Voltage Flicker Assessment in Distribution Feeders with Large Wind Farms

By Diego Mascarella

Master of Engineering

Department of Electrical and Computer Engineering

McGill University, Montreal, Quebec

October 2012

A thesis submitted to McGill University in partial fulfillment of the requirements for the degree of Master of Engineering in Electrical Engineering

Abstract

In recent years, Doubly Fed Induction Generator (DFIG) wind turbines connected to rural distribution feeders represents an emerging trend that has experienced growth. Higher penetration levels of embedded wind generation has interesting benefits (i.e. peak-shaving, congestion alleviation, reduction of losses, etc.) but raises important issues concerning the quality of power delivered to utility consumers. This thesis investigates the technical limitations involved with integrating large DFIG based wind farms into existing distribution feeders with regard to voltage flicker. This dissertation includes an overview of firstly, the applicable Electromagnetic Compatibility (EMC) standards related to the measurement and assessment of flicker emissions produced by distribution-connected wind farms. Secondly, aerodynamic, turbine and feeder characteristics which influence voltage flicker. Thirdly, the level of modeling required to conduct a pre-connection flicker study. Based on these three aspects, flicker emissions produced by a DFIG are quantified and a rule of thumb and a set of guidelines are presented for the acceptance of a 10 MW to 14 MW distributed wind farm, compliant to the allocated flicker emission quota. If the rule of thumb does indeed reveal a problem, both passive and active flicker mitigation techniques are proposed such that EMC of the power system is preserved.

Résumé

Au cours des dernières années, les éoliennes à base de génératrice asynchrone à double alimentation (DFIG) connectées à des réseaux de distribution rurale représentent une tendance émergente en croissance. Le niveau de pénétration plus élevé d'énergie éolienne présente des avantages intéressants (i.e. écrêtement des pointes, la réduction de la congestion, la réduction des pertes, etc.) mais il soulève d'importantes questions liées à la qualité de l'énergie livrée aux consommateurs. Cette thèse étudie les limites techniques liées à l'intégration des grands parcs éoliens dans les réseaux de distribution existants au niveau du scintillement. Cette thèse comprend, premièrement, une vue d'ensemble des normes applicables sur la compatibilité électromagnétique concernant la mesure et l'évaluation des émissions produites par des parcs éoliens connectés à des réseaux de distribution. Deuxièmement, l'aérodynamisme, la turbine et les caractéristiques du réseau de distribution sont étudiés pour leurs influences sur le scintillement. Troisièmement, le niveau de la modélisation requis pour mener une étude de pré-connexion sur le scintillement est évalué. Sur la base de ces trois aspects, les émissions de scintillements induites par les éoliennes DFIG sont quantifiées. Une méthode empirique et un ensemble de directives sont présentés pour l'intégration d'un parc éolien de 10 MW à 14 MW afin d'assurer une conformité au quota alloué pour l'émission de scintillement. Si la méthode empirique révèle un problème, des techniques passives et actives d'atténuation de scintillement sont proposées afin que la compatibilité électromagnétique du réseau électrique soit préservée.

Acknowledgements

First and foremost, I would like to thank my supervisor, Prof. Géza Joós, for his continuous guidance and support throughout my engineering master's degree. Through the many discussions we had, his insight, knowledge and perspective have helped me develop the engineering skills required to tackle any challenge.

Furthermore, I acknowledge the assistance provided by Dr. Anthony J. Rodolakis. I also thank Prof. François Bouffard and Prof. Boon-Teck Ooi who helped me gain ample knowledge of power engineering fundamentals through our discussions and courses lectured. I extend my thanks to all my power engineering research colleagues, especially, Moataz Ammar and Ali Shojaei, who enriched my work through many discussions, suggestions and comments.

I appreciate the financial and technical support of the Hydro-Québec industrial research fund, Natural Sciences and Engineering Research Council of Canada (NSERC), and McGill University.

Finally, I would like to dedicate this work to my family, Santo, Anna, Francesco and Marco Antonio, whose help, support and encouragement have been greatly appreciated during all my years of study.

Table of Contents

List of Figures

List of Tables

List of Abbreviations

CDF	*Cumulative Distribution Function*
CL	*Compatibility Level*
DG	*Distributed Generator*
DFIG	*Doubly Feed Induction Generator*
EHV	*Extra High Voltage*
EMC	*Electromagnetic Compatibility*
ESS	*Energy Storage System*
FS	*Fixed Speed*
GSC	*Grid Side Converter*
HV	*High Voltage*
IEC	*International Electrotechnical Commission*
IFL	*Instantaneous Flicker Level*
IGBT	*Insolated Gate Bipolar Transistor*
MPPT	*Maximum Power Point Tracking*
MV	*Medium Voltage*
PCC	*Point of Common Coupling*
PEC	*Power Electronic Converter*
PFC	*Power Factor Control*
PI	*Proportional Integral*
PL	*Planning Level*
PMSG	*Permanent Magnet Synchronous Generator*
PSD	*Power Spectral Density*
RSC	*Rotor Side Converter*
SCC	*Short Circuit Capacity*
SCR	*Short Circuit Ratio*
STATCOM	*Static Synchronous Compensator*
SVC	*Static Var Compensator*
VC	*Voltage Control*
VS	*Variable Speed*
VSC	*Voltage Source Converter*
WRIG	*Wound Rotor Induction Generator*
WRSG	*Wound Rotor Synchronous Generator*
WTG	*Wind Turbine Generator*

List of Acronyms

α	*Empirical wind shear exponent*
a	*Tower radius*
A	*Area swept by rotor blades*
β	*Blade pitch angle*
C	*Capacitance*
C_P	*Power coefficient*
D_m	*Shaft mutual damping*
f_s	*Sampling frequency*
H	*Hub height*
H_G	*Generator inertia*
H_T	*Turbine inertia*
i'_{dr}	*d-axis rotor current*
i_{ds}	*d-axis stator current*
i'_{qr}	*q-axis rotor current*
i_{qs}	*q-axis stator current*
I_{dc}	*DC link current*
I_n	*Turbulence intensity*
K	*Reactive compensation gain*
K_{shaft}	*Shaft stiffness*
λ	*Tip-speed ratio*
λ^*	*Optimal tip-speed ratio*
L	*Turbulence length*
L'_{lr}	*Rotor leakage inductance*
L_{ls}	*Stator leakage inductance*
L_m	*Magnetizing inductance*
L'_r	*Total rotor inductance*
L_s	*Total stator inductance*
N_{wt}	*Number of wind turbines*
ω_r	*Generator rotor speed*
$\omega_{r,ref}$	*Reference generator rotor speed*
$\omega_{r,meas}$	*Measured generator rotor speed*
ω_s	*Synchronous speed*
ω_T	*Turbine rotor speed*
ϕ	*Azimuthal angle*
φ'_{dr}	*d-axis rotor flux*
φ_{ds}	*d-axis stator flux*
φ_{grid}	*Grid impedance angle*
φ_{pf}	*Power factor angle*
φ'_{qr}	*q-axis rotor flux*

φ_{qs}	*q-axis stator flux*
p	*Number of pole pairs*
P	*Real power*
P_{dc}	*DC link power*
P_g	*Grid side converter power*
P_{lt}	*Long term flicker severity index*
P_m	*Mechanical power*
P_r	*Rotor side converter power*
P_{st}	*Short term flicker severity index*
Q	*Reactive power*
Q_{meas}	*Measured reactive power*
Q_{ref}	*Reference reactive power*
ρ	*Air density*
R	*Rotor radius*
R_L	*Line resistance*
R_r'	*Rotor resistance*
R_s	*Stator resistance*
θ_r	*Generator rotor angle*
θ_T	*Turbine rotor angle*
T_e	*Electromagnetic torque*
T_s	*Sampling time*
T_T	*Turbine mechanical torque*
v	*Wind speed*
V_{dc}	*DC link voltage*
V_{dr}'	*d-axis rotor voltage*
V_{ds}	*d-axis stator voltage*
V_{ll}	*Line-to-line voltage*
V_{qr}'	*q-axis rotor voltage*
V_{qs}	*q-axis stator voltage*
x	*Distance from blade origin to tower midline*
X_L	*Line reactance*

Chapter 1: Introduction

1.1 Proliferation of wind energy

In recent years, the proliferation of wind power has been mainly driven by the deregulation of the power industry, technological advancements and the continuing push for cleaner energy sources. According to the Global Wind Energy Council, the total installed wind power capacity now operating stands at 237,669 MW; refer to Figure 1-1 [1].

Canada reached a record year in 2011, installing 1,267 MW of wind power. Heading in the right direction to meet the industry-set target of 10 GW by 2015, up to 1,500 MW is scheduled to be installed in 2012, adding to Canada's current total installed capacity of 5,265 MW [2].

Provincially, Hydro-Québec has signed contracts for a total of 3,000 MW, as a result of two tender calls for the purchase of wind power, dated February 2005 and June 2008. In April 2009, two additional calls for tenders for the purchase of 500 MW of wind power were issued. Thus, by 2013, 3,500 MW of wind power will be under contract as a result of the Hydro-Québec's tender calls [3].

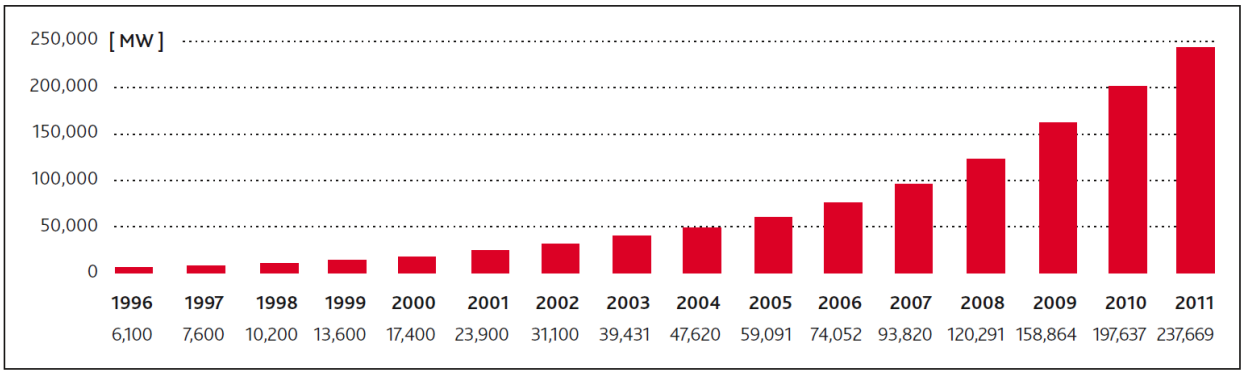

Figure 1-1 Global cumulative installed wind capacity [1]

The large-scale integration of wind power, particularly that which is distribution-connected, projected to be as high as 30% of all new generation [4], however, gives rise to new challenges for the power system. The highly fluctuating nature of the wind constitutes the main challenge towards a harmonious integration of the wind power [5], yet regional grid code requirements must be abided. Thus, as the penetration levels of distribution-connected wind power increases, it becomes necessary to ensure that the proper studies and measures are taken such that power system operates smoothly.

1.2 Wind turbine technologies

1.2.1 Overview

Wind Turbine Generator (WTG) designs have progressed mainly with regards to the rotational speed, Power Electronic Converter (PEC) and drive train components. Referring to the rotation speed, WTG topologies can be classified into Fixed Speed (FS), limited variable speed and Variable Speed (VS) [8]. VS wind turbines, which include a PEC in their topology, can be further classified into WTGs with a partial-scale and a full-scale PEC, based on the relative rating of the PEC to the WTGs generation capacity. Furthermore, referring to the drive train system, the WTG topologies can be classified into geared-drive and direct-drive wind turbines [6]-[8].

WTGs are commonly classified as Type 1, Type 2, Type 3 and Type 4 [8],[31]. Type 1 and Type 2 WTGs consist of FS and limited variable speed topologies. Whereas, Type 3 and Type 4 WTGs consist of VS topologies and represent the dominant modern day design and hence, will be further discussed.

1.2.2 Variable speed configurations

A Type 3 WTG, as illustrated is figure 1-2, corresponds to a VS wind turbine with a Wound Rotor Induction Generator (WRIG) and a partial-scale PEC on the rotor circuit [8]. This configuration is also known as the Doubly-Fed Induction Generator (DFIG) topology and is widely used in wind power generation. In this topology, the stator is directly connected to the grid, whereas the rotor is connected through a cascade of two Voltage Source Converters (VSC),

typically rated 30% of the machine power. The Rotor Side Converter (RSC) excites the generator rotor winding at variable frequency, thus permitting the WTG to operate at a variable rotational speed. The WTG is able to support a wide speed range operation which is typically $\pm 30\%$ around the synchronous speed [6].

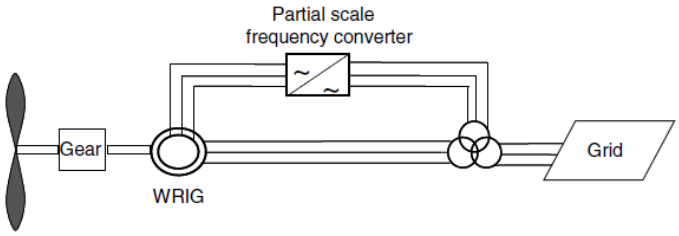

Figure 1-2 Type 3, Variable speed WTG with partial-scale PEC [8]

For Type 4, WTGs, as illustrated is Figure 1-3, the generator is entirely decoupled from the grid via a full-scale PEC. In this case, the PEC handles the total generated power delivered to the grid. Therefore, the PEC must be fully rated, resulting in an increase in cost, power losses and harmonic emissions compared to the DFIG topology [7]. The generator can be a Permanent Magnet Synchronous Generator (PMSG), Wound Rotor Synchronous Generator (WRSG), or WRIG [8].

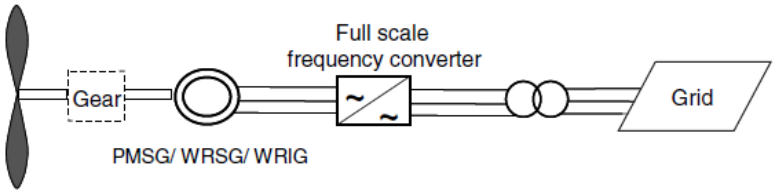

Figure 1-3 Type 4, Variable speed WTG with full-scale PEC [8]

1.3 Impact of large distribution-connected wind farms on the power system

Distribution networks were not designed to deal with the large fluctuating power injections produced by wind farms, hence, the proliferation of wind power on the power system results in a number of adverse impacts. A subset of these impacts include voltage variations, degraded protection, altered transient stability, and bi-directional power flow [9],[10]. At the distribution level, voltage variations which induce flicker are considered to be

one of the main power quality problems associated with large penetrations wind power. These voltage variations are mainly due to the stochastic and non-dispatchable nature of the local wind resource by which the typical 25 kV North American rural distribution feeder is less suitable to handle, due to network characteristics, leading to objectionable flicker levels.

Generally, the normal tolerances of feeder voltage levels are $\pm 10\%$, however, rapid voltage variations become a nuisance at levels as low as 0.3%, in weak feeders which are often located in rural areas where the wind farms are connected [11]. This nuisance is termed as flicker, which is defined as a subjective phenomenon that is experienced by human beings when exposed to the fluctuating luminous flux of light sources. Utility surveys have shown that most people are tolerant to an occasional light flicker event, but when light flicker is frequent and/or continuous, consumers are annoyed and start to complain [12],[13]. Hence, light flicker can be the limiting factor determining the amount of wind power which can be connected to a distribution feeder and thus, the phenomenon must be studied.

1.4 Description of the light flicker phenomenon

1.4.1 Voltage fluctuations and flicker

Voltages fluctuations and flicker are linked terms and are commonly used indistinctly. Nonetheless, these terms are defined differently, although they frequently can occur at the same time [14]. Therefore, it is essential to clearly differentiate these two terms:

Voltage fluctuations are defined entirely from an electrical point of view and are described as variations of the voltage waveform whose amplitudes are bound to $\pm 10\%$ of the nominal voltage level. The magnitude of these voltage fluctuations are typically well below the thresholds of sensitivity of most electrical equipment and are not likely to result in operating problems [14],[16]. However, for some specific cases, voltage fluctuations can induce variations in the luminous flux of light sources, hence, affecting the light bulbs operation [14].

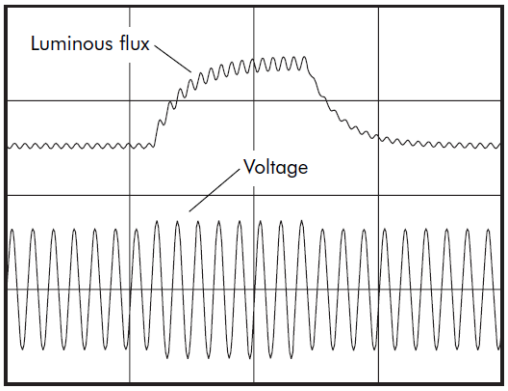

Figure 1-4 Change in luminous flux resulting from a temporary voltage change, (informative, not to scale) [13]

The International Electrotechnical Commission (IEC) standard IEC 61000-3-7 [48], defines flicker as an impression of unsteadiness of visual sensation induced by a light stimulus whose luminance or spectral distribution fluctuates with time. Essentially, flicker corresponds to the visual discomfort experienced by a person, when exposed to variations in the luminous flux of light sources. These luminous flux variations are induced by voltage fluctuations, as can be seen in Figure 1-4, thus, there is a clear connection between flicker and voltage fluctuations. However, a human factor is involved in the definition of flicker, while voltage fluctuations are defined entirely from an electrical point of view [14]. This implies that in order for a flicker problem to occur, the following two factors are required: 1) voltage fluctuations causing variations in luminous flux, defined as the objective factor and 2) a person exposed to these luminous flux variations, defined as the subjective factor [14],[16]. Thus, as the human physiological process has a significant influence in quantifying the flicker disturbance, thorough knowledge of the human visual perception is essential for the measurement of the flicker.

1.4.2 Physiology of flicker perception

As mentioned in the previous section, flicker is basically a physiological phenomenon that can at certain severity levels cause significant discomfort to the person exposed to it. The work conducted by de Lange [18], in the 1950s and Rashbass [19] in the 1970s, demonstrated that the response of the human eye has the behavior of a band-pass filter between 0.5 Hz and 42 Hz, with the highest sensitivity to the luminous flux at a frequency around 8 to 9 Hz. Physiological effects also depend on several other key factors (i.e. the amplitude of the

fluctuations, the duration of the disturbance, the activity/state of the person and the color of the lighting source). They also concluded that the brain response to light stimulus has a memory effect with a time constant of around 300 ms, implying that slow changes in luminous flux are more noticeable than fast changes in luminous flux which are smoothed out [14],[18],[19],[53]. Based on these results, the IEC Flickermeter was progressively developed to simulate the human physiological process in order to quantify the flicker disturbance and will be discussed in chapter 2.

1.5 Factors influencing flicker

1.5.1 Overview

The connection of a large wind farm to a distribution network may greatly influence the flicker level in the supply voltage provided to utility customers. The main factor contributing to the deterioration of voltage quality are the rapid variations of the wind farm's output power, which induce fluctuations in the feeder's voltage, attributing to flicker [78]. Flicker emissions arise in consequence of the fluctuating nature of the wind farm's output power which is composed of both deterministic components (due to tower shadow and wind shear) and stochastic components (due to wind gusts, wind turbulence and wind speed variability) [11],[20]-[31],[78]. Furthermore, network characteristics such as the short circuit capacity, grid impedance angle and the local load will be the determining factors attenuating or aggravating the feeder's flicker level [21]-[26].

1.5.2 Wind flow and local characteristics

Flicker emissions produced by a distributed wind installation during continuous operation are in most part induced by power fluctuations originating from variations in the rotor torque. Aerodynamic factors influencing variations in rotor torque of the WTG, contributing to increased amounts of flicker emissions, initiate from three main sources:

- Mean wind speed
- Wind gusts and turbulence intensity
- Blade passing effects

Site characteristics, notably the annual mean wind speed and turbulence intensity influence the quantity of flicker emissions produced by the WTG. Typically, the flicker emissions produced by the WTG will increase linearly with respect to the mean wind speed and turbulence intensity in the range below the WTG rating [22],[24]. On another note, gust components present in the wind resource, which are defined as rapid changes in the wind speed, have a direct influence on the flicker level produced.

Aerodynamic factors which influence the flicker level produced by a WTG and are not present in the wind resource include wind shear and tower shadow. These two deterministic effects are an inherent characteristic of any wind turbine and will result in periodic fluctuations in rotor torque. Wind shear is defined as the variation in wind speed with height. Hence, the WTG's blades will experience a greater wind speed facing upwards and a reduction in wind speed facing downwards during a revolution. Tower shadow is defined as the reduction in wind flow due to the presence of the tower. Thus, when the turbine blade crosses the tower, the WTG experiences a reduction in wind flow. Consequently, these 3p frequencies, typically in the range of 0.5 Hz – 2 Hz, result in fluctuations in the supply voltage at the Point of Common Coupling (PCC) [30] and contribute to the total amount of flicker produced by the WTG.

1.5.3 Wind turbine topology and wind penetration

The smoothing of these wind power fluctuations originating from aerodynamic variations fed to the distributed wind farm are highly dependent on:

- Type of wind turbine and associated reactive power control
- Rated capacity of the wind farm

1.5.3.1 Type of wind turbine and associated reactive power control

The WTG technology applied has a great influence on the magnitude of output power fluctuations produced by the distributed wind installation [22]. The use of PECs utilized in Type 3 (partial-scale converter) and Type 4 (full-scale converter) variable speed turbines to interface with the grid, provides better performance related to flicker emissions in comparison with their fixed speed, Type 1 and Type 2 counterparts [28]. The main reasoning is that in the Type 3 WTG topology, the incoming power fluctuations can be attenuated by slightly changing the turbine

rotor speed, hence, using the VS operation of the machine to smooth power fluctuations [22],[26]. On a similar note, Type 4 WTGs are fully decoupled from the grid via a PEC, hence the energy stored in the DC-link of the PEC provides a buffer to smooth out power fluctuations. Furthermore, for Type 3 and Type 4 WTGs the output active and reactive power can be controlled independently. Thus, the reactive power can be controlled to reduce the voltage fluctuations caused by active power fluctuations as opposed to operating the WTG at a unity power factor [27].

1.5.3.2 Rated capacity of wind farm

As the wind farm capacity increases, the flicker emissions produced by the distributed wind installation at PCC will tend to increase as well. A measure of the distributed wind penetration is the Short Circuit Ratio (SCR) defined by:

$$SCR = \frac{SCC}{S_n} \tag{1.1}$$

Where S_n is the rated apparent power of the wind farm. Thus, as the rated apparent power of the wind installation increases, the SCR will decrease, indicating an increased relative penetration and increased level of flicker emissions. In fact, it is well noted that the flicker level is inversely proportional to the SCR [21]-[24]. Factors that influence the SCC at a particular node in the distribution feeder will be discussed in the next section.

1.5.4 Distribution feeder characteristics

The inherent characteristics of a weak rural distribution feeder represent a bothersome concern that a utility may have prior to the connection of a large embedded wind farm. The reasoning is that the wind farms highly fluctuating power injections, associated with the turbines mode of operation, in combination with distribution feeder parameters, may cause significant fluctuations in the feeder voltage which may lead to objectionable flicker levels. The relative voltage change due to a fluctuation in power flow on a distribution feeder can be approximated using eqn. (1.2).

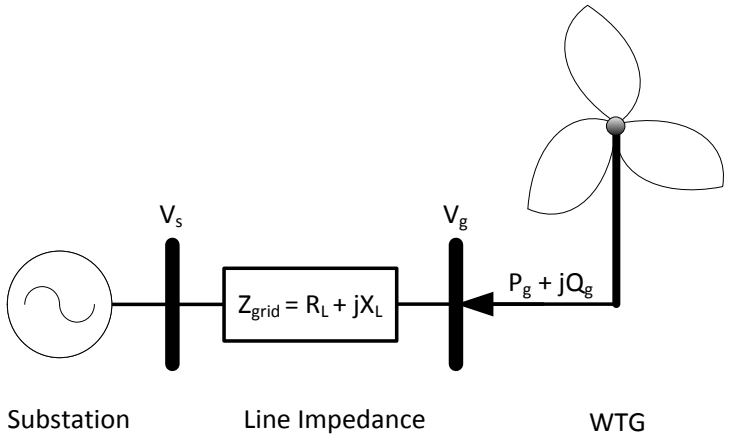

Figure 1-5 Voltage change over a distribution network with wind power

$$\left.\begin{aligned} \Delta V = V_g - V_s = Z_{grid} I_g = (R_L + jX_L)\left(\frac{\Delta P_g - j\Delta Q_g}{V_g}\right) \\ \Delta V = \frac{R_L \Delta P_g + X_L \Delta Q_g}{V_g} + j\frac{X_L \Delta P_g - R_L \Delta Q_g}{V_g} \\ \Delta V = \Delta V_p + j\Delta V_q \end{aligned}\right\} \quad (1.2)$$

Whereby, ΔV is the change in voltage, ΔP_g is the change in active power, ΔQ_g is the change in reactive power, R_L and X_L are the distribution feeder line resistance and reactance respectively. In the case of distribution networks, it is common to ignore the imaginary term $j\Delta V_q$, assumed negligibly small [32], and thus, eqn. (1.2) simplifies to:

$$\Delta V = \frac{R_L \Delta P_g + X_L \Delta Q_g}{V_g} \quad (1.3)$$

1.5.4.1 Impact of the network impedance angle (X/R ratio)

The X/R ratio is a significant parameter in terms of its influence on voltage flicker due to the fact that it determines whether the active or reactive power will dominate voltage fluctuations at the PCC. Depending on the network impedance angle denoted by eqn. (1.4), the ability for the network to attenuate flicker emissions will vary.

$$\varphi_{grid} = \tan^{-1}\left(\frac{X_L}{R_L}\right) \quad (1.4)$$

The determining factor that influences the severity of flicker emissions is the difference between grid impedance angle and the wind turbine power factor angle φ_{pf} [24]. This can be shown analytically with the reformulation of eqn. (1.3):

$$\Delta V = \frac{R_L \Delta P_g \cos(\varphi_{pf} - \varphi_{grid})}{V_g \cos(\varphi_{pf}) \cos(\varphi_{grid})} \tag{1.5}$$

Usually the DFIG wind farm is set to operate at unity power factor, which implies that no reactive power is supplied to or absorbed from the feeder [22]. In this scenario, the line resistance, typically high for distribution feeders, is the determining factor that influences the flicker emissions produced by the wind farm. Thus, for higher grid impedance angles, implying a higher X/R ratio, a reduction in flicker emission is observed. When the difference between the grid impedance angle and the power factor angle approaches 90 degrees, flicker emissions are minimized [22],[24], as can be verified by eqn. (1.5).

1.5.4.2 Impact of network short-circuit capacity

The short circuit capacity is a relative indicator of the voltage stiffness of a particular node in the distribution feeder. The higher the SCC, the higher the voltage stiffness of that node, and hence, flicker levels should be relatively low. Stated otherwise, the SCC is a measure of the feeder's ability to absorb voltage fluctuations and although not directly a parameter of voltage quality, has a great influence [11]. It has been noted that the flicker level is approximately inversely proportional to the short circuit capacity at the PCC of the distributed wind farm [24].

Distribution feeder characteristics that primarily influence the SCC at the PCC are the voltage interconnection level and the grid impendence.

$$SCC = \frac{V_{ll}^2}{\sqrt{R_L^2 + X_L^2}} \tag{1.6}$$

With reference to eqn. (1.6), the higher the interconnection voltage level and the lower the grid impendence at PCC, the greater the SCC. The equivalent grid impedance determined by looking back into the distribution feeder from the PCC and is dependent on multiple factors,

including the size of the substation transformer, distribution conductor type and distance from the substation [20],[39].

1.5.4.3 Load Type

Fluctuating industrial loads of substantial size connected to the distribution feeder can cause severe flicker levels to other customers connected to the same feeder. Typical flicker emitting loads consist of electric arc furnaces, electric boilers, frequently starting and stopping induction motors, and welders [14],[33]-[36]. If these loads are connected near or at the PCC of the distributed wind installation, the summation of flicker emissions originating from different sources may reach to objectionable levels. Hence, the load type connected at or near the PCC may be a serious technical limitation to the quantity of distributed wind to be installed, especially if the occurrences of emissions are simultaneous and/or within the same frequency range.

1.6 Flicker mitigation

Several solutions are available to mitigate the flicker emissions caused by distribution-connected wind turbines. The most widely adopted techniques are based on reactive power compensation; however, other methods are possible and include reducing the line impedance and the use of an Energy Storage System (ESS).

The passive flicker mitigation measure to reduce the line impedance, with the intent to strengthen the SCC at PCC, is not common, but can be done in the two following manners. The reduction of the line impedance can be achieved by physically moving the PCC closer to the substation transformer or by reinforcing the existing distribution network [20],[32]. However, it may not always be possible to relocate the wind farm closer to the substation transformer as these areas are typically more densely populated and may violate municipal legislation. Moreover, the reinforcement of the distribution feeder is likely to render the wind farm project infeasible from a financial standpoint, as the costs of re-conductoring sections of the feeder will be fairly significant [32].

Flicker mitigation techniques utilizing an ESS connected at the DC-link of the WTG PEC, for power smoothing can also reduce flicker emissions. The main notion is that flicker emissions are attenuated by storing or injecting fluctuating active power components at the DC-link of the WTG. In ref. [37] an ESS is employed to reduce tower shadow and wind shear flicker emissions while ref. [38] employs an ESS to suppress all flicker components. However, economic feasibility of these approaches is questionable.

Reactive power based mitigation techniques reduce the flicker level by dispatching reactive power in the opposite direction to that of active power fluctuations and hence, reducing ΔV, refer to eqn. (1.3). Reactive power compensation can be employed to distributed wind installations by conventional equipment such as a Static Var Compensator (SVC) or Static Synchronous Compensator (STATCOM) as mentioned in ref. [20],[39],[40]. The purchase of this additional equipment, however, raises the project cost considerably and presents an infeasible solution for distributed-wind applications. Moreover, variable speed WTG topologies have an inherent ability to control reactive power, therefore, the WTGs PEC can be utilized in a similar fashion to that of a STATCOM in order to reduce flicker emissions [22]. Thus, reactive power based, flicker mitigation techniques may be embedded within the WTG and assume the form of either Voltage Control (VC) or Power Factor Control (PFC).

The voltage control technique involves using the difference between the voltage measured at the WTG terminal to a reference voltage, in order to set the reactive power needed to be absorbed or supplied by the machine. This in consequence reduces voltage fluctuations and hence, the flicker level. However, distribution networks containing an On-Load Tap Changing transformer (OLTC) and capacitor banks, both which are voltage control devices will require a more sophisticated and coordinated voltage control scheme, if the voltage control mitigation technique embedded in the WTG is employed [20],[41]. The main reasoning is such that the multiple voltage control devices within the network are not “chasing” each other, stimulating excessive switching occurrences, resulting in distribution equipment degradation, particularly the OLTC and circuit breaker [41].

The main notion of the PFC mitigation technique is based on eqn. (1.5). Essentially the PFC technique adjusts the power factor angle φ_{pf}, such that $(\varphi_{pf}-\varphi_{grid})$ is equal to 90° by controlling the reactive power output [22],[23],[37],[38],[42]-[44]. Nevertheless, the PFC mitigation technique shows its limitations when the grid impedance angle is low, inherent to weak rural distribution networks which tend to be much more resistive that transmission networks [22]. If the total reactive power required to mitigate flicker is in excess of the WTG ratings, the flicker level may still stand at objectionable levels. Active power curtailment is one technique applied to provision for a reactive power margin in the case when the power limits of the converter may be exceeded in order to mitigate flicker by absorbing reactive power [31]. Yet, curtailing active power has unfavorable financial implications as the power sent to the grid is decreased. Moreover, for weak distribution networks, the PFC mitigation technique will require the WTG to operate at very poor power factors which may not meet local grid code requirements and may in fact bring upon new problems to the distribution network with regard to reactive power supply.

In a more practical scenario of the PFC implementation, manufacturers provide electrical WTG ratings 10% in excess of their prospective active power rating [75]. This allows the WTG to operate constantly at a slightly leading power factor, (i.e. absorbing reactive power) and still reduce flicker emission levels without the need for active power curtailment. Although, WTG flicker emissions may not be reduced to their minimum levels, this method provides a way to reduce the flicker level and comply with grid codes. Yet, operating at a constant power factor, other that unity, implies continuously absorbing significant amounts of reactive power, which comes at a dollar cost and increases the burden on network reactive power sources.

Thus, there is a need for a reactive power based mitigation technique which directly addresses flicker emissions, such that reactive power is used efficiently, rendering the technique practically viable. An improved flicker mitigation technique based on reactive power which operates within a specified power frequency band is explored in chapter 4 of this dissertation.

1.7 Problem statement & project description

The quantity of flicker emissions produced by a distribution-connected wind farm is a bothersome issue for utilities. In order to make the most efficient penetration of wind energy into rural distribution feeders without compromising EMC of the power system, the utility must be able to assess the dependence of voltage flicker on site characteristics, wind turbine characteristics and feeder characteristics which were all discussed in the previous section. Thus, a set of guidelines and a rule of thumb for the design and interconnection of a large distributed wind installation, with regard to flicker, will be of great benefit.

In order to determine if a distributed wind installation will impose technical limitations with regard to flicker, a parametric study will be conducted, in accordance to factors that influence flicker in order quantify and assess emissions. Flicker studies tend to be computationally expensive, due to the 10 minute voltage sampling period and 50 μs simulation time step, thus, the modeling will be oriented for a flicker study and the parameters which influence flicker will only be tested within a logical and practical range. Moreover, based upon these studies, a subset of factors which are deemed to greatly influence voltage flicker will be further studied for the development of a generalized rule of thumb.

These studies will serve as guidelines on how flicker is influenced from individual characteristics and later used to develop rule of thumb with appropriate mitigation corresponding to flicker level, grid characteristics and applicable regional grid codes. Thus, the overall goal of this research is to aid in the design and interconnection of a large distributed wind installation with a certain degree of confidence, without the need for a detailed network simulation.

1.8 Thesis outline

The remainder of the thesis is organized as follows:

Chapter 2 details flicker evaluation, measurement and modeling. This includes a revision of applicable standards, notably IEC 641000-4-15, IEC 61400-21 and IEC 61000-4-7 which cover the Flickermeter instrument, flicker measurement guidelines for wind turbines, summation of flicker originating from multiple sources as well as compatibility, planning and emission levels for flicker in MV networks.

Chapter 3 details the level of modeling required to conduct a flicker study. This entails assuring that factors which influence flicker are incorporated and may be adjusted in the modeling such that emissions are well quantified. Both, the modeling requirements of the wind speed model as well as the wind turbine model are discussed in this chapter.

Chapter 4 quantifies and analyses the behavior of wind farm flicker emissions according to factors that are known to influence flicker. This includes the influence wind, aerodynamic and grid parameters on DFIG induced flicker emissions. Moreover, the effectiveness of reactive power based mitigation techniques are compared in terms of reactive power use and viability.

Chapter 5 details a flicker study conducted on a real distribution network, using the Opal-RT® real time simulator. Varying levels of wind penetration are connected at several PCCs and flicker behavior is studied and quantified. The interaction between flicker emitting loads and the wind farm are also studied. Finally the effectiveness of reactive power based flicker mitigation is tested.

Chapter 6 presents the formulated rule of thumb for flicker assessment in a pre-connection study and summarizes the main conclusions drawn from this thesis.

Chapter 2: Flicker Evaluation, Measurement and Modeling

2.1 Overview

This chapter presents two methods for quantifying flicker emissions produced by a distribution-connected wind farm during a pre-connection phase, as specified in [46]. Both methods entail the use of the IEC Flickermeter, which is detailed. The first method involves a detailed simulation, involving the network under study, the wind farm and the measurement of flicker at the node of interest, using an IEC Flickermeter emulator. The second method uses universally applicable flicker tables provided by the WTG manufacturer compliant to the IEC 61400-21 standard [47] to quantify flicker emissions at the desired PCC. Also mentioned, is how flicker is summed when originating from multiple sources and the flicker emission limits provided by the IEC 61000-4-7 standard [48].

2.2 Perspective, description, limitations and modeling of the IEC Flickermeter

2.2.1 Perspective and description of the IEC Flickermeter

Currently, the most prevalent and widely accepted standard for flicker is IEC 641000-4-15, also referred to as the IEC Flickermeter. The IEC Flickermeter standard specifies the function and design of a flicker instrument based on human perception to the luminous flux variations of a standard 60W incandescent light bulb induced by voltage variations. The major advantage of the IEC Flickermeter is that it automatically incorporates the contributions of numerous flicker disturbances and non-standard (i.e. not square or sine wave) modulating waveforms [16] into unified and comparable flicker measure, which was considered a major shortcoming of the historical GE flicker curves [16],[40].

The IEC Flickermeter essentially processes the input voltage measurement at the node under study and outputs two main indices, notably, the short term flicker severity, P_{st}, and the long term flicker severity, P_{lt}. These two main indices are derived statistically from the level of perceptible flicker over periods of 10 minutes and 2 hours respectively.

2.2.2 Limitations of the IEC Flickermeter instrument

The IEC Flickermeter specifies a measurement instrument based on human perception to a 120V, 60W incandescent lamp supplied with a fluctuating voltage waveform. Controversially, some governments are considering stronger measures to entirely remove incandescent lamps from the market. These measures include taxation or bans on the production of incandescent lamps that do not meet energy efficiency requirements [49]. It is important to note, the IEC Flickermeter standard specifically states that the characteristics of discharge lamps are totally different than incandescent lamps and that substantial modifications to this standard would be necessary if they were taken in account. Thus, the IEC Flickermeter has limitations with regards to accessing flicker in modern lighting which is based on a different technology than the incandescent lamp and sought to be less sensitive to voltage fluctuations inducing flicker. Recently, studies [11],[50]-[54] have been demonstrated that inter-harmonics originating from the supply voltage can also cause both incandescent and fluorescent lamps to flicker. However, the mechanisms and the involved frequency ranges, as well as light flicker amplitudes, are quite different.

2.2.3 Modeling and implementation of the IEC Flickermeter instrument

2.2.3.1 Overview

In order to conduct a flicker study, without the use of flicker tables provided by the IEC 61400-21 standard, a flickermeter emulator must be constructed, as in [70]-[74]. Thus, a discrete time flickermeter, compliant with ref. [15], implemented in Matlab® and to be used for voltage flicker studies is required. The main objective is to develop a measurement tool which will output a short term flicker severity P_{st} from a 10 minute input voltage array, generated in any simulation package. Thus, a script based flickermeter function which takes an input voltage array V, at a specified sampling frequency f_s and specified instrument warm up time (time for

instrument to reach steady state due to the fact the embedded filters are not initialized) and outputs the corresponding P_{st} and Instantaneous Flicker Level (IFL) will be implemented. The IFL is essentially the measured flicker emissions as a function of time from which the P_{st} is statistically computed from.

It is important to note that a minimum sampling frequency f_s for compliant results as well as a minimum warm up time for the instrument filter transients to settle will need to be reported. Respecting these two conditions will ensure correct usage of the newly developed flickermeter emulator.

2.2.3.2 Implementation of the IEC Flickermeter Instrument

The structure of the IEC Flickermeter is shown in figure 2-1. The major steps of the flickermeter algorithm which need to be implemented are 1) input processing 2) eye-brain-lamp response, 3) statistical analysis of the flicker signal for the computation of the P_{st} level [16].

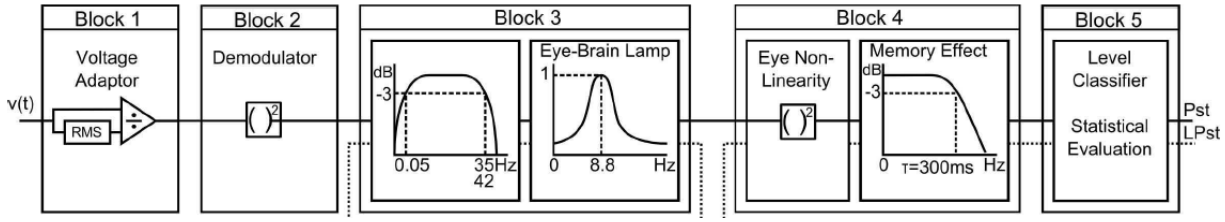

Figure 2-1 IEC Flickermeter processing diagram [15]

Please note that ref. [15] describes a physical flickermeter device and not a flickermeter emulator. Thus, sections regarding transformer sizing, operating temperatures etc. can be disregarded. In addition, all filter transfer functions in the standard are in s domain. To model the filters as discrete blocks, as opposed to continuous blocks, it is necessary to express the filter transfer functions from s domain to z domain. The bilinear transformation, also known as the Tustin transformation is a well-known discretization method and will be employed. The transformation is the following:

$$s \approx \frac{2}{T_s} \cdot \left(\frac{z-1}{z+1}\right) \tag{2.1}$$

Whereby, T_s is the sampling time.

Block 1: Input voltage adaptor & calibration checking circuit

The input of the first block is a 10 minute time series of the voltage and the node under evaluation. This block contains a voltage adaptor whose objective is to scale the 1 minute mean RMS value, updated every half cycle, down to an internal reference level. This step allows for flicker measurements to be done independently of the input voltage supply level. The output of this block is the normalized RMS value of the input voltage.

Block 2: Square law demodulator

The function of the second block is to recover the voltage fluctuation by squaring the input voltage which has been scaled to an internal reference level, thus simulating the light output behavior of an incandescent lamp which is proportional to its instantaneous power.

Block 3: Weighting filters

Block 3 is composed of a cascade of two filters. The first filter models the sensitivity of the human eye-brain to light stimulus and incorporates a band-pass filter consisting of a 1st order high pass filter and a 6th order Butterworth low pass filter with cutoff frequencies at 0.05 Hz and 42 Hz respectively. The 1st order high pass filter which eliminates the DC component is given as follows:

$$F_{HP}(s) = \frac{s \cdot \tau_{HP}}{s \cdot \tau_{HP} + 1} \tag{2.2}$$

Whereby τ_{HP} is the filter time constant given as follows:

$$\tau_{HP} = \frac{1}{2\pi \cdot f_{HP}} \tag{2.3}$$

Whereby f_{HP} is the cut off frequency of the high pass filter having attenuation of 3dB at $f_{HP} = 0.05Hz$. The 6th order Butterworth low pass filter transfer function can be given in cascade form as follows:

$$F_{LPBW} = \frac{1}{\left[\left(\frac{s}{\omega_{lp}}\right)^2 + a\left(\frac{s}{\omega_{lp}}\right) + 1\right] \cdot \left[\left(\frac{s}{\omega_{lp}}\right)^2 + b\left(\frac{s}{\omega_{lp}}\right) + 1\right] \cdot \left[\left(\frac{s}{\omega_{lp}}\right)^2 + b\left(\frac{s}{\omega_{lp}}\right) + 1\right]} \tag{2.4}$$

Whereby $a \approx 0.5176,\ b \approx 1.4142,\ c\ \approx 1.9319$ and $\omega_{lp} = 2\pi f_{lp}$. Whereby, f_{lp} is the cut off frequency of the low pass filter with attenuation of 3dB at a frequency of 42 Hz.

The second filter incorporates a weighting function, simulating the frequency response of the eye-brain and lamp and peaks at a frequency of 8.8 Hz. The decomposition of the IEC weighting curve of the eye-brain lamp model is obtained by 1) eye-brain response to flicker, 2) the lamps response to voltage disturbance. The transfer function for the weighting filter is defined by ref. [15] and consists of these two parts:

$$F_W(s) = [Eye - brain\ response\ to\ flicker] \cdot [Lamp\ response\ to\ flicker] \tag{2.5}$$

$$F_W(s) = \frac{k\omega_1 s}{s^2+2\lambda s+\omega_1^2} \cdot \frac{1+\frac{s}{\omega_2}}{\left(1+\frac{s}{\omega_3}\right)\left(1+\frac{s}{\omega_4}\right)} \tag{2.6}$$

Whereby, the variables are listed in table 8 of ref. [15].

For illustrative and validation purposes, figure 2-2 plots the frequency response of the weighting filter for both 50 Hz and 60 Hz systems. As expected, the filter response peaks at 8.8Hz.

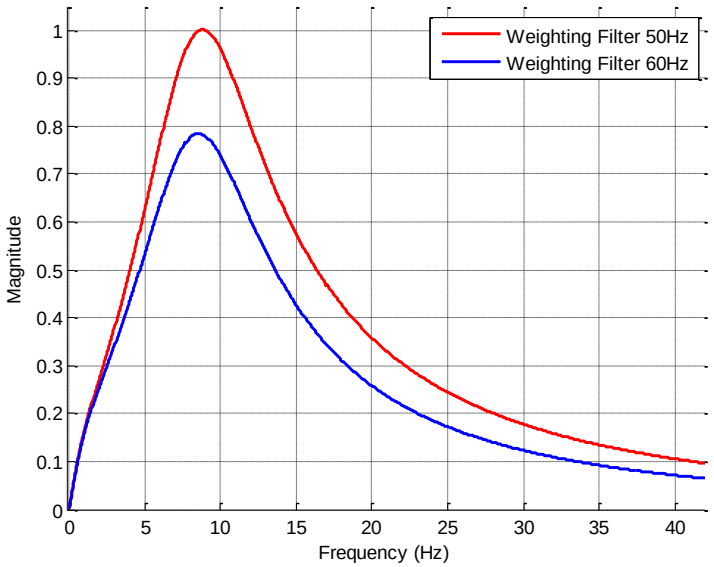

Figure 2-2 Weighting filter frequency response

Block 4: Squaring & smoothing

Block 4 is composed of a squaring multiplier, first order low-pass filter and a calibration gain and outputs the IFL. In the first two sub-blocks, the flicker signal is squared and then is filtered to simulate the memory effect in the brain using the first order low-pass filter with following transfer function:

$$F_{LP}(s) = \frac{s}{1+s\cdot\tau_{LP}} \tag{2.7}$$

Whereby τ_{LP} is the time constant of the brains memory effect to light stimulus and is equal to $\tau_{LP} = 300\ ms$.

Once again, for illustrative and validation purposes, figure 2-3 plots the frequency responses of all the filters incorporated in the implementation of the flickermeter for 60 Hz systems.

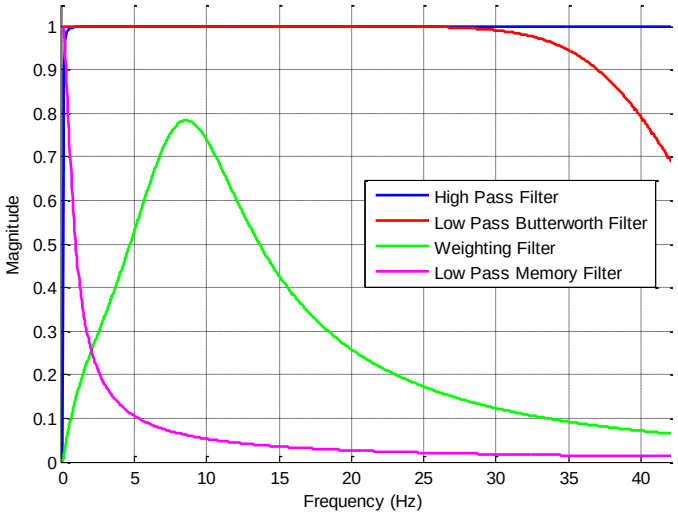

Figure 2-3 Filter frequency responses

The third sub-block takes the filtered signal and then normalizes it. This is done by using a calibration gain factor to give a maximum value of $IFL = 1$, for a given modulation frequency and depth given by ref. [15]. The Flickermeter standard specifically indicates to calibrate the flicker instrument using a sine wave, modulated input signal with fundamental frequency $f = 60\ Hz$, a modulation frequency $f_{mod} = 8.8\ Hz$ and a modulation depth $\frac{\Delta V}{V} = 0.323\%$.

Figure 2-4 illustrates the IFL with respect to time for the above mentioned case. As was previously noted, there is an initial filter transient at the start of the simulation due to the long time constants of the filters. Thus, part of the voltage signal, which includes the Flickermeter's filter start transients must be removed in order to yield correct measurements. The specified warm up time determined graphically is 15 seconds.

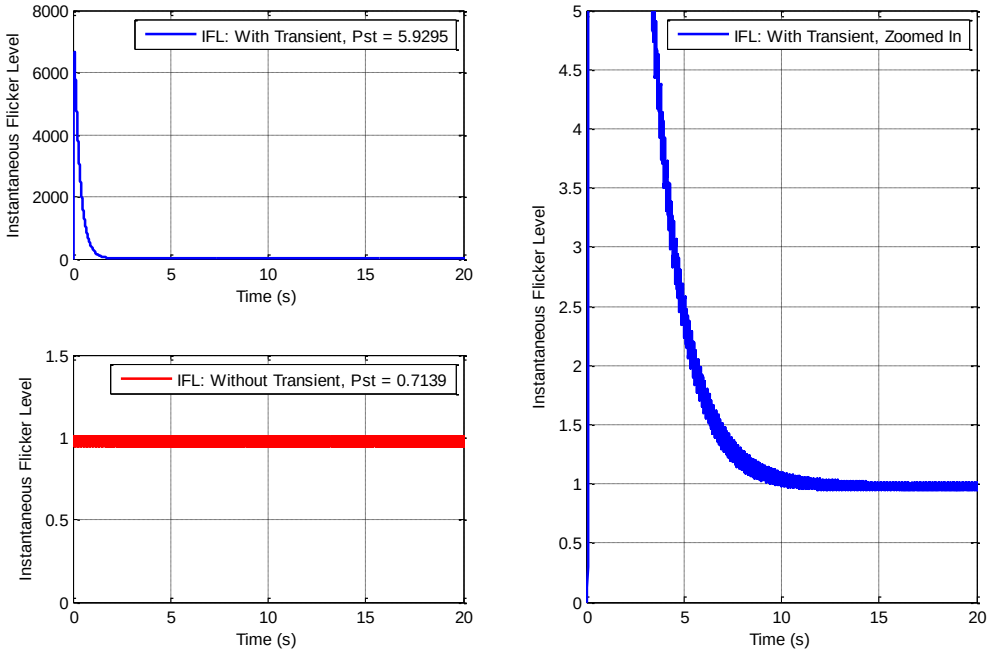

Figure 2-4 Calibration of flicker instrument & removal of filter start transient

Block 5: Statistical analysis

The function of Block 5 is to evaluate the annoyance to the human eye produced by fluctuations in luminous flux. This block calculates P_{st} by performing a statistical classification of IFL signal over 10 minutes. First, the IFL is classified within an adequate number of classes as defined by [15]. From this classification, the Cumulative Distribution Function (CDF) of the IFL is calculated. The process is visually illustrated in figure 2-5 [17].

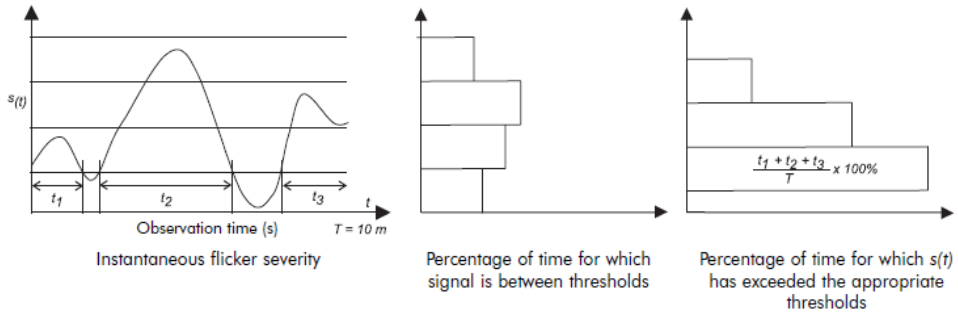

Figure 2-5 The process of CDF evaluation [17]

Finally, the short-term flicker severity index P_{st} is calculated from the P_X percentiles as follows:

$$P_{st} = \sqrt{0.0314P_{0.1s} + 0.0525P_{1s} + 0.0657P_{3s} + 0.28P_{10s} + 0.08P_{50s}} \tag{2.8}$$

Whereby P_x is the *x%* percentile (i.e. the flicker level which exceeded for *x%* of the time), calculated from the P_{st} duration curve. The subscript "s" denotes the smoothed values, obtained by averaging the neighboring values of the duration curve. These are obtained from the following equations:

$$\left.\begin{aligned} P_{50s} &= \frac{P_{30}+P_{50}+P_{80}}{3} \\ P_{10s} &= \frac{P_6+P_8+P_{10}+P_{13}+P_{17}}{5} \\ P_{3s} &= \frac{P_{2.2}+P_3+P_4}{3} \\ P_{1s} &= \frac{P_{0.7}+P_1+P_{1.5}}{3} \end{aligned}\right\} \tag{2.9}$$

Although, only P_{st} levels will be used for this research, the long term severity index P_{lt} consisting of a combination of 12 P_{st} measurements is calculated as follows:

$$P_{lt} = \sqrt[3]{\frac{\sum_{i=1}^{12} P_{sti}^3}{12}} \tag{2.10}$$

Whereby, P_{sti} are consecutive P_{st} readings.

2.2.4 Compliance testing of the IEC Flickermeter instrument

Section 6.1 of the IEC 61000-4-15 standard details the required performance tests to be completed such that the newly constructed flickermeter can claim compliance. This entails conducting a benchmark test to verify if, 1) the overall input/output response up to block 4 is correct and 2) the statistical analysis implemented in block 5 is correct.

2.2.4.1 Compliance test: Block 4

To carry out the compliance test, two tables (respectively sinusoidal and rectangular amplitude modulation) are reported in the standard with nominal values, at given frequencies of $\frac{\Delta V}{V}\%$ which should give a maximum $IFL = 1$. The flickermeter instrument complies with the standard if the modulating signals, as specified by the standard, produce a peak IFL of $1.00 \pm 5\%$. As can be visually seen by figure 2-6, the developed flicker instrument complies with both tables 1 and 2 of ref. [15].

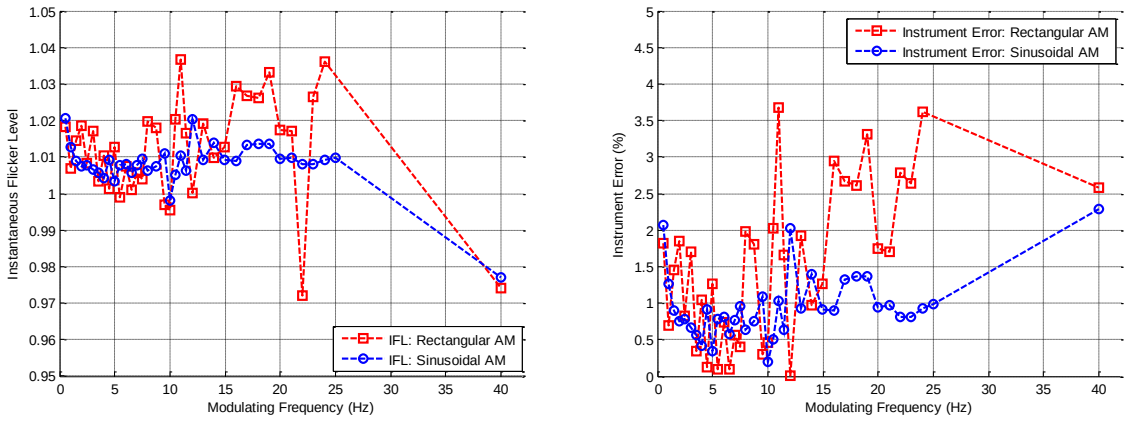

Figure 2-6 IFL vs. modulation frequency (left), Instrument error vs. modulation frequency (right)

2.2.4.2 Compliance test: Block 5

To carry out the compliance test for block 5, table 5 specifies nominal values of a rectangular amplitude modulated signal, at given repetition rates of $\frac{\Delta V}{V}\%$ which should yield $P_{st} = 1$. The flickermeter instrument complies with the standard if the all specified modulating signal yield $P_{st} = 1 \pm 5\%$. As illustrated in figure 2-7, the developed flicker instrument complies with table 5 of ref. [15].

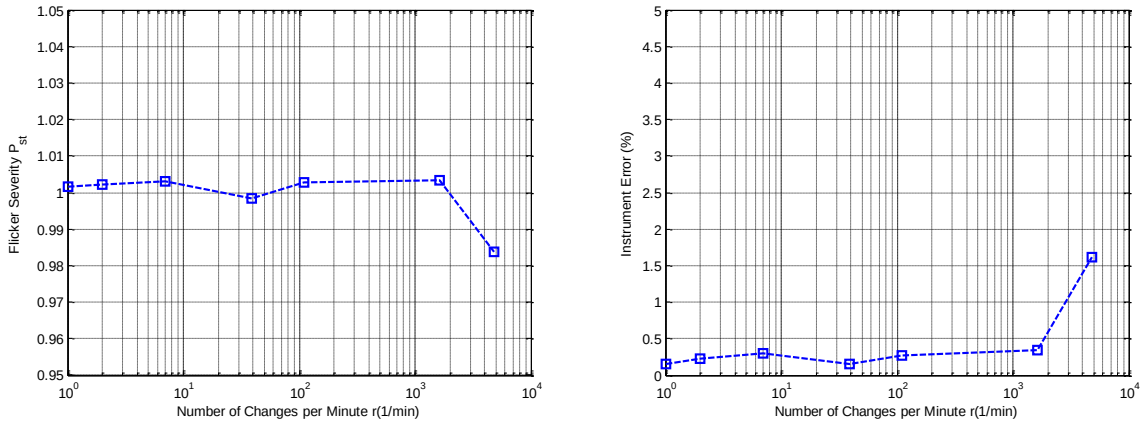

Figure 2-7 Pst vs. repetition rate (left), Instrument error vs. repetition rate (right)

2.3 Flicker measurement guidelines for wind generators

The IEC 61400-21 standard [47] was developed for the testing and the assessment of power quality characteristics of grid-connected WTGs in a consistent and accurate way [77]. To compare WTGs of different types, it defines a list of parameters to be measured and reported. Of interest, is the section detailing flicker in continuous operation and due to switching operations. IEC 61400-21 also refers to other IEC standards, for example, flicker measurements have to take into account IEC 61000-4-15.

The procedure to evaluate the flicker emissions produced by a WTG during continuous operation is two-part, consisting of a "testing stage" for a single specific WTG and followed by an "assessment stage" on a particular site. During the WTGs testing stage, flicker coefficients $c(\psi_k, v_a)$ are obtained for four grid impedance angles $\psi_k = (30°, 50°, 70° \text{ and } 85°)$ and four mean wind speeds $v_a = (6, 7.5, 8.5, \text{and } 10)\frac{m}{s}$. Once the look-up table of flicker coefficients $c(\psi_k, v_a)$ from the WTG under test has been completed, one can assess the flicker emission from a WTG of the same type, installed at a specific site, described by short circuit power S_k, ψ_k, and v_a. The flicker emissions can then be assessed with eqn. (2.11), by linear interpolation of the flicker look-up table, given the site characteristics ψ_k and v_a.

$$P_{st} = P_{lt} = c(\psi_k, v_a)\frac{S_n}{S_k} \tag{2.11}$$

Whereby, S_n represents the rated apparent power of the wind turbine.

Moreover, the above mentioned IEC standard defines a method for assessing the flicker emissions from a number of wind turbines based on the measurements on a single wind turbine. The flicker emission from a wind farm can be assessed as follows:

$$P_{st\Sigma} = \frac{1}{S_k}\sqrt{\sum_{i=1}^{N_{wt}}\left(c_i(\psi_k, v_a)S_{n,i}\right)^2} \tag{2.12}$$

Whereby, N_{wt} corresponds to the total number of wind turbines at the PCC and $S_{n,i}$ corresponds to the rated apparent power of the individual wind turbine. If all wind turbines are identical, eqn. (2.12) equates to:

$$P_{st\Sigma} = P_{st}\sqrt{N_{wt}} \tag{2.13}$$

2.4 Summation law of flicker originating from multiple sources

IEC 61000-3-7 [48] provides rules of thumb to consider the summation effect of flicker emissions produced by multiple flicker sources. The P_{st} resulting from several fluctuating installations operating simultaneously can be obtained from the following expression:

$$P_{st} = \sqrt[\alpha]{\sum_i P_{st_i}^{\alpha}} \tag{2.13}$$

Whereby P_{st_i} are the individual flicker levels emitted by each of the flicker sources. The value of the coefficient α depends upon how the fluctuating load or generator is characterized. Generally α is classed into the following four categories:

- α = 4: This value is used uniquely for the summation of flicker when coincident fluctuations are very unlikely.
- α = 3: This value used is when the probability of coincident voltage fluctuations are small. The majority of the studies combining the effect of unrelated flicker sources belong to this category.
- α = 2: This value is used when there is coincident voltage fluctuations are likely to occur.
- α = 1: This value must be used when there is a high probability of coincident voltage fluctuations.

2.5 Compatibility, planning and emission levels for flicker

The IEC 61000-4-7 standard defines the assessment of flicker emission limits for the connection of fluctuating installations to Medium Voltage (MV), High Voltage (HV) and Extra High Voltage (EHV) networks. The standard uses two reference values, notably the Planning Level (PL) and Compatibility Level (CL) to coordinate the flicker emissions produced by fluctuating network devices and to ensure that EMC of the power system is preserved. Figure 2-9, taken from ref. [48], illustrates the relation between the PLs and CLs. The planning levels are typically set lower than the compatibility levels and are used as reference values for setting flicker limits at different voltage levels.

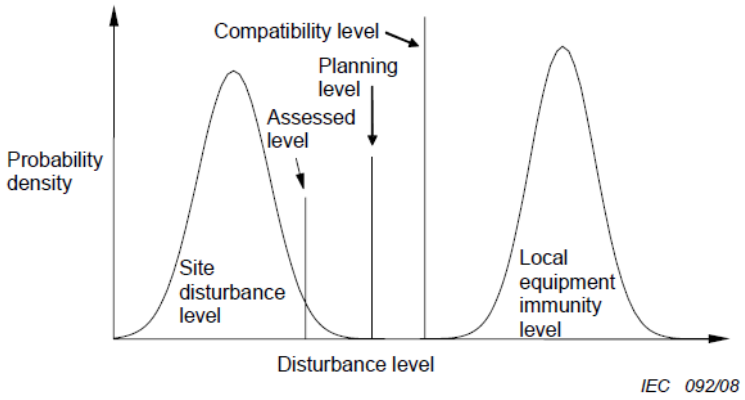

Figure 2-8 Electromagnetic compatibility [56]

The IEC 61000-3-7 standard gives both PLs, the total flicker level which must not be exceeded and emission levels, the flicker level from an individual installation which must not be exceeded. The recommended values specified by the standard are given in table 2-1 [56].

Flicker severity factor	Planning levels		Emmission levels
	MV	HV	MV and HV
P_{st}	0.9	0.8	0.35
P_{lt}	0.7	0.6	0.25

Table 2-1 Flicker planning and emissions levels [57]

However, the specified emissions limits may hinder the installation of a large distribution-connected wind farm and may be viewed as overly restrictive. In fact, the maximum theoretical flicker level that a distribution-connected wind farm can produce while complying with PLs and preserving EMC in the system is defined by eqn. (2.14) [56]. Although this theoretical emission limit may be in violation of applicable grid codes and standards, EMC of the system will be preserved and flicker related complaints are not likely to occur.

$$P_{st\ max} = \sqrt[\alpha]{L_{Pst,MV}^{\alpha} - T_{Pst,UM}^{\alpha} * L_{Pst,US}^{\alpha} - B_{Pst,MV}^{\alpha}} \quad (2.14)$$

Whereby:

- $P_{st\ max}$: is the theoretical maximum flicker contribution produced by the wind farm that will preserve EMC of the system
- $L_{Pst,MV}$ is the planning level for flicker in the MV system
- $L_{Pst,US}$: is the planning level for flicker in the upstream system
- $T_{Pst,UM}$: is the transfer coefficient of flicker from the upstream system to the MV system and generally taken as 0.9
- $B_{Pst,MV}^{\alpha}$: is the background flicker produced by other installations on the MV feeder
- α: is a summation law exponent and generally taken as 3

On a similar note, the French grid code enforces IEC 61000-3-7 for Distributed Generators (DG) up to 5 MW, but allocates a linear increase in flicker emissions to the fluctuating installation, with an upper limit of $P_{st} = 0.44$. The flicker emission limit as a function of the DGs power is shown in figure 2-9 [56]. Thus, the re-allocation of emission limits to favor the installation of a wind farm is possible and is subject to utility policy and strategy.

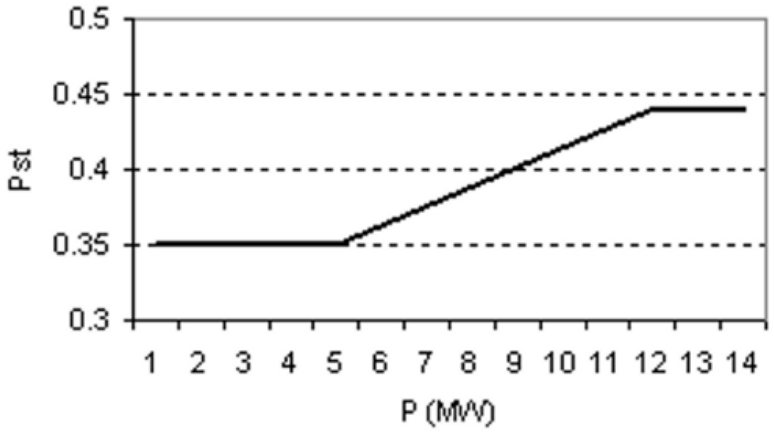

Figure 2-9 Flicker emission limit for DG connection [56]

Chapter 3:

Flicker Oriented Modeling

3.1 Overview

The goal of this chapter is to detail the level of modeling required to conduct a flicker study. This entails assuring that factors which influence flicker are incorporated in the modeling such that emissions are well quantified. Both, the modeling requirements of the wind speed model as well as the wind turbine model are discussed in this chapter.

3.2 Wind speed modeling

3.2.1 Description of the equivalent wind speed model

The modeling of the wind resource is imperative in order to simulate and obtain representative power fluctuations produced by a wind farm. Thus, an appropriate representation of the wind resource must be used. Typically, when performing large time scale studies in the range of days, weeks and years, the wind is normally modeled to fit a Weibull or Rayleigh (simplification of Weibull) distribution in order to take into account the long term seasonal components of the wind [57]. However, when performing studies in the range of minutes, such as in the case of a flicker study, long term components are irrelevant and only short term wind speed fluctuations are of particular interest. These short term fluctuations are typically described by a Power Spectral Density (PSD). Both, Von Karmon and Kaimal spectrum models, refer to eqn. (3.1) are commonly used to simulate the stochastic behavior of the wind [58], which are then superimposed onto a mean wind speed assumed constant on the scale of the 10 minute flicker measurement timeframe.

$$S_{t,Kaimal}(f) = \frac{\sigma^2 L}{v\left(1+6f\frac{L}{v}\right)^{\frac{5}{3}}} \qquad S_{t,Von\ Karmon}(f) = \frac{4\sigma^2 L}{v\left(1+70.8\left(f\frac{L}{v}\right)^2\right)^{\frac{5}{3}}} \tag{3.1}$$

Flicker emissions produced by a wind farm can be divided into two categories, flicker originating from: 1) stochastic variations of the local wind speed profile and 2) aerodynamic deterministic blade passing effects (i.e. tower shadow, wind shear). Thus, for a flicker study to be comprehensive, both components must be incorporated in the equivalent wind speed model.

The equivalent wind speed that will be fed to each individual wind turbine has three components. The first v_{eq0}, the equivalent hub height wind speed, the second $v_{eq_{ws}}$, the equivalent wind shear component, and the third $v_{eq_{ts}}$, equivalent tower shadow component. The first component v_{eq0} is considered to reflect the stocastic variations in the wind while the second and third components incorporate the deterministic aerodynamic blade passing phenomenon. Thus, the equivalent wind speed as a function of time t and blade position ϕ, can be written as follows:

$$v_{eq}(t,\phi) = v_{eq0}(t) + v_{eq_{ws}}(t,\phi) + v_{eq_{ts}}(t,\phi) \tag{3.2}$$

3.2.2 Description of the stochastic component

The equivalent stochastic wind speed $v_{eq0}(t)$ at the hub height of the turbine is considered to be of the form:

$$v_{eq0}(t) = v_{mean} + v_t(t) \tag{3.3}$$

Whereby v_{mean} represents the mean wind speed component and $v_t(t)$ represents the turbulence component. For the purpose of flicker studies, the site specific wind speed profile is defined for a fairly short period of 600 seconds, thus, the corresponding turbulence component is computed based on the assumption that v_{mean} remains constant. The frequencies of the turbulence component $v_t(t)$ corresponding to realistic variations in the wind are generated using the Kaimal shaping filter, refer to eqn. (3.4).

$$H_F(s) = \frac{K_F}{\left(1+s\frac{L}{v_{mean}}\right)^{\frac{5}{3}}} \tag{3.4}$$

The Kaimal shaping filter's coefficients depend on v_{mean}, and the turbulence length scale L. The gain factor K_F is adjusted such that the output of the filter, referred to as the colored noise, has a standard deviation equal to one.

3.2.3 Implementation of the stochastic component

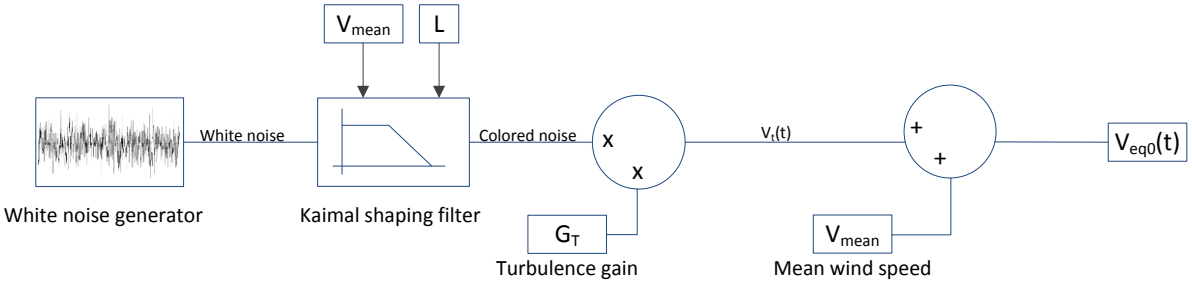

Figure 3-1 Implementation of the stochastic component

Figure 3-1 illustrates the Simulink® implementation for the generation of the equivalent wind speed $v_{eq0}(t)$ at the hub height of the turbine, similar to [57]-[61]. The algorithm for stochastic wind speed generation is as follows:

1. White noise is generated with a sampling period of 20Hz.
2. White noise is passed through a low pass Kaimal shaping filter and outputs a colored noise representing the Kaimal PSD.
3. Colored noise is scaled to correspond to the desired turbulence intensity I_n.
4. Equivalent wind speed $v_{eq0}(t)$ is computed via the addition of the mean wind speed component v_{mean} and turbulence component $v_t(t)$.
5. Sampling frequency converter is used to interface with other modules (not shown in figure 3-1).

Figure 3-2 illustrates a sample wind speed profile generated with a mean wind speed of $13m/s$ and turbulence intensity of 15%.

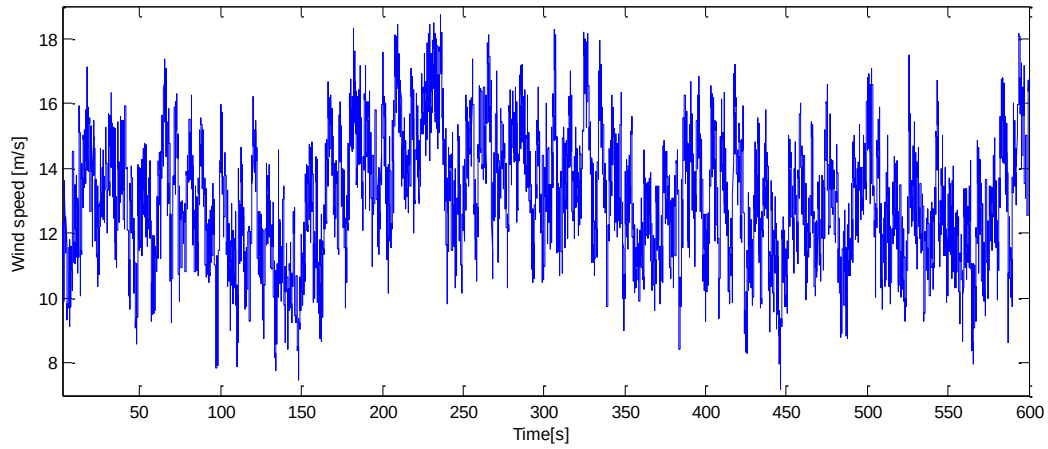

Figure 3-2 Stochastic wind speed profile

3.2.4 Description of the deterministic component

3.2.4.1 Description of the tower shadow & wind shear component

The inclusion of blade passing effects (i.e. wind shear and tower shadow) as part of the equivalent wind speed model in order to represent the periodic oscillations of turbine torque is essential. The blade passing effect model, as specified in [29],[30], incorporates the components corresponding to: 1) torque variations due to wind shear and 2) torque variations due to tower shadow. The equivalent deterministic wind speed components $v_{eq_{ts}}(t,\phi)$ and $v_{eq_{ws}}(t,\phi)$, mainly influenced by the mechnical structure of the turbine are considered to be of the form:

$$\left.\begin{aligned} v_{eq_{ts}}(t,\phi) &= \frac{m v_{eq0}(t)}{3R^2}\sum_{b=1}^{3}\left[\frac{a^2}{\sin^2\phi}\ln\left(\frac{R^2 sin^2\phi}{x^2}+1\right)-\frac{2a^2R^2}{R^2\sin^2\phi+x^2}\right] \\ v_{eq_{ws}}(t,\phi) &= v_{eq0}(t)\left[\frac{\alpha(\alpha-1)}{8}\left(\frac{R}{H}\right)^2+\frac{\alpha(\alpha-1)(\alpha-2)}{60}\left(\frac{R}{H}\right)^3\cos(3\phi)\right] \\ m &= 1+\frac{\alpha(\alpha-1)R^2}{8H^2} \end{aligned}\right\} \quad (3.5)$$

Whereby R represents the blade radius, H the hub height, a the tower radius, x the blade origin from the tower midline and α the wind shear component.

3.2.5 Implementation of the deterministic component

Figure 3-3 illustrates the Simulink® implementation the wind shear and tower shadow module. The algorithm to compute the contribution of wind shear and tower shadow components is as follows:

1. Convert the rotational speed of the turbine shaft from pu to rad/s.
2. Integrate the rotational speed to find the relative blade position.
3. Compute the wind shear and tower shadow component in accordance with the above mentioned functions given the blade position and mechanical turbine parameters.

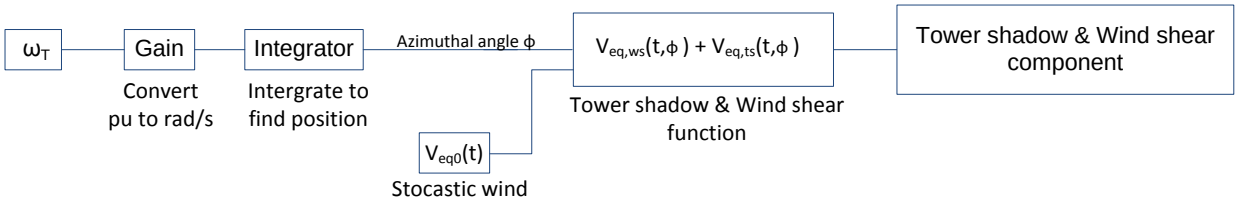

Figure 3-3 Implementation of the deterministic components

As illustrated in figure 3-4, the wind shear and tower shadow components oscillate 3 times per cycle. Thus, every 120° there is a drop in the relative wind speed. Note that the tower shadow component is much more pronounced that the negligibly small wind shear component.

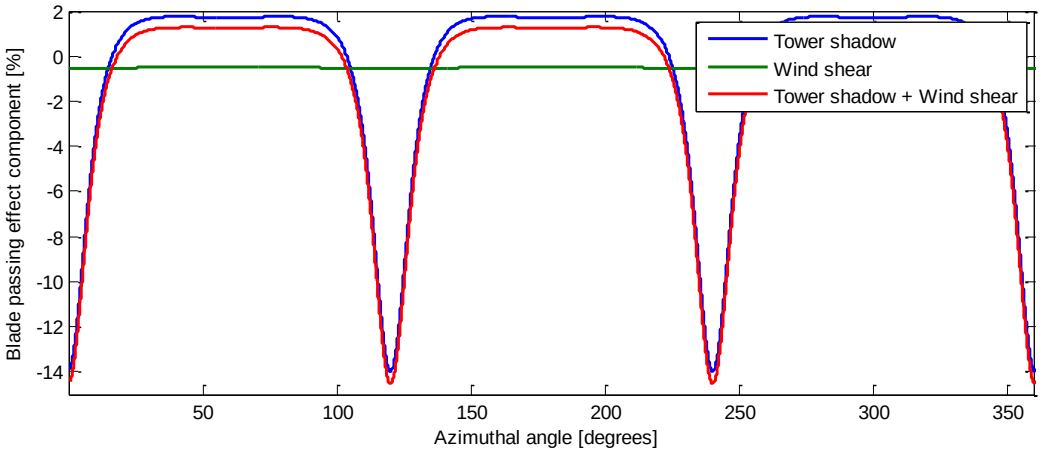

Figure 3-4 Blade passing effect components

Figure 3-5 demonstrates the effective torque and power oscillations that are resultant from a dip in wind speed 3 times per turbine shaft rotation given a fixed wind speed of 12.2$\frac{m}{s}$. It is clear that this module produces oscillations at approximately 1.2 Hz which is the equivalent 3p frequency of this turbine. On another note, although the oscillations are pronounced in the turbine torque, the converter control and large machine inertia greatly damps the resulting fluctuations in the output power of the turbine.

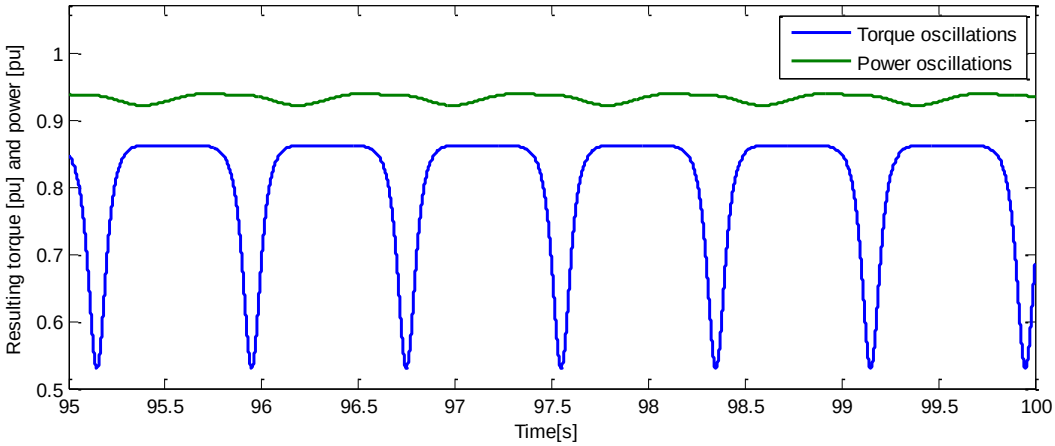

Figure 3-5 Resulting torque and power fluctuations

Figure 3-6 illustrates first the equivalent stochastic wind speed $v_{eq0}(t)$ at the hub height of the turbine, secondly the the equivalent wind speed model $v_{eq}(t, \phi)$ with deterministic blade passing effects included and thirdly a comparision of the power spectral densities of the wind with and without the inclusion of blade passing effects. The power spectral density of the equivalent wind speed model clearly demontrates the addition of the 3p, 6p and 9p components to the wind.

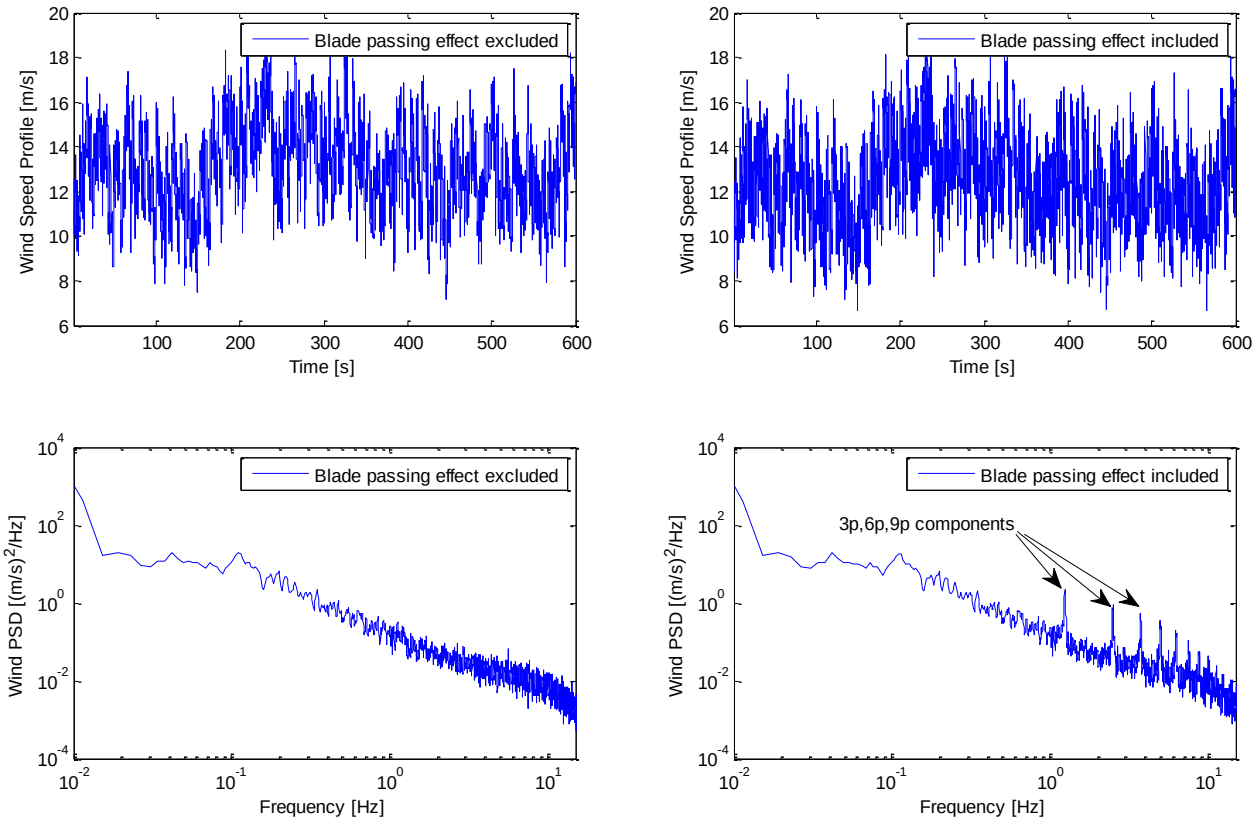

Figure 3-6 Time and frequency domain representation of the deterministic component

3.3 Wind turbine modeling

3.3.1 Overview

This section of chapter 3 details the main components and controls of the wind turbine model, notably the aerodynamic model, mechanical model, generator model, converter model, speed and pitch controller. The specifications of the WTG modeled are listed in the Appendix.

3.3.2 Aerodynamic model

The mechanical power of the wind turbine is obtained from the energy drawn from the wind and can be expressed as follows:

$$P_m = \frac{1}{2}\rho A v^3 C_P(\lambda, \beta) \tag{3.6}$$

Whereby P_m is the mechanical power extracted from the wind, ρ is the air density in $\frac{kg}{m^3}$, A is the area swept by the rotor blades in m^2, v is the wind speed in $\frac{m}{s}$, C_P is the power coefficient, β is the blade pitch angle and λ is the tip-speed ratio. The tip-speed ratio λ is defined by:

$$\lambda = \frac{\omega_T R}{v} \tag{3.7}$$

Whereby ω_T is the rotational speed of the wind turbine $\left(\frac{rad}{s}\right)$ and R is the rotor radius (m). The power coefficient C_P is a highly nonlinear function and depends on the aerodynamic characteristics of the wind turbine as well as the turbine rotational speed and the wind speed. $C_P(\lambda, \beta)$ is defined as follows:

$$C_P(\lambda, \beta) = c_1\left(\frac{c_2}{\lambda_i} - c_3\beta - c_4\right)e^{-\frac{c_5}{\lambda_i}} + c_6\lambda \tag{3.8}$$

$$\frac{1}{\lambda_i} = \frac{1}{\lambda + c_7\beta} - \frac{c_8}{\beta^3 + 1} \tag{3.9}$$

Figures 3-7 and 3-8 illustrate the C_p curves associated with the aerodynamic model. With reference to figure 3-7, one notes that the C_p reaches it maximum value of 0.5 at a λ =

9.9495. With reference to figure 3-8, the λ^* occurs at a wind speed of $11\frac{m}{s}$, with β kept constant at its optimal value of $0°$.

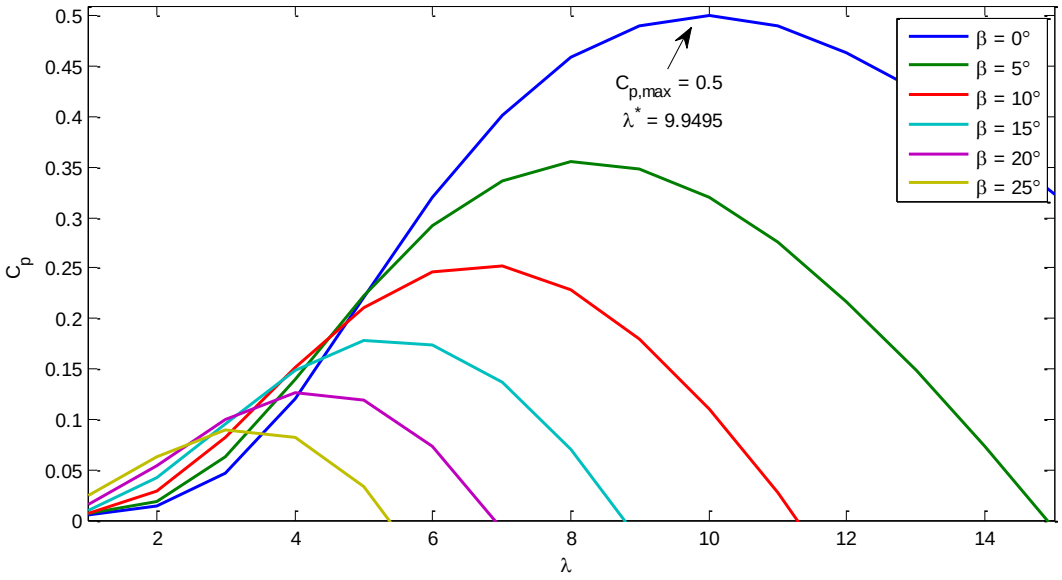

Figure 3-7 C_p vs. λ curves

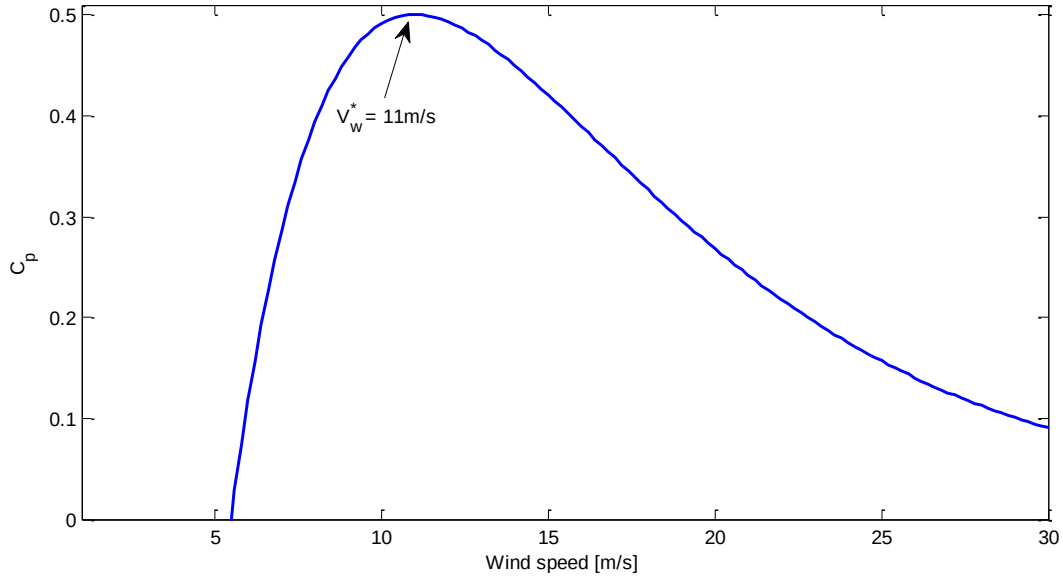

Figure 3-8 C_p vs. v curve

To conclude, the aerodynamic block implemented, shown in figure 3-9, consists of four main modules:

1. Tip speed ratio λ computation
2. Power coefficient $Cp(\lambda, \beta)$ computation
3. Mechanical power computation
4. Aerodynamic torque computation

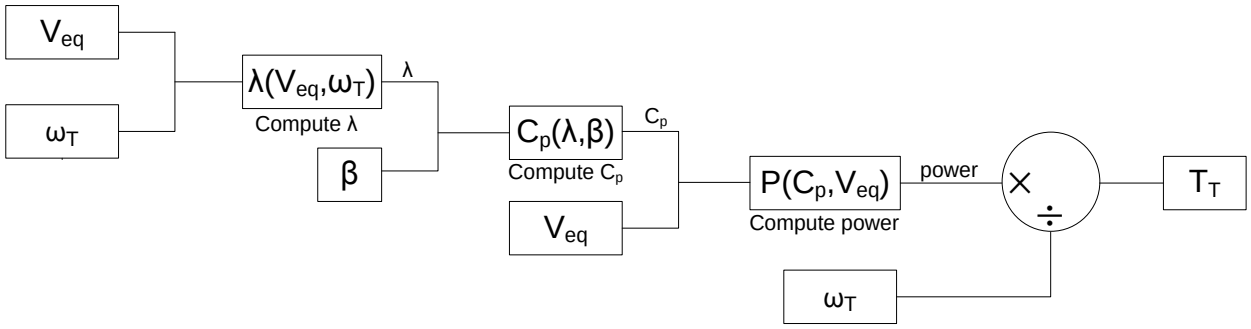

Figure 3-9 Aerodynamic model

3.3.3 Mechanical Model

The mechanical model illustrated in figure 3-10 essentially consists of a 2-mass model representing the turbine drive train system in terms of two inertias. The two masses correspond to the large turbine inertia constant H_T, representing the turbine blades and small inertia constant H_G representing the generator rotor. These two masses are linked by the shaft modeled as a spring with stiffness K_{shaft} and damper with mutual damping D_m [62].

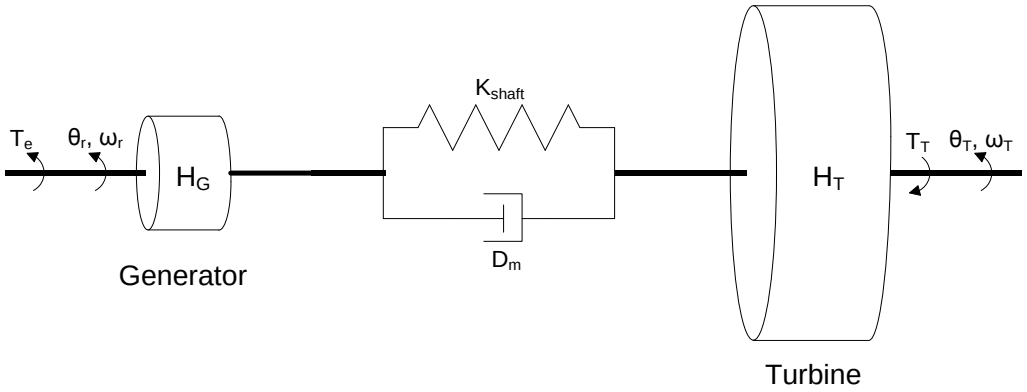

Figure 3-10 Mechanical model

The dynamic equations can be written as follows:

$$\left.\begin{aligned} 2H_T \frac{d\omega_T}{dt} &= T_T - K_{shaft}(\theta_T - \theta_r) - D_m(\omega_T - \omega_r) \\ 2H_G \frac{d\omega_r}{dt} &= -T_e - K_{shaft}(\theta_r - \theta_T) - D_m(\omega_r - \omega_T) \end{aligned}\right\} \quad (3.10)$$

Whereby, T_T is the turbine torque, T_e is the generator torque, ω_T & ω_r are the turbine and generator rotor speed respectively and θ_T & θ_r are the turbine and generator rotor angle respectively.

With respect to flicker, the mechanical dynamics of the wind turbine filter out the high frequency power variations, which lead to flicker attenuation. As the inertia constants increase given a fixed turbine rating, the cut-off frequency of the mechanical low pass filter will decrease leading to a reduction in flicker emissions.

3.3.4 Generator Model

The basic equations governing the dynamic model of the DFIG machine behavior are taken from [76], listed below in the dq0 frame with subscripts d and q denoting the d-axis and q-axis vector components and subscripts r and s denoting the rotor and stator quantities. Please note that the rotor quantities are referred to the stator side.

$$\left.\begin{aligned} V_{qs} &= R_s i_{qs} + \frac{d}{dt}\psi_{qs} + \omega_s \psi_{ds} \\ V_{ds} &= R_s i_{ds} + \frac{d}{dt}\psi_{ds} - \omega_s \psi_{qs} \\ V'_{qr} &= R'_r i'_{qr} + \frac{d}{dt}\psi'_{qr} + (\omega_s - \omega_r)\psi'_{dr} \\ V'_{dr} &= R'_r i'_{dr} + \frac{d}{dt}\psi'_{dr} - (\omega_s - \omega_r)\psi'_{qr} \end{aligned}\right\} \quad (3.11)$$

The stator and rotor fluxes can be expressed as:

$$\left.\begin{aligned} \psi_{ds} &= L_s i_{ds} + L_m i'_{dr} \\ \psi_{qs} &= L_s i_{qs} + L_m i'_{qr} \\ \psi'_{dr} &= L'_r i'_{dr} + L_m i_{ds} \\ \psi'_{qs} &= L'_r\, i'_{qr} + L_m i_{qs} \end{aligned}\right\} \quad (3.12)$$

Whereby the total stator and rotor inductance are calculated as follows:

$$\left.\begin{aligned} L_s &= L_{ls} + L_m \\ L'_r &= L'_{lr} + L_m \end{aligned}\right\} \quad (3.13)$$

Finally the electromagnetic torque can be calculated as follows:

$$T_e = -1.5p(\psi_{ds} i_{qs} - \psi_{qs} i_{ds}) \tag{3.14}$$

3.3.5 Converter model

Flicker studies focus on low frequency voltage fluctuations in the range of 0.5-42Hz. There is no interest in harmonic content nor high frequency voltage fluctuations. Hence, the average model is a great method to model the PEC compared to a detailed Insolated Gate Bipolar Transistor (IGBT) switch model and is used with the intent to significantly improve computational speed performance.

In the average model, the IGBT converter switches are replaced by controlled voltage sources. These voltage sources are controlled by the modulating voltage references typically fed to the Pulse Width Modulation (PWM) converters. The average model is built on the energy conservation principle between the DC and the AC side [63]. The DC capacitor voltage variations are also reflected in this converter model, since the instantaneous power is kept equal on both sides. The DC capacitor power can be expressed as:

$$P_{dc} = P_g - P_r \tag{3.15}$$

Whereby P_{dc} represents the DC capacitor power, P_g represents the Grid Side Converter (GSC) power and P_r represents the RSC power. The DC capacitor current can be expressed as:

$$I_{dc} = \frac{P_{dc}}{V_{dc}} \tag{3.16}$$

Whereby V_{dc} is the capacitor voltage. The capacitor voltage is recursively computed based on the capacitor current as follows:

$$V_{dc} = \frac{1}{C} \int I_{dc} \tag{3.17}$$

Whereby C is the capacitance of the DC bus capacitor. Thus, according to eqn. (3.15) to eqn. (3.17), the DC bus voltage variations will be represented based on current variations corresponding to the differences in power between both AC sides. Finally, in order to regulate the DC bus capacitor voltage, the GSC output power will be controlled.

3.3.6 Associated MPPT controls

3.3.6.1 Speed Controller (power optimization)

The WTG speed is controlled in order to follow a pre-defined power-speed characteristic curve, named the Maximum Power Point Tracking (MPPT) curve. The MTTP curve is illustrated in figure 3-11.

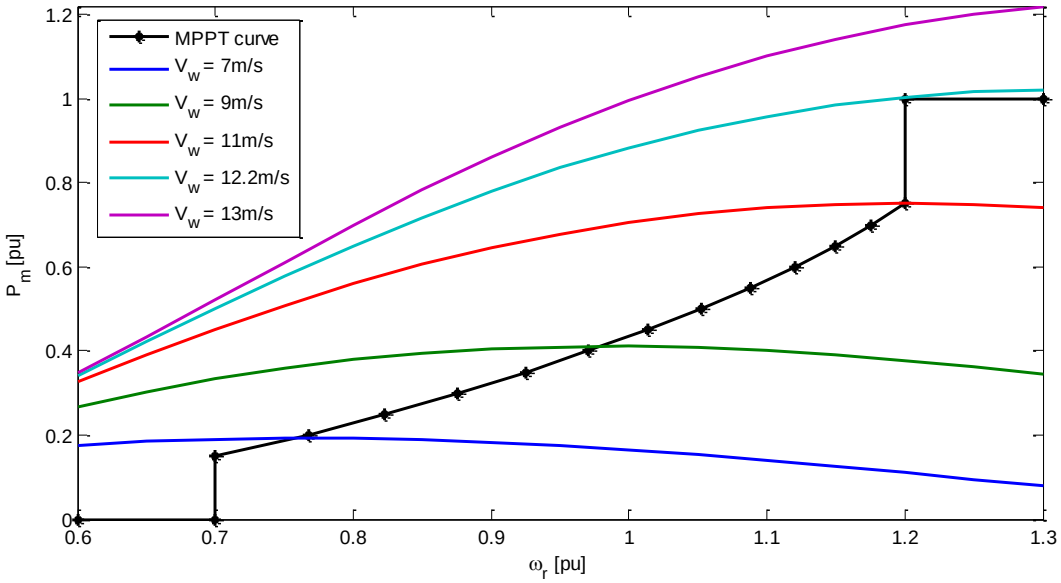

Figure 3-11 Maximum power point tracking curve

Figure 3-12 illustrates the incorporated speed controller. A power measurement is used as the input of the tracking curve to set the rotor speed. Optimal tracking will occur up to wind speed of $11\frac{m}{s}$ and a measured power of 0.75pu. For wind speeds and power measurements above this level, the rotor speed will be set to 1.2pu. The saturation block ensures that the rotor speed reference stays between 0.7pu and 1.2pu. The $\omega_{r,error}$ which is defined as the difference between the measured and reference speed is then sent to a Proportional Integral (PI) controller to set the d-axis rotor current.

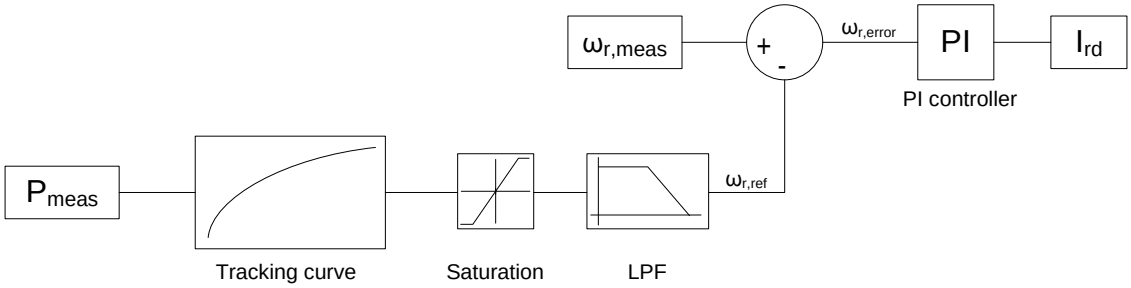

Figure 3-12 Speed controller

3.3.6.2 Pitch controller (power limitation)

Wind turbines are also equipped with a pitch controller in order to protect itself in high wind periods. Figure 3-13 illustrates the pitch controller implemented. This pitch controller utilizes the difference between the measured rotational speed of the machine $\omega_{r,meas}$ and a reference value $\omega_{r,ref}$ of 1.2pu to set the pitching of the blades. One can note that the pitching of the blades will only occur once the reference speed of 1.2pu has been exceeded. Cases where $\omega_{r,meas} \leq 1.2pu$, the pitch angle β is set to its optimal value of 0°. The dynamics of the pitch actuator is modelled by three blocks, the rate limiter, which limits the rate of change of the pitch angle to $\pm 10°/s$, the saturation block limits the pitch angle from 0° to 27° and the low pass filter which represents the time constant of the pitch mechanism.

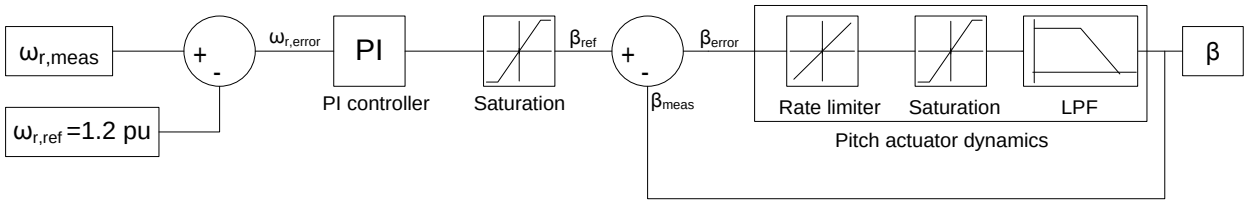

Figure 3-13 Pitch controller

Chapter 4:

Quantification of DFIG Flicker Emissions & Potential Mitigation Techniques

4.1 General methodology and approach

In order to develop guidelines and a rule of thumb for the selection of a distributed wind installation with respect to flicker, a parametric study will be conducted, in accordance to factors that influence flicker, as detailed in chapter 1, in order determine and quantify their level of severity. Flicker studies tend to be computationally expensive, due to the 10 minute voltage sampling period and 50 μs simulation time step required for a WTG flicker measurement. Thus, the parameters which influence flicker will only be tested within a logical and practical range pertaining to distribution networks. Based upon these studies, a subset of parameters were deemed to greatly influence voltage flicker will further studied in order to help formulate a generalized rule of thumb. In addition reactive power based flicker mitigation techniques mentioned in chapter 1, will be implemented to get a measure of their flicker reduction performance and associated reactive power demand.

For the purpose of simplicity and universal applicability, these studies will be conducted for one 2 MW DFIG wind turbine, on a test network, represented by a Thevenin equivalent impedance, as described in the next section.

4.2 Test network topology

A test network, as illustrated in figure 4-1, has been used for the parametric study and is commonly used in the literature for voltage quality studies [22]-[24]. The Thevenin equivalent representation is an appropriate benchmark network when no specific distribution feeder is provided and generalized conclusions are sought [24]. The main components of this test network are:

- Grid (vary voltage level)
- Equivalent Thevenin network impedance (vary SCC & X/R ratio)
- Wind speed profile generator (vary mean wind speed & turbulence intensity)
- MV/LV distribution transformer
- DFIG wind turbine

The goal of the test network is to provide the flexibility and ease to change key parameters for the assessment and quantification of flicker emissions. For instance, the evaluation of flicker emissions under different system conditions such as short circuit capacity and X/R ratio and wind variability. The base case parameters are given in Table 4-1.

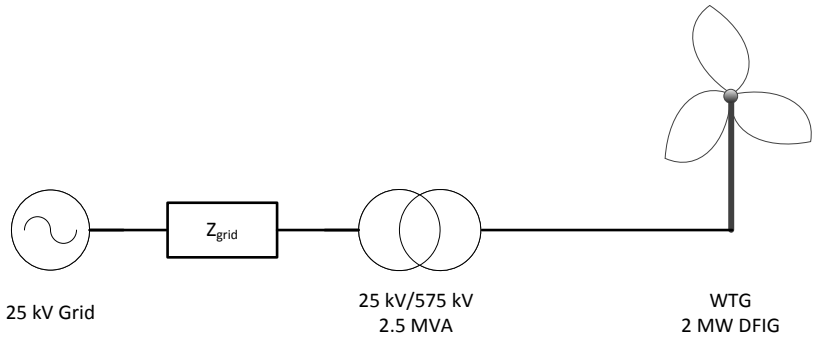

Figure 4-1 Parametric test network

Mean wind speed	13 m/s
Turbulence intensity	15 %
Grid line-to-line voltage	25 kV
Short circuit capacity	20 MVA
X/R ratio	3

Table 4-1 Base case parameters

4.3 Sensitivity analysis based on factors that influence flicker

4.3.1 Influence of wind and aerodynamic effects on flicker emissions

4.3.1.1 Overview

Flicker emissions produced by the distributed wind installation during continuous operation are in most part induced by power fluctuations originating from variations in the rotor torque. As mentioned in chapter 1, aerodynamic factors influencing variations in the rotor torque of the WTG, contributing to increased amounts of flicker emission, initiate from 3 main sources:

- Mean wind speed
- Turbulent and gusty winds
- Blade passing effects

4.3.1.2 Mean wind speed

In the case of DFIG WTGs, the flicker emissions will vary according to changes in the mean wind speed. Referring to figure 4-2, at low wind speeds, flicker emissions are minimal, due to a small amount of output power injected at the PCC. At higher wind speeds, ranging beyond cut-in but until the nominal speed, flicker emissions increase with an approximate linear relation to mean wind speed until the rated wind speed of the turbine, whereby the flicker emissions are at their maximum. The flicker emissions increase at the PCC in this region due and increase in the power delivered and due to the fact that increases in the mean wind speeds are associated with increases in turbulent components, as the turbulence intensity is fixed at 15%.

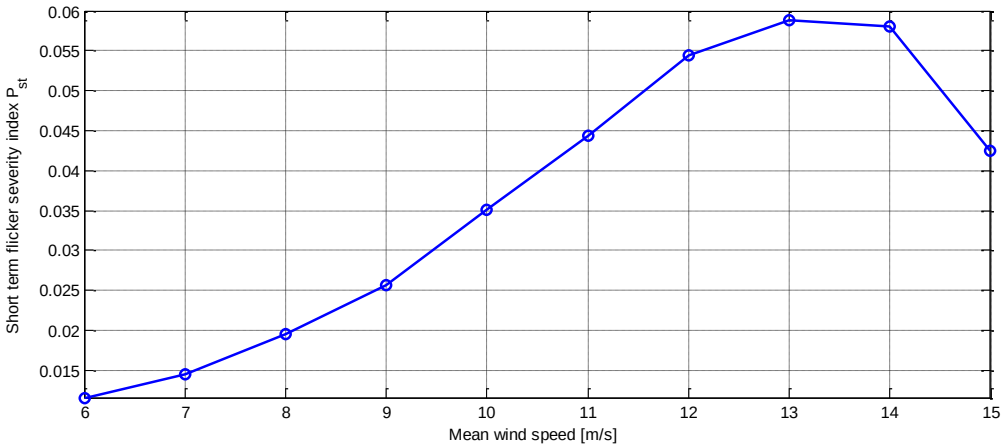

Figure 4-2 Flicker emissions due to changes in mean wind speed

For wind speeds above the nominal wind speed of the wind turbine, the flicker level tends to decrease. The reason is that the combination of the pitch control and the variable speed operation of the WTG can effectively attenuate stochastic fluctuations in the output power, hence, limiting the flicker emissions produced.

4.3.1.3 Turbulence intensity

The turbulence intensity of the wind has a significant influence on the flicker emissions produced by the distributed-connected WTGs due to the magnitude of its stochastic pulsations on the rotor torque. Turbulence intensity is defined as, $I_n = \frac{\Delta v}{v}$ where Δv is the wind speed standard deviation and v is the mean wind speed. Thus, as the turbulence intensity of the wind increases, the magnitude of the stochastic pulsations on the rotor torque increases. As a consequence, the flicker emissions produced by the WTG are aggravated. Figure 4-3, illustrates flicker emissions due to changes in mean wind speed and turbulence intensity. As expected, the higher the turbulence intensity, the more pronounced the WTG flicker emissions.

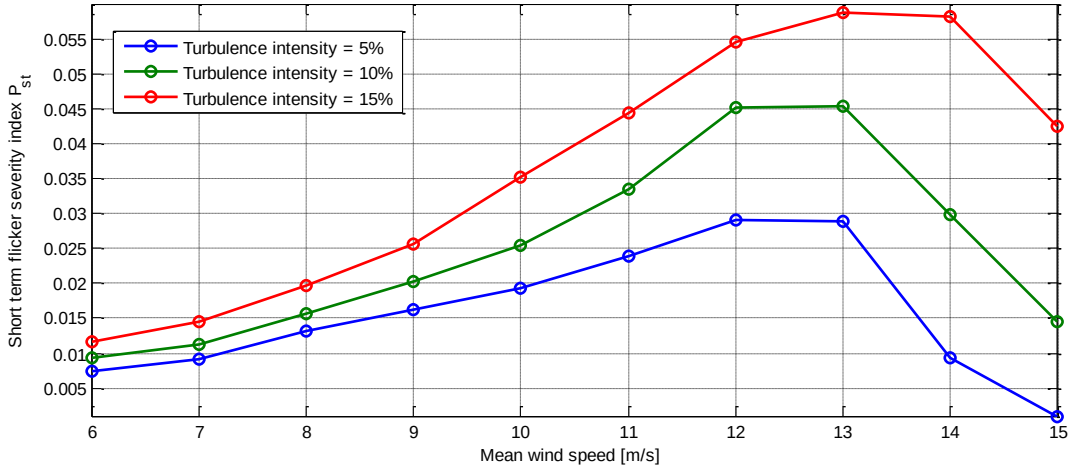

Figure 4-3 Flicker emissions due to changes in mean wind speed and turbulence intensity

4.3.1.4 Blade passing effects

Blade passing frequencies are referred to as the np frequencies, where p is the rotational frequency and n is the number of blades. As mentioned in chapter 1, these deterministic frequencies are induced by variations in rotor torque due to two phenomena

known as wind shear and tower shadow. Consequently, these 3p frequencies result in the addition of periodic components to the feeder's voltage at the PCC of the WTG and contribute to the total flicker level. Figure 4-4 illustrates the contribution of flicker emissions, with and without blade passing effects over a range of wind speeds. Flicker emissions originating from blade passing effects account for roughly 10% to 15% of the total flicker level produced by the WTG.

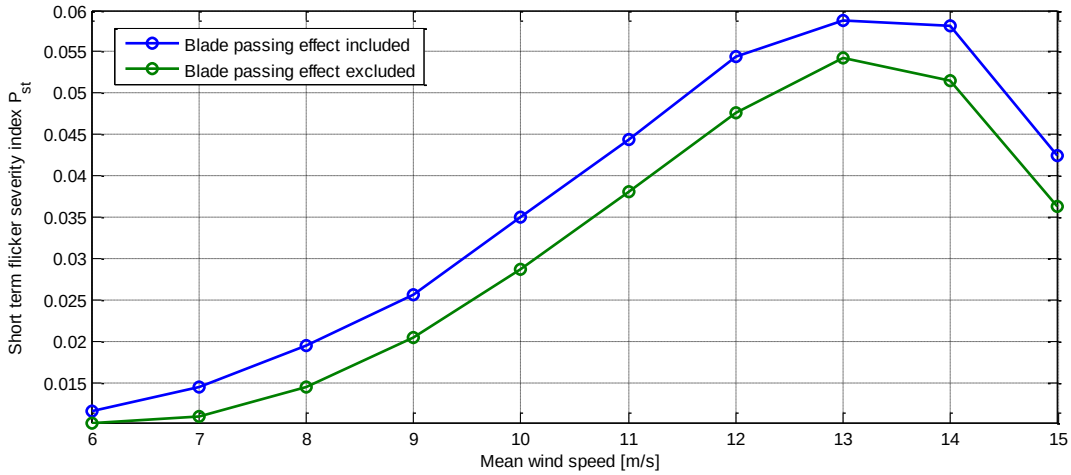

Figure 4-4 Flicker emissions due to changes in mean wind speed and the inclusion of deterministic blade passing effects

4.3.1.5 Mode of operation

The wind turbine has two main modes of operation: 1) power optimization mode and 2) power limitation mode. It would be interesting to assess flicker emissions from the turbines mode of operation and thus the IFL measurement is deemed to be more appropriate for this test. With reference to figure 4-5 once can note that in the power limitation mode, the IFL is greatly reduced. Also, one can note that gust components, characterized by rapid changes in wind speed generate spikes in the IFL chart.

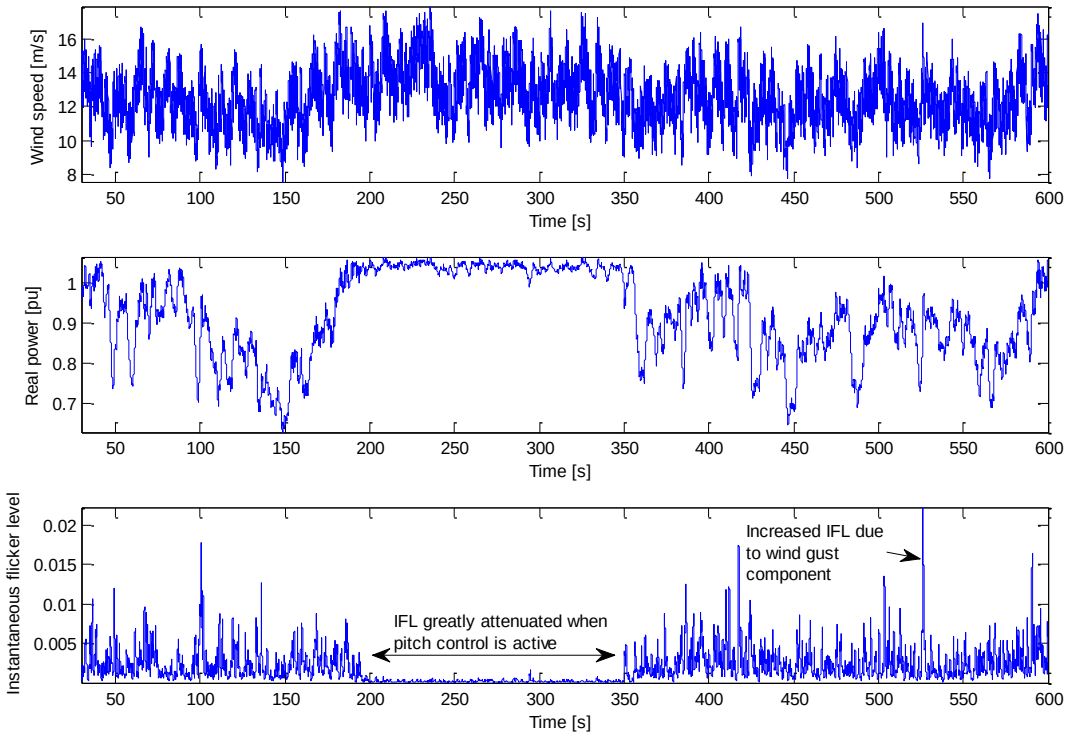

Figure 4-5 Flicker emissions due to mode of operation

4.3.2 Influence of grid parameters on flicker emissions

4.3.2.1 Short circuit capacity

As mentioned in chapter 1, the short circuit capacity is a relative indicator of the voltage stiffness of a particular node in the distribution feeder. The higher the SCC, the higher the voltage stiffness of that node, and hence, flicker levels should be relatively low. With regard to figure 4-6, the flicker level is approximately inversely proportional to the SCC at the PCC of the distributed wind farm. As expected, flicker levels are more pronounced in weak networks, characterized by low SCCs, than in stronger networks, characterized by high SCCs.

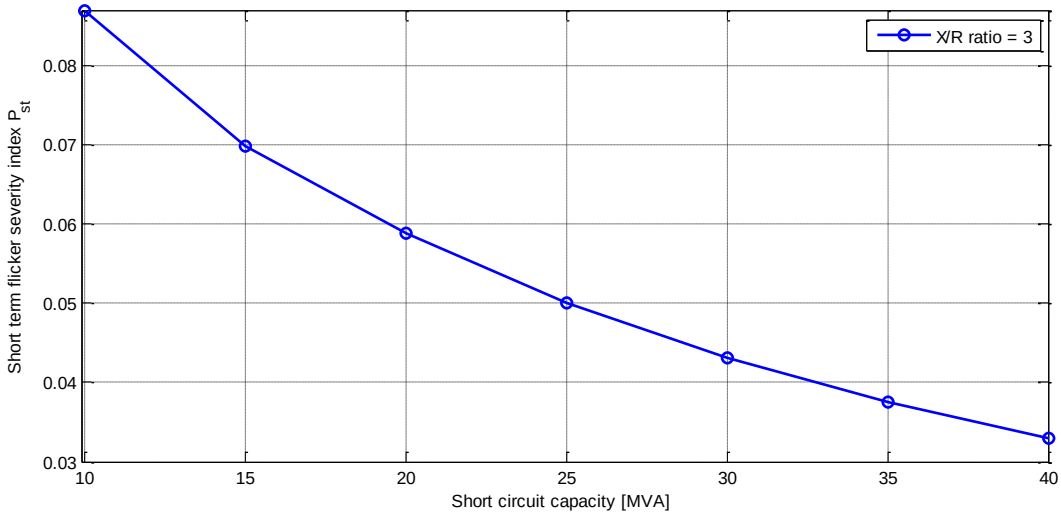

Figure 4-6 Influence of short circuit capacity on flicker emissions

4.3.2.2 Network impedance angle (X/R ratio)

The X/R ratio is a significant parameter in terms of its influence on voltage flicker, due to the fact that it determines whether the active or reactive power will dominate voltage fluctuations at the PCC. Depending on the network impedance angle denoted by $\theta_{grid} = \tan^{-1}\left(\frac{X_L}{R_L}\right)$, the active power flow may be offset by reactive power flow. As previously mentioned, the determining factor that influences flicker emissions is the difference between grid impedance angle and the WTG power factor angle, i.e. $\Delta V = \frac{\Delta P R_L cos(\theta_{pf} - \theta_{grid})}{V cos(\theta_{pf}) * \cos(\theta_{grid})}$.

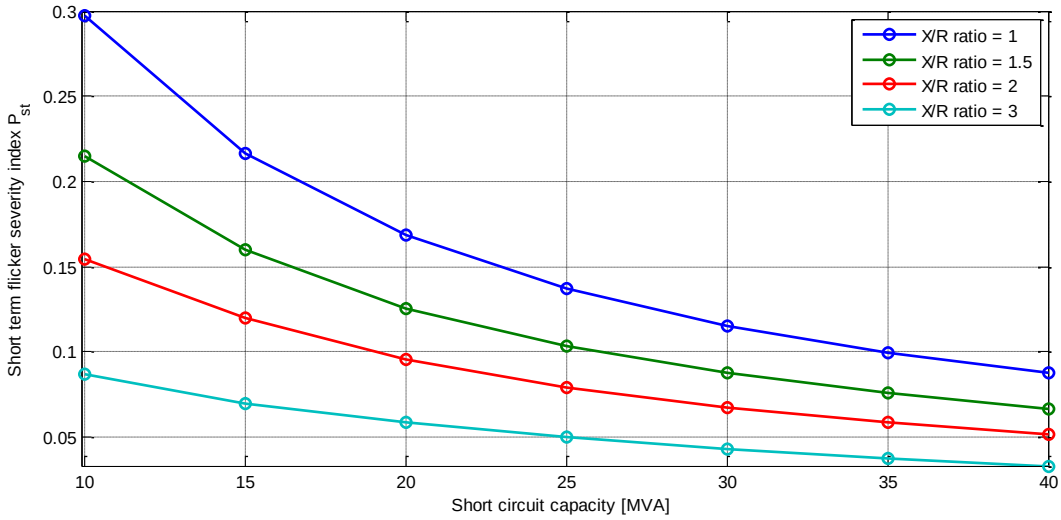

Figure 4-7 Influence of grid parameters on flicker emissions

Since the DFIG wind turbine is set to operate at a unity power factor in this study, only the grid impedance angle, which is relatively fixed, will determine the level of flicker produced by the WTG. Thus, for feeders characterized by a high impedance angle, implying a high X/R ratio, flicker emissions measured are relatively low compared to a feeder characterized by a lower impedance angle; refer to figure 4-7. Figure 4-7 also graphically illustrates how flicker is influenced from both the SCC and the X/R ratio combined.

4.3.2.3 Voltage level

The voltage level is another important characteristic that plays a role is the attenuation of flicker emitted from a distributed wind installation. Typically, higher voltage levels are associated with higher short circuit capacities and the X/R ratios, thus, implying a greater ability of the grid to absorb voltage fluctuations. As illustrated in figure 4-8, it is important to note that given a fixed short circuit capacity and X/R ratio, flicker emissions remain constant regardless of the voltage level.

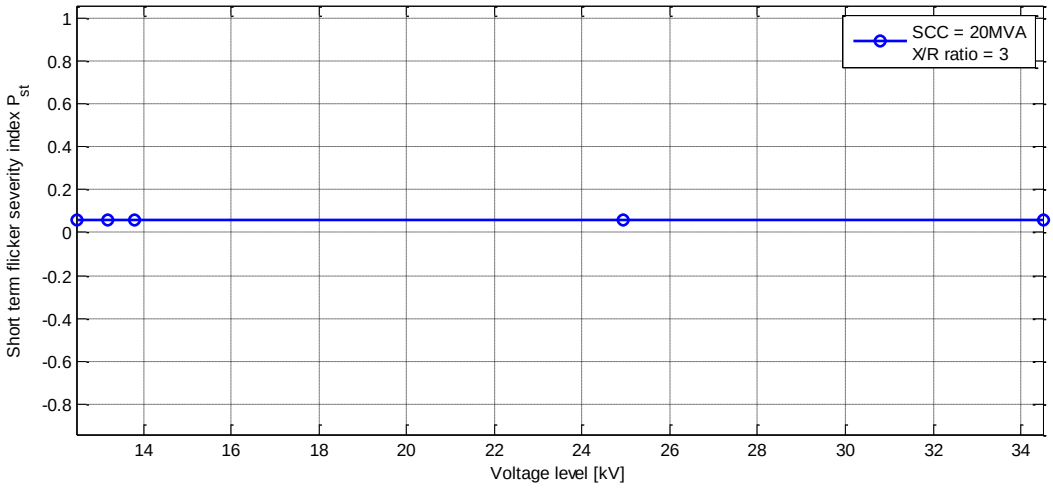

Figure 4-8 Flicker emissions due to changes in the voltage connection level

4.5 Flicker mitigation via reactive power control

4.5.1 Overview

Chapter 1 had detailed flicker mitigation techniques via reactive power compensation. The objective of this section is to implement these embedded controls and get a quantifiable measure of their flicker mitigation performance and reactive power usage. A sensitivity analysis will also be conducted to understand how reactive power can be used in a more efficient manner to mitigate flicker. Furthermore, an improved reactive power based technique is developed to directly address power fluctuations generating flicker, which allows for a practical implementation.

4.5.2 Power factor control

4.5.2.1 Concept

Power factor control is a reactive power based flicker mitigation technique. As previously stated, the general concept is that the wind farm's flicker emissions are reduced by operating the wind farm at a leading power factor such that power factor angle φ_{pf} and the grid's impedance angle φ_{grid} differ by $90°$. In accordance to eqn. (4.1), this should result in $\Delta V \rightarrow 0$, thus implying a reduction in flicker emissions.

$$\Delta V = \frac{PR_L + QX_L}{V} \rightarrow \frac{PR_L \cos(\varphi_{pf} - \varphi_{grid})}{V \cos(\varphi_{pf}) \cos(\varphi_{grid})} \tag{4.1}$$

4.5.2.2 Setting the WTG power factor or Q_{ref}

The WTG will operate at a constant power factor, which will be controlled by modifying the RSC's control loop, from constant Q control, inherent of the design provided in Simulink®, to PFC, in accordance to figure 4-9. Essentially, Q_{ref} is set by a pre-determined power factor and compared to the measured WTG output reactive power Q_{meas}. The difference between both quantities is defined as the error signal, which is feed to a PI controller to set the quadrature-axis rotor current. The WTGs power factor is set in accordance to eqn. (4.2).

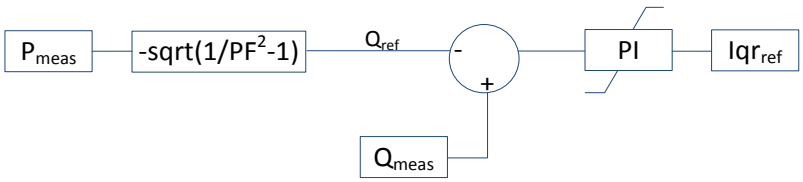

Figure 4-9 Power factor angle controller, version 1

$$Power\ Factor = \cos(90° - \varphi_{grid}) \tag{4.2}$$

Figure 4-10 illustrates a similar controller applying the identical concept based on eqn. (4.1). In this controller, Q_{ref} is set by eqn. (4.3). Both controls will yield identical results since Q_{ref} is the equal in both cases.

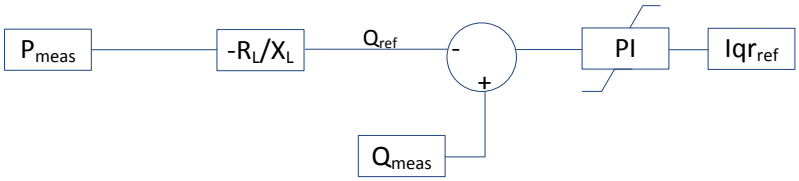

Figure 4-10 Power factor angle controller, version 2

$$Q_{ref} = -\frac{R_L}{X_L}P \tag{4.3}$$

4.5.2.3 Example

Test network

The test network, illustrated in figure 4-1, utilizes a Thevenin equivalent network with feeder characteristics listed in table 4-2. The wind speed profile feed to the WTG will be characterized by a Kaimal PSD with a mean wind speed of $13m/s$ and a turbulence intensity of 15%, as described in chapter 3. This network will serve as a benchmark to observe the effectiveness of the flicker mitigation technique.

Short circuit capacity	20MVA
X/R ratio	3
Grid impedance angle φ_{grid}	$\tan^{-1}(3) = 71.56°$

Table 4-2 Test network properties

With reference to eqn. (4.2), the wind installations power factor is set, refer to eqn. (4.4), to its optimal value of 0.95 leading which implies it is absorbing reactive power from the grid.

$$\left.\begin{aligned} \varphi_{pf} &= 90° - \varphi_{grid} = 90° - 71.56° = 18.44° \\ Power\ Factor &= \cos(18.44°) \approx 0.95 \end{aligned}\right\} \quad (4.4)$$

Simulation & sensitivity analysis

Figure 4-11 illustrates the fluctuating power profile of a one, 2 MW DFIG unit. In order to mitigate the power fluctuations which lead to voltage fluctuations and consequently flicker, reactive power is absorbed from the grid, for different power factors, as seen in figure 4-12. One can easily note that large amounts of reactive power are needed to mitigate flicker. This is mainly due to the large DC component present, which has no impact in mitigating flicker, leading to an unrealistic practical implementation of the mitigation scheme. Thus, the flicker mitigation technique shows its limits, particularly when the grid impedance angle is low, which requires operating at a poor power factor.

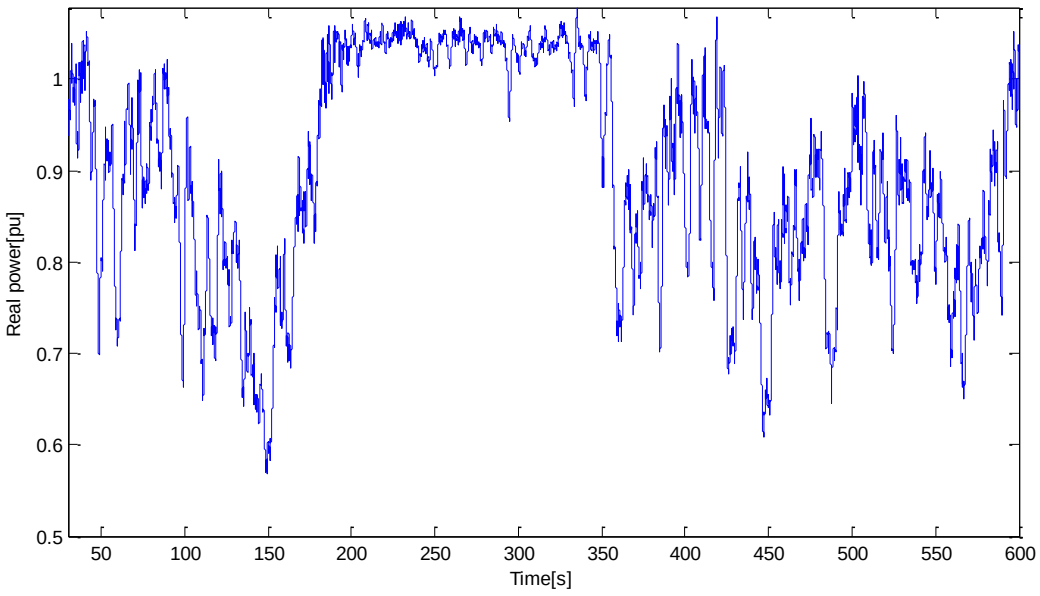

Figure 4-11 Wind installations real power produced

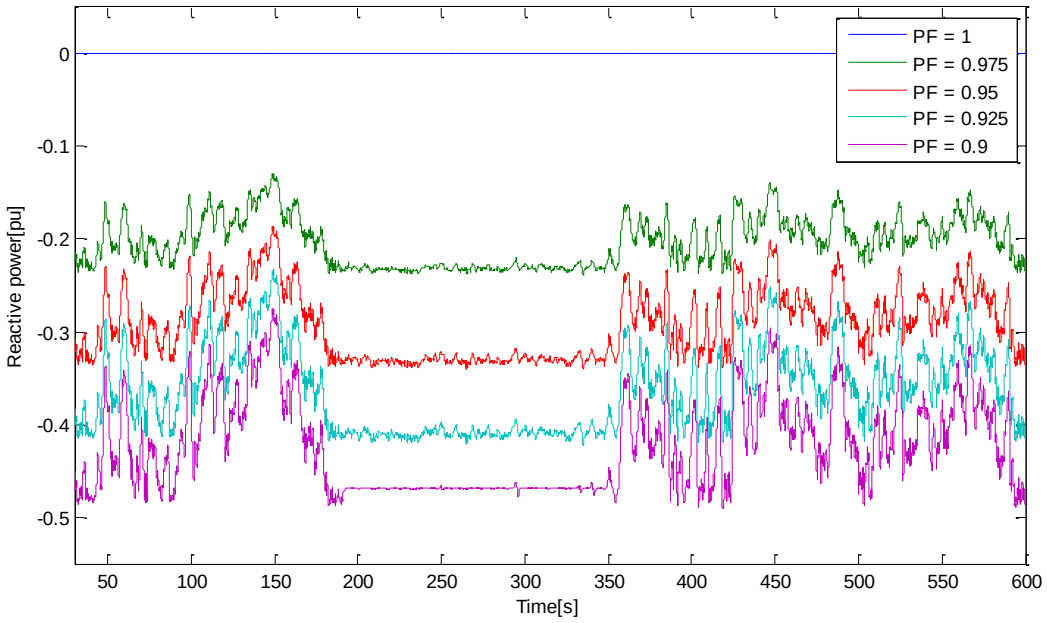

Figure 4-12 Reactive power absorbed from the grid in order to mitigate flicker

With reference to figures 4-13, 4-14 and table 4-3, one can note that the flicker mitigation scheme does indeed work as flicker emissions are reduced from $P_{st} = 0.0588$ to $P_{st} = 0.0250$. This represents a 57.5% reduction in flicker emissions. However, there is a marginal difference in the reduction of flicker emissions when operating the turbine at a power factor of 0.975 as opposed to 0.95, this is similar to what is noted in [64]. This implies that much less reactive power needs to be absorbed from the grid, reducing the network technical limitations and cost related to the reactive power supply. Thus, the utility can operate the turbine at a slightly leading power factor as opposed to the optimal power factor (i.e. when the angle difference between φ_{pf} & φ_{grid} is 90°, as shown in figure 4-14) in order to partially reduce flicker emissions. This mitigation technique may be a pragmatic and brute-force solution to solve a potential flicker problem. It is important to note that if the WTG operates at a power factor poorer that the optimal power factor, power fluctuations will be compensated in excess and the flicker level will be aggravated.

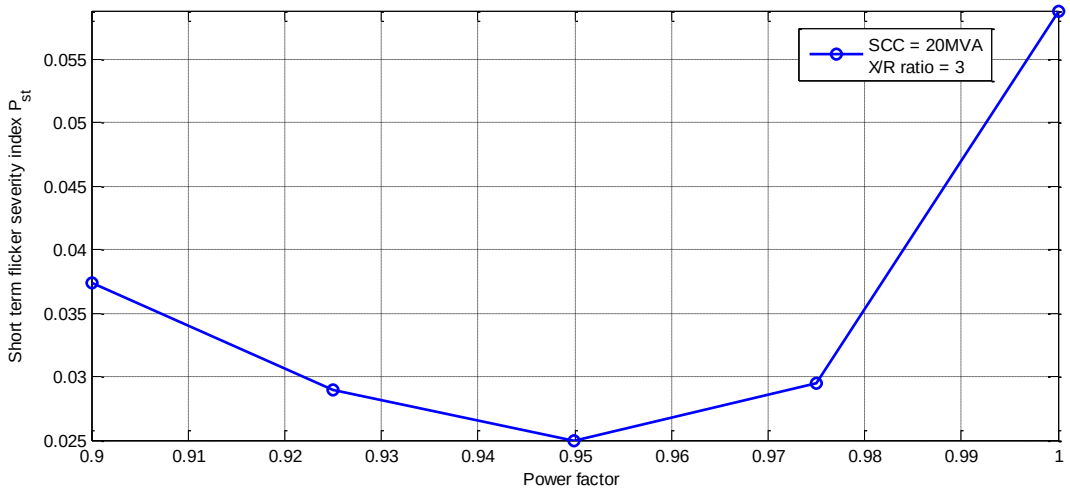

Figure 4-13 Influence of turbine power factor on flicker

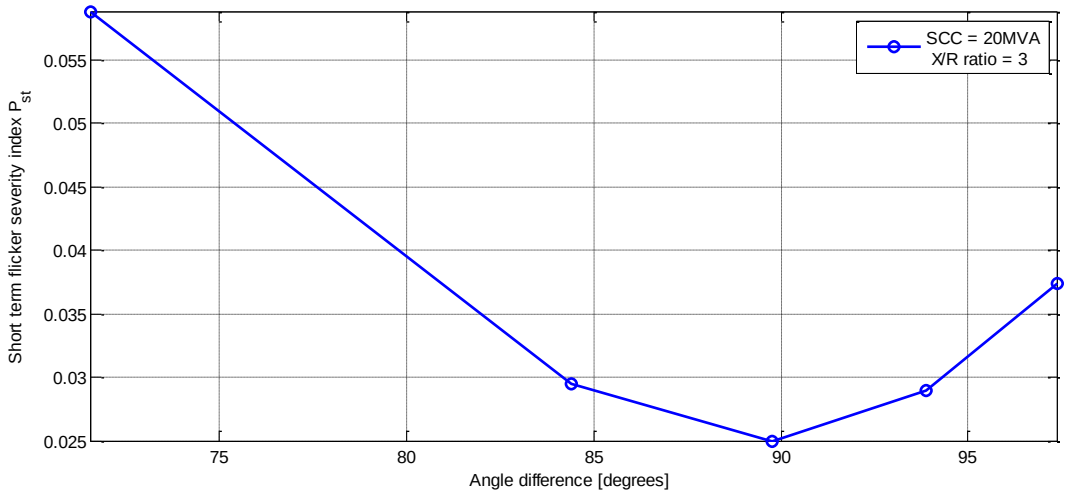

Figure 4-14 Influence of the angle difference between the φ_{pf} and φ_{grid}

Power Factor	0.9	0.925	0.95	0.975	1
Angle Difference	97.4°	93.89°	89.75°	84.4°	71.56°
P_{st}	0.0374	0.0290	0.0250	0.0295	0.0588

Table 4-3 Sensitivity analysis

4.5.3 Improved controller for flicker mitigation

4.5.3.1 Concept

The improved controller developed is similar to the reactive power based flicker mitigation technique previously mentioned; refer to figure 4-15. The difference is that a specified bandwidth is associated to the controller and the power factor is not maintained constant. This technique based on operating only within a frequency band is similar to [44] which uses average value deviations in the power to set the amount of reactive power needed to be supplied/absorbed by the WTG to attenuate the flicker level. Ultra low frequencies present in the power fluctuations are filtered out by a second order Low Pass Filter (LPF) as they do not influence flicker emissions. The second order LPF is characterized with a cut-off frequency and damping factor equal to 0.05 Hz and 0.707 respectively. The upper limit of frequencies present in the fluctuating power waveform is set by the mechanical filters of the turbine and is much lower that the upper limit of the flicker frequency range of 0.5 Hz to 42 Hz. Hence, the objective of the improved controller is to operate within a specific frequency band, targeting solely flicker emissions, such that the intake of reactive power is deeply reduced. Hence, the efficiency of reactive power to mitigate flicker would be greatly increased.

In order for the controller to be more flexible, Q_{ref} will be composed of two components. The first component Q_{Pst}, will dispatch the reactive power needed to be absorbed or supplied in order to minimize flicker emissions. The second component Q_{ss} will handle the steady state reactive power level that the WTG is required to provide.

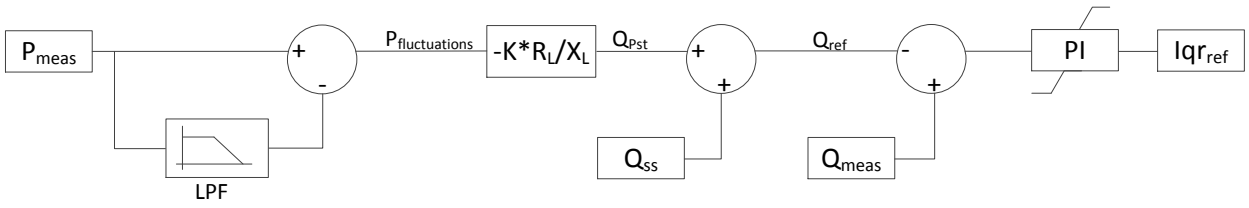

Figure 4-15 Improved reactive power based flicker mitigation controller

4.5.3.2 Example

The same test network, as illustrated in figure 4-1, utilizing a Thevenin equivalent network with feeder characteristics listed in table 4-2 is used to observe the performance of the

improved mitigation scheme. Figure 4-16 illustrates the reactive power supplied and absorbed by the turbine installation in order to mitigate flicker, i.e. Q_{Pst}. In this case, $Q_{ss} = 0$. One can note that the reactive power absorbed and supplied by the WTG solely targets the frequency band of power fluctuations linked to flicker emissions, thus resulting in a more efficient use of reactive power. Table 4-4, benchmarks three scenarios: 1) No mitigation scheme, 2) PFC mitigation scheme and 3) Improved mitigation scheme. One can note that not only does the improved mitigation scheme utilize substantially less reactive power but also further reduces DFIG flicker emissions compared to the PFC mitigation scheme.

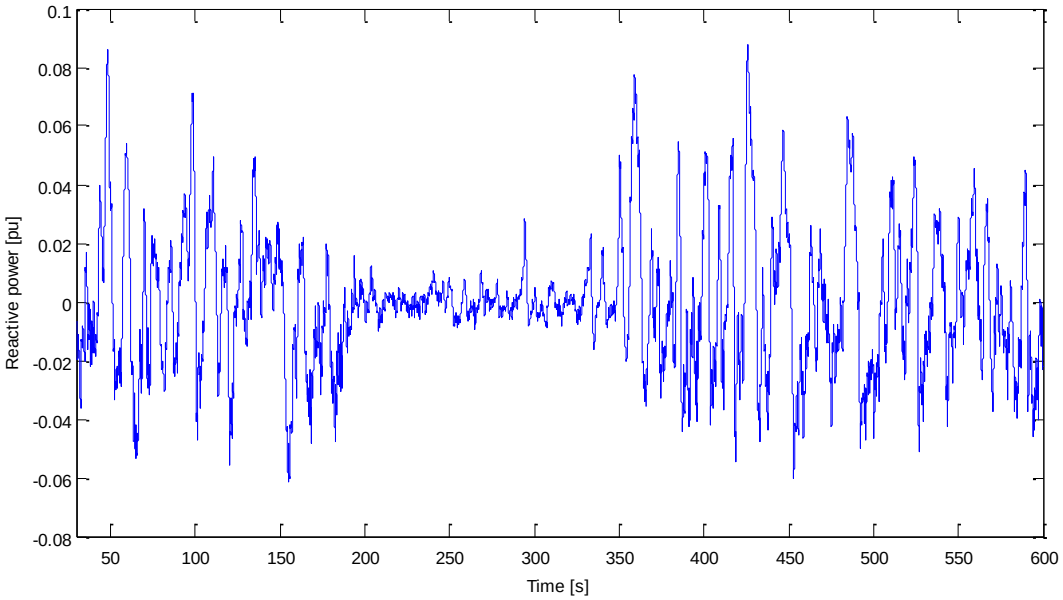

Figure 4-16 Reactive power absorbed/supplied by the installation to mitigate flicker emissions (i.e. Q_{Pst})

	No mitigation	Power factor control	Improved controller
P_{st}	0.0588	0.0250	0.0240

Table 4-4 Summary of results

4.5.3.3 Sensitivity analysis

With reference to figure 4-17, table 4-5 and eqn. (4.6), one can observe the changes in flicker emissions, subject to changes in the gain constant K. Once again, some cases present marginal differences in flicker emissions for large changes in reactive power supply and absorption. For instance, for $K = 1$, the optimal gain, $P_{st} = 0.0240$, yet for $K = 0.75$, which implies 25% less use of reactive power, $P_{st} = 0.0271$. Note, for $K > 1$, power fluctuations are

over compensated and thus, flicker is aggravated as opposed to attenuated. Thus, by slightly reducing K from its optimal value of $K = 1$, emissions can be partially reduced to achieve a desired level, to have less of a burden on reactive power sources present in the distribution network.

$$Q_{Pst}^{*} = -K \frac{R_L}{X_L} P_{fluctuations} \tag{4.6}$$

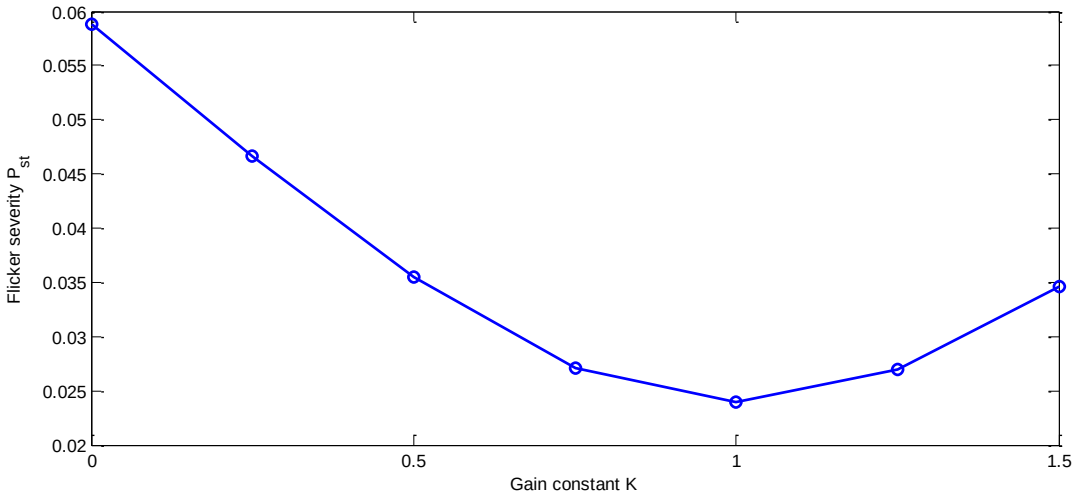

Figure 4-17 Sensitivity analysis

K	0	0.25	0.5	0.75	1	1.25	1.5
P_{st}	0.0588	0.0467	0.0355	0.0271	0.0240	0.0269	0.0346

Table 4-5 Sensitivity analysis

Chapter 5:
Flicker Study on a Real Distribution Feeder

5.1 Overview

The goal of chapter 5 is to conduct a flicker study on a real distribution feeder using the Opal-RT® real time simulator. This will allow for a more comprehensive flicker study on a distribution feeder scheduled for the interconnection of a large embedded wind farm installation, executed in real time. Flicker emissions will be quantified and assessed under the following scenarios:

- Sweeping the level of wind penetration
- Changing the interconnection point
- Adding flicker emitting loads
- Using a reactive power based flicker mitigation technique

5.2 Description of the distribution feeder under study

The balanced rural distribution feeder under study has a nominal line-to-line voltage of 25 kV at 60 Hz and supplies an 11 MW, 2.5 MVar load, being dominantly of residential nature, yet some industrial loads are present. With reference to figure 5-1, the substation generator is connected to the HV/MV transformer through a grid impedance modeled by a resistive inductive line. The HV/MV transformer is delta-connected at the 120 kV source side and wye-connected on the 25 kV feeder side. The network also contains an in-line voltage regulator located between bus 8 and bus 10, modeled as a fixed tap transformer and a 1200kVar shunt capacitor bank at bus 15. Both are used to provide compensation for voltage drops toward the end of feeder length. Unless otherwise specified, distribution feeder loads are represented as constant impedances and do not contribute to flicker emissions. The network is represented in Simulink®, maintaining grid, line and transformer parameters.

The distributed wind installation, consisting of 2 MW DFIG units, will be connected to the feeder through a delta-connected transformer at the 575 V generator side and wye-connected on the 25 kV feeder side. Buses 1, 8, 9 and 18 will be the studied distributed wind farm interconnection points. For more details on the distribution feeder, refer to the Appendix.

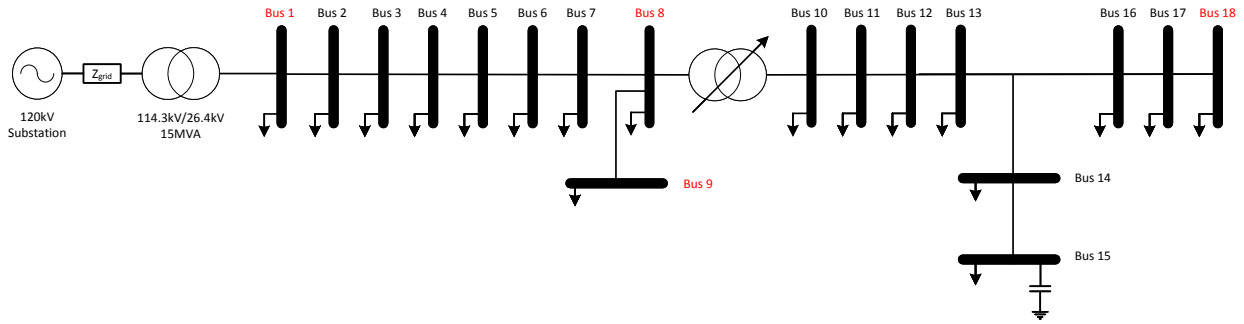

Figure 5-1 Distribution feeder under study

5.3 Grid characteristics at potential interconnection points

As previously stated buses 1, 8, 9 and 18 have been selected as potential points of common coupling. Table 5-1 lists the grid characteristics, notably short circuit capacity and X/R ratio of these selected points. Grid characteristics were obtained by measuring the equivalent impedance at 60Hz for each of the potential points of common coupling using Simulink®'s impedance measurement tool. The short circuit capacity and X/R ratio were calculated from the equivalent impedance using eqn. (5.1) and (5.2).

$$Short\ circuit\ capacity = \frac{V_{ll}^2}{\sqrt{R^2+X^2}} \tag{5.1}$$

$$X/R\ ratio = \frac{X}{R} \tag{5.2}$$

Point of common coupling	Short circuit capacity	X/R ratio
Bus 1	148 MVA	5.85
Bus 8	49 MVA	2.25
Bus 9	36 MVA	2.5
Bus 18	35 MVA	1.8

Table 5-1 Distribution feeder grid characteristics

5.4 Decoupling of the distribution feeder using RT-LAB

The Opal-RT® real time simulator allows for a distribution feeder model to be distributed over a cluster of processors running in parallel to achieve a significant improvement in computational speed performance. RT-LAB® is Opal-RT®'s software application that allows one to readily convert Matlab®/SPS models to a real-time model to be distributed over a cluster of processors. In order to decouple a distribution feeder into sub-networks, one must use the provided ARTEMiS® library line blocks (i.e. stublines). The stubline block permits the decoupling of state-space system equations of the feeder on both sides where the stubline is inserted. Essentially, this method takes advantage of the natural propagation delay of the line to buffer the communication time required between two processors. Consequently, it is possible to distribute smaller portions of the large impedance matrix pertaining to the feeder amongst a cluster of processors, to be solved in parallel [79]. Solving a reduced impedance matrix as opposed to a large impedance matrix greatly decreases the computational effort allowing for a significant improvement in simulation speed. However, in order to permit the insertion of a stubline, the following condition must hold: $\tau = \sqrt{LC}$ [80]. Whereby, τ is the simulation time step and L & C are the line inductance and capacitance respectively.

With reference to figure 5-2 the distribution feeder under study is separated into three sub-networks. Each sub-network runs on a dedicated processor allowing computational speed-ups via parallel processing. These three networks are connected by two stubline blocks which are located between bus 7 and 8 and between bus 8 and 9 and are represented by green lines.

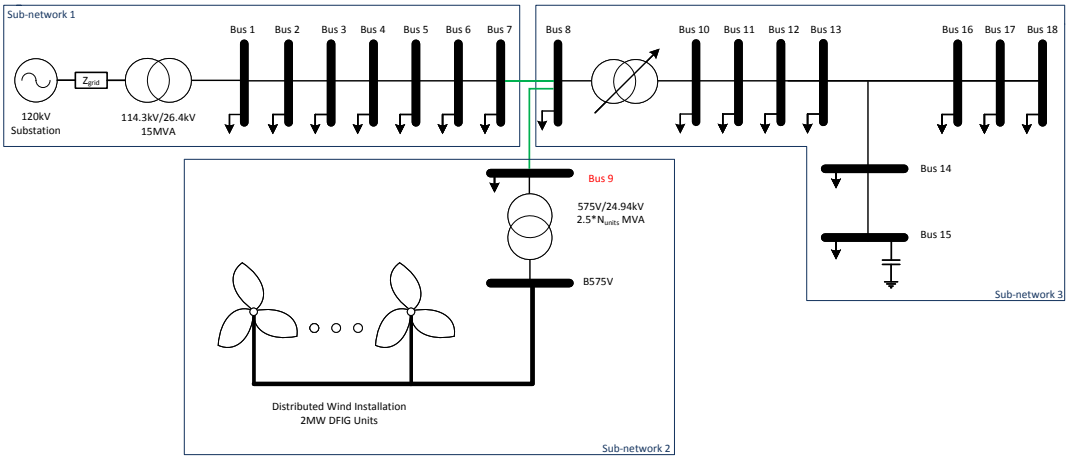

Figure 5-2 Decoupled distribution feeder

5.5 Flicker study using the detailed distribution feeder model

5.5.1 Influence of varying levels of distributed wind penetration

In the base case study, varying levels of wind penetration, ranging from 2 MW to 14 MW are interconnected at bus 9. If each 2 MW WTG to be incorporated in the wind farm were to be feed identical wind speed profiles, flicker emissions would most likely be highly overstated. The main reasoning is that power fluctuations originating from the stochastic nature of the wind and deterministic blade passing effects would be fully synchronized, not representing realistic occurrences. Thus, for this study, flicker emissions produced by the distribution-connected wind installation are measured under two scenarios. Scenario 1, all turbines are feed identical wind speed profiles characterized by a Kaimal PSD with a mean wind speed of $13m/s$ and a turbulence intensity of 15%. Scenario 2, the wind turbines are assumed to have a geographical spacing of 5 times the rotor diameter. In our case, this evaluates to wind speed profiles, identical to that of scenario 1, time shifted by 30 seconds between turbines. With reference to figure 5-3, the influence of increasing the penetration of wind power, thus decreasing the SCR is inversely proportional to flicker emissions and is consistent with the literature [21]-[24]. It can be noted that flicker emissions are more pronounced at lower SCR's, specifically when the $SCR < 4$. This observation is coherent with ref. [65].

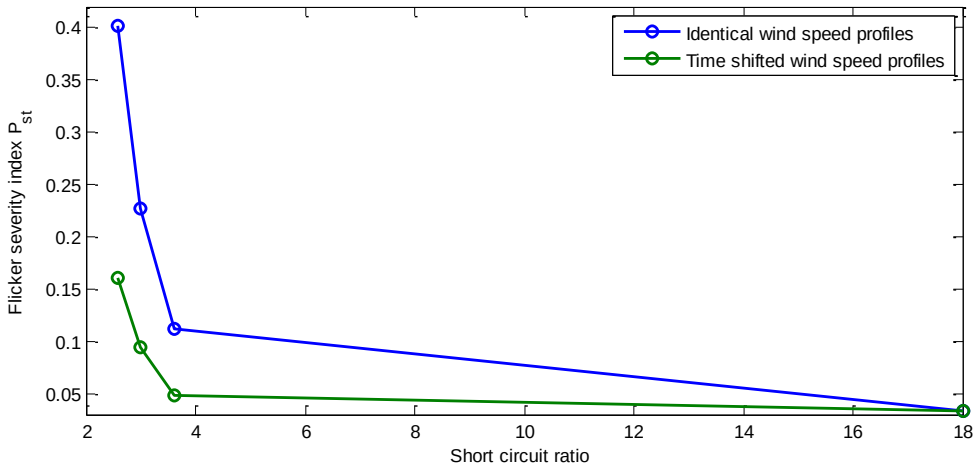

Figure 5-3 Influence of Short circuit ratio on flicker emissions

With reference to figures 5-3 and 5-4, by time shifting the wind speed profiles, power fluctuations are unsynchronized, which results in a more realistic wind farm flicker emission measurement.

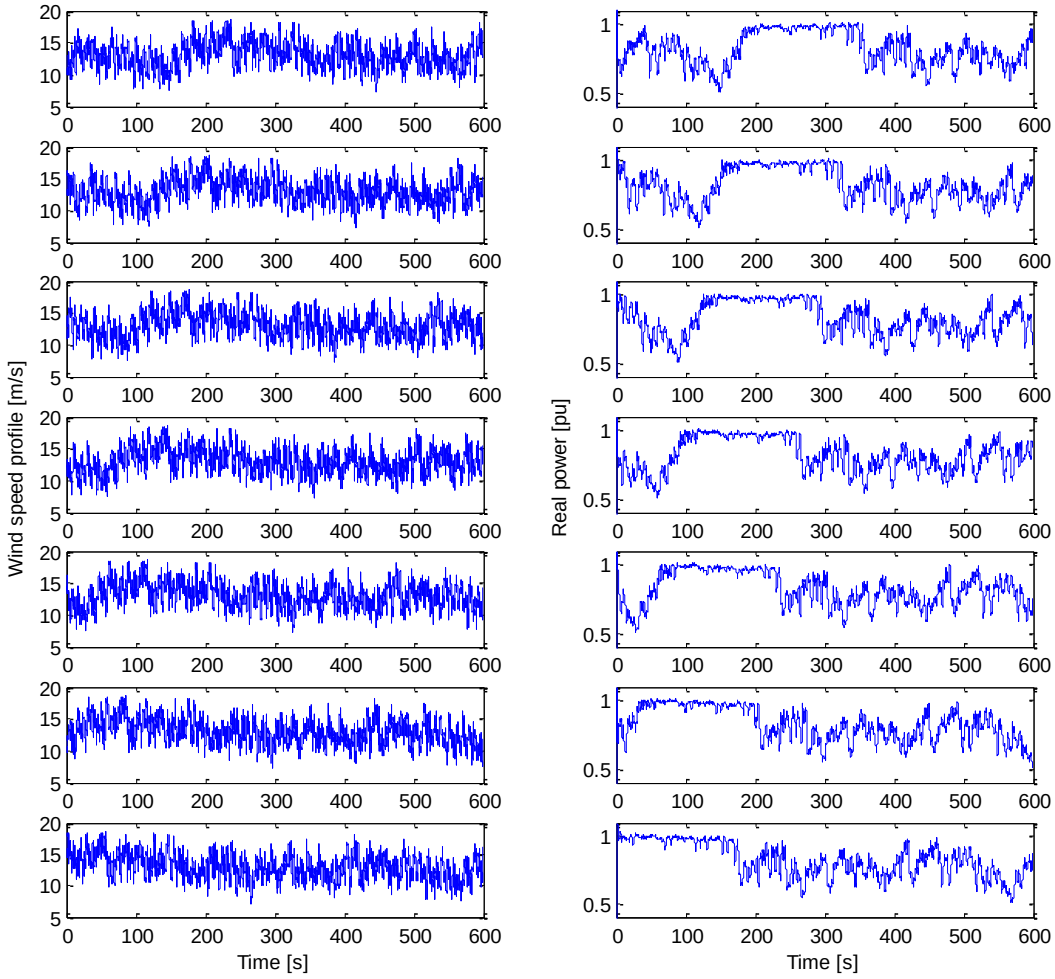

Figure 5-4 Time shifted wind speed profiles and associated output power waveforms

5.5.2 Influence of changing the interconnection point

Given the choice of four potential interconnection points, notably bus 1, 8, 9 and 18, flicker emissions for different wind penetration levels ranging from 10MW to 14MW are measured. Each turbine in the wind farm is represented and feed a time shifted wind speed profile identical to the previous section. With reference to figure 5-5 and table 5-2, given the grid characteristics at each of the potential points of common coupling, one can note that stiffer connections points characterized by a bus 1 and 8 result in much lower flicker emissions

compared to geographically distant bus 9 and 18. Bus 1 located at the distribution HV/MV transformer terminals has the stiffest point of common coupling, whereby, flicker does not seem to impose any technical limitation. In fact reference [11] claims that up to 40 MW may be connected at this point if the network infrastructure allows. Conversely, bus 18, located at the end of the feeder, characterized by a fair short circuit capacity but low X/R ratio is not deemed cautionary, but is the most aggravated by the installation of a large distributed wind project. Thus, as the PCC of the wind farm approaches the HV/MV transformer, the SCC and SCR are increased and flicker attenuates.

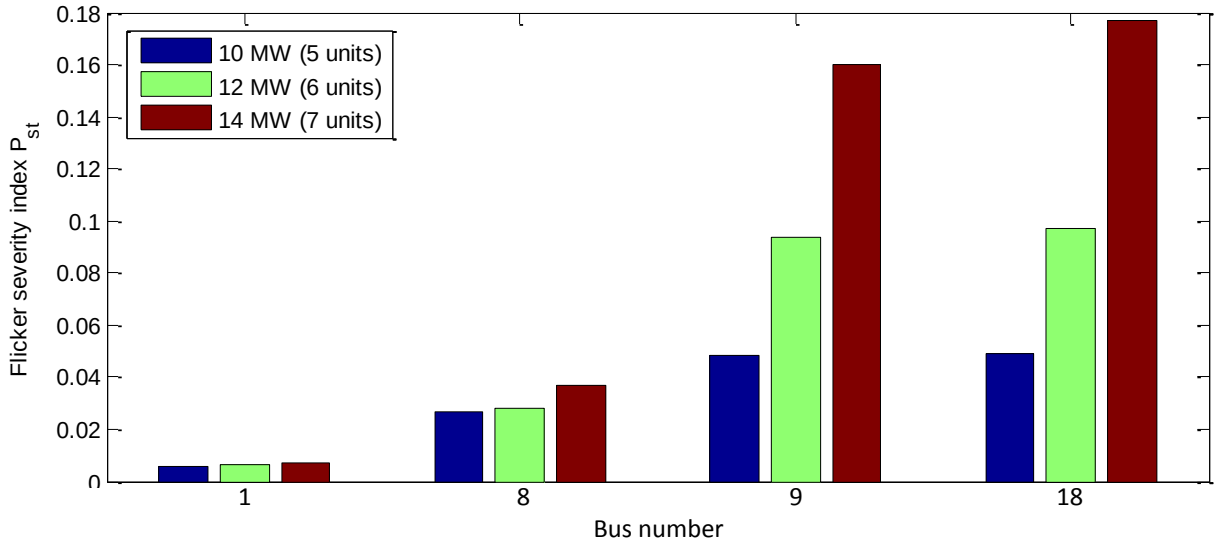

Figure 5-5 Flicker emissions at difference interconnection points

Point of common coupling	P_{st} (5 units)	P_{st} (6 units)	P_{st} (7 units)
Bus 1	0.0059	0.0064	0.0073
Bus 8	0.0264	0.0284	0.0371
Bus 9	0.0487	0.0938	0.1602
Bus 18	0.0492	0.0968	0.1768

Table 5-2 Summary of flicker measurements

5.5.3 Flicker profile

Also of interest is the flicker profile across the distribution feeder. In other words, how flicker propagates throughout the MV network. Table 5-2 tabulates the measured flicker emissions at a subset of buses given the connection of 7 DFIG units (i.e. 14 MW) at bus 9, as

illustrated in figure 5-6. Once again, this simulation demonstrates that as the fluctuating voltage waveform approaches the substation transformer, flicker is attenuated. However, for buses not approaching the substation transformer, flicker is not attenuated and remains constant.

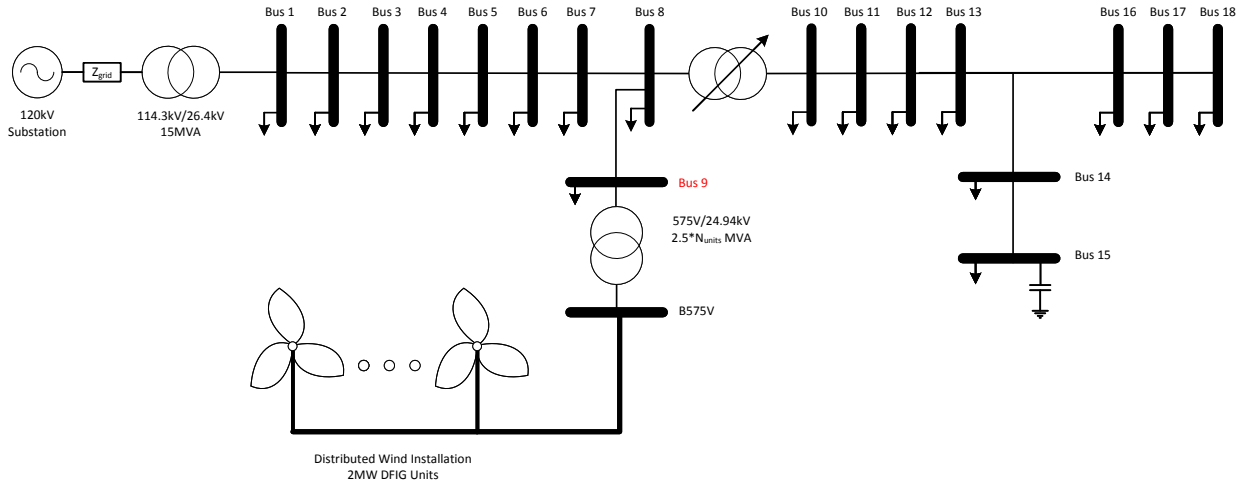

Figure 5-6 Interconnection to Bus 9

	Bus 1	Bus 5	Bus 7	Bus 8	Bus 9	Bus 13	Bus 18
P_{st}	0.0422	0.0588	0.0698	0.1251	0.1602	0.1251	0.1251

Table 5-3 Flicker profile

5.5.4 Addition of flicker producing loads

With reference to figure 5-6, two flicker emitting loads are introduced to the network at bus 8 and bus 13. These two loads are identical and consist of a 750 horsepower, frequently starting motors, represented by squirrel cage induction machines. These motors have switching events corresponding to 12 motor starts per hour. Please note that switching events between both flicker producing loads are unsynchronized. In the first simulation, the flicker generated from these loads is of interest and thus a constant wind speed profile is feed to the wind installation. The flicker emissions measured, only due to flicker emitting loads corresponds to $P_{st} = 0.1261$. In the second simulation, the interaction between the flicker producing wind farm and loads is studied. The flicker level measured due to all flicker sources combined equates to $P_{st} = 0.1945$. Figure 5-7 illustrates flicker emissions as a function of time, notably the IFL due to 1) solely flicker loads, 2) solely the wind farm and 3) both the wind farm and flicker loads.

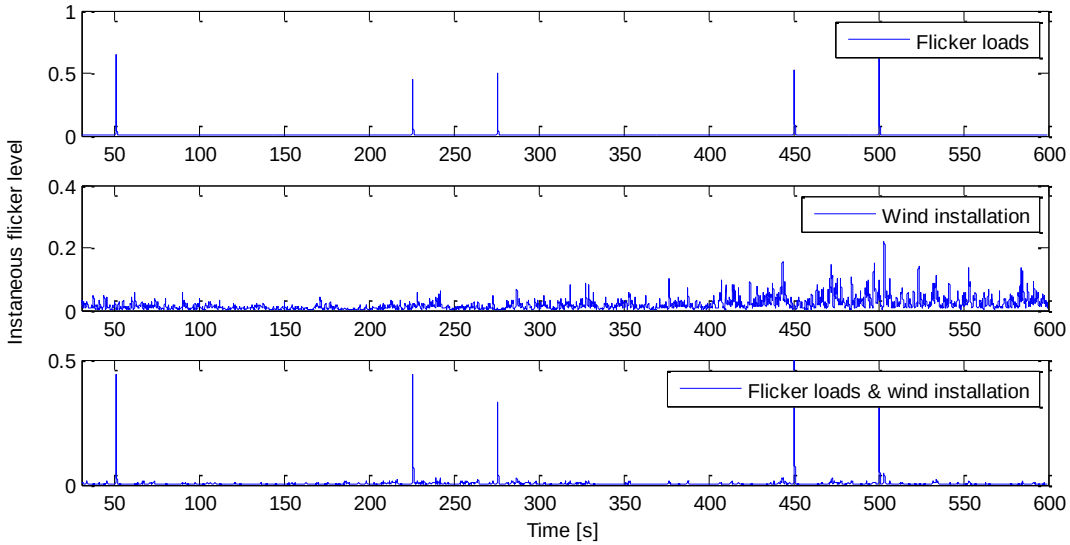

Figure 5-7 Instantaneous flicker emissions due to three scenarios

With reference to figure 5-7, flicker emissions from motor starts occur at distinct times while emissions from the wind farm are continuous. Also note that flicker emissions from the more distant frequently starting motor located at bus 13 are less than those generated at bus 8. This has to do with the fact that flicker is attenuated as it moves upstream the feeder. Flicker measurements from all three scenarios indicate that flicker emissions due to multiple flicker emitting loads are not the linear addition of flicker producing loads and generators, refer to figure 5-8. The relation is consistent with the summation law specified by the IEC 61000-4-7.

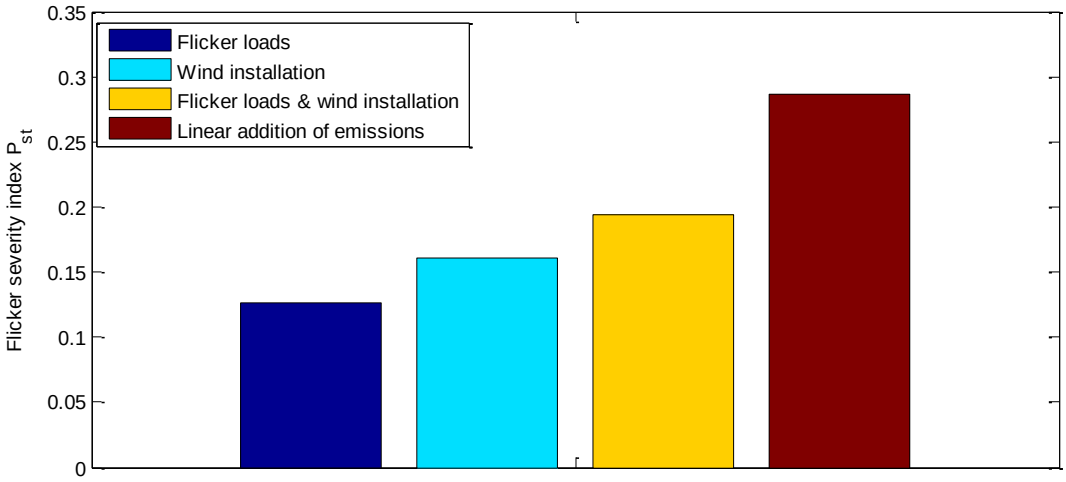

Figure 5-8 Influence of flicker generating loads

5.5 Flicker mitigation via reactive power control

Chapter 4 detailed several reactive power based techniques to mitigate flicker. It would be interesting to use the improved mitigation technique mentioned in section 4.5.3 which controls the reactive power absorbed/supplied by the wind turbine to strictly handle power fluctuations which generate flicker, termed Q_{Pst}. This results in a less abusive use of reactive power and viable technique to mitigate flicker generated by a large wind farm. With reference to figure 5-9, four scenarios are presented. The first two scenarios deal with flicker solely originating from the wind installation, with and without mitigation. The latter two scenarios deal with flicker originating from both the wind installation and flicker loads, with and without mitigation. It is important to note that the flicker mitigation technique utilized only mitigates flicker produced by the wind installation. One can note that the mitigation technique clearly works under both circumstances.

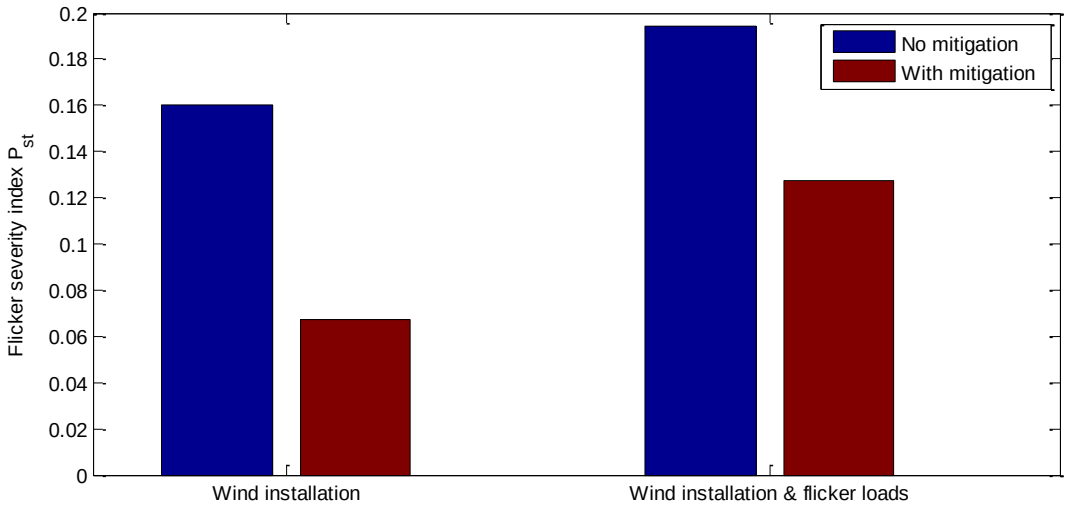

Figure 5-9 Influence of reactive power based mitigation technique on flicker emissions

With reference to figure 5-10, the reactive power supplied/absorbed by each individual WTG is plotted. Figure 5-11 illustrates the net reactive power supplied/absorbed at the PCC. Thus, this mitigation technique is clearly viable as the use of reactive power use is efficient, manageable and compliant to grid codes.

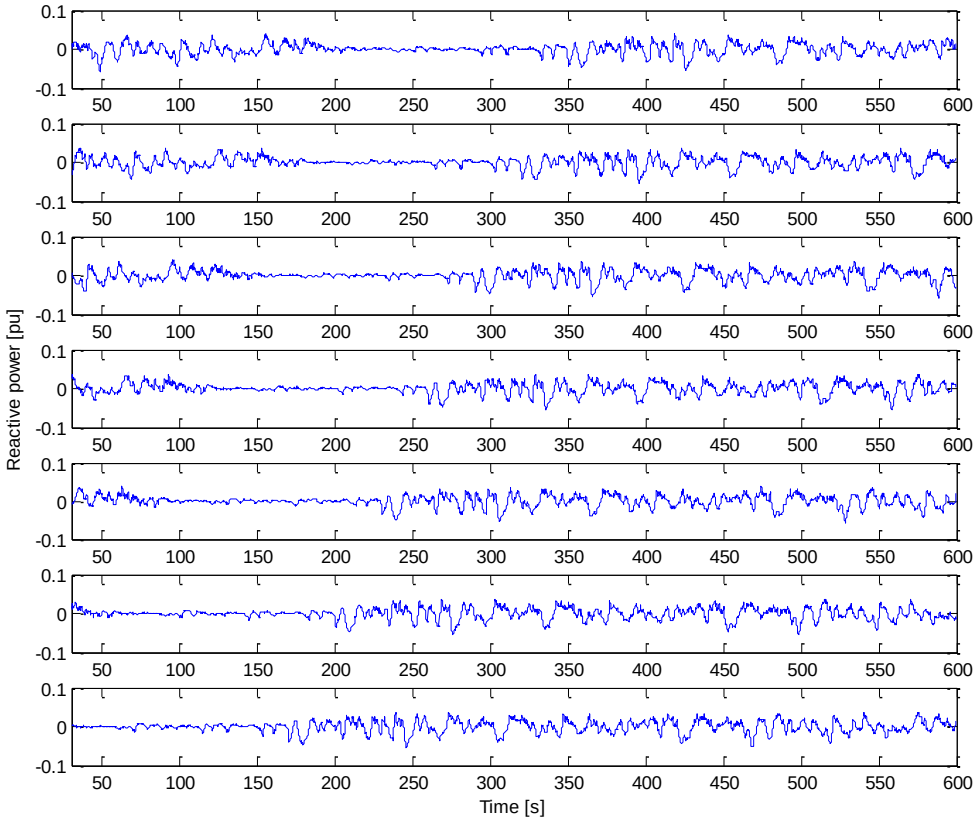

Figure 5-10 Reactive power supplied or absorbed by each turbine needed to mitigate flicker

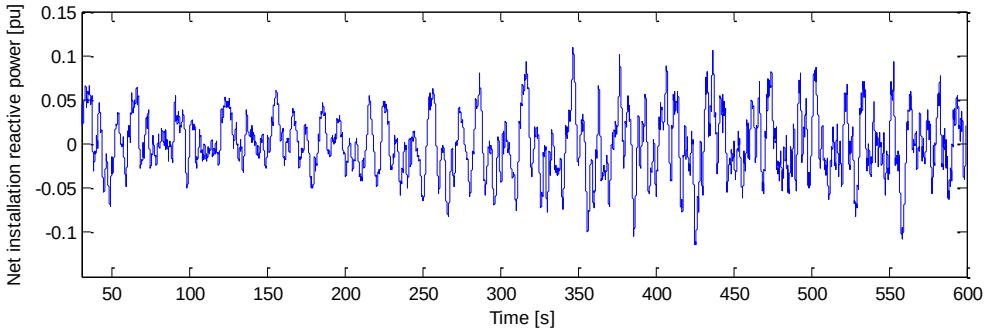

Figure 5-11 Net reactive power absorbed by the wind installation to mitigate flicker

5.7 Summary

Chapter 5 dealt with the interconnection of large wind farms to a distribution feeder, executed in real time. Flicker emissions were assessed and quantified to a variety of scenarios. Finally, the effectiveness and viability of the reactive power based flicker mitigation technique developed in chapter 4 was demonstrated.

Chapter 6: Conclusions & Recommendations for Future Work

6.1 Presentation of the Rule of Thumb

The quantity of flicker emissions produced by a distribution-connected wind farm is likely to be the limiting factor which determines the greatest level of wind penetration possible. In order to make the most efficient penetration of wind energy into distribution feeders, without violating flicker limits and the need for detailed studies, a rule of thumb has been developed based on figure 6-1 and is presented in figure 6-2. Essentially, figure 6-1 quantifies the flicker emissions produced by DFIG wind turbines connected to a parametric network, as in chapter 4, feed identical wind speed profiles characterized by $v_{mean} = 13\, m/s$ & $I_n = 15\%$, and benchmarks the flicker emissions produced to an emission limit. Events which result in wind farm emissions above the green plane, notably the emission limit, are in violation of emissions limits, whereas events resulting in wind farm emissions below the green plane are in compliance to emission limits.

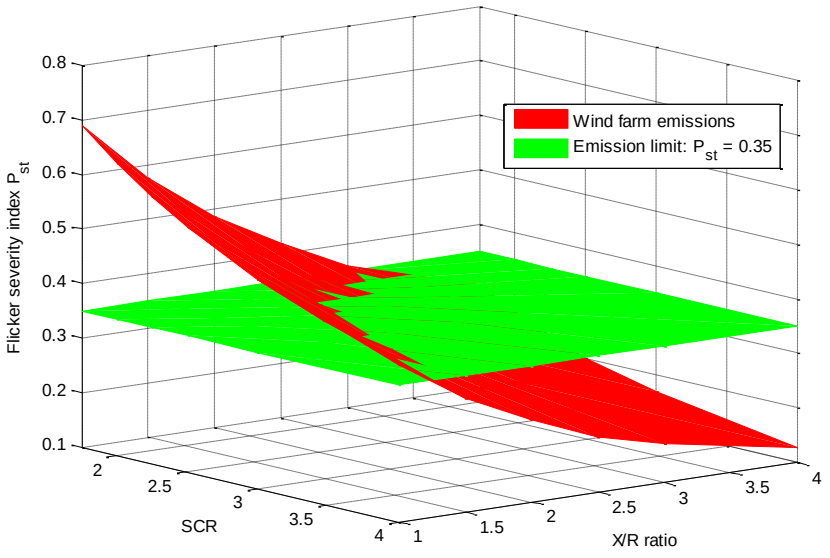

Figure 6-1 Wind farms flicker emission plane with reference to the emission limit

The rule of thumb screens a large distribution-connected wind installation, typically ranging from 10 MW - 14 MW with regard to flicker, based on grid characteristics, notably the SCC and the X/R ratio. Compliance is based on the minimum flicker emission limit in accordance to IEC 61000-3-7, which is equal to $P_{st} = 0.35$ for MV flicker producing generators.

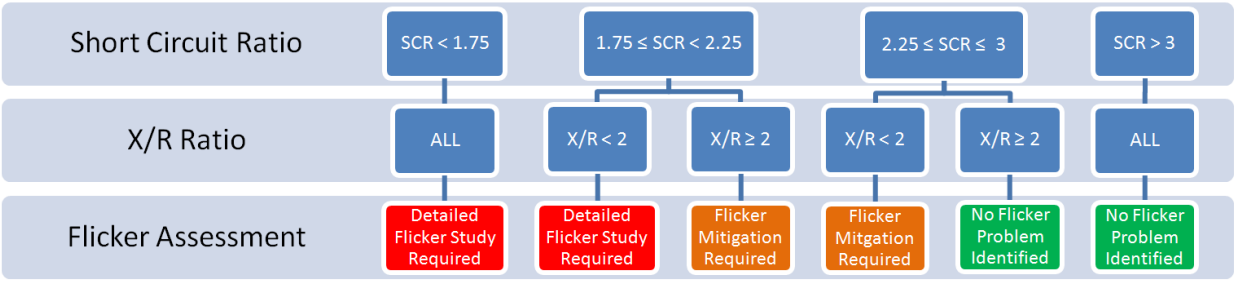

Figure 6-2 Rule of Thumb developed to screen for flicker problems due to large distribution-connected wind farms

The rule of thumb presents three flicker assessment results, 1) No Flicker Problem Identified, 2) Flicker Mitigation Required and 3) Detailed Flicker Study Required.

In the first scenario, whereby no flicker problem is identified, the desired wind penetration passes the flicker screening test and can be installed without the need for detailed studies and the provisioning of flicker mitigation. The fundamental assumption is that a global flicker analysis on the distribution feeder was conducted and there is indeed an emission limit of $P_{st} = 0.35$ that can be allocated to the wind farm.

In the second scenario, whereby flicker mitigation is required, a more cautious approach needs to be taken before the installation of the wind farm. The most universally applicable approach to render the desired wind penetration possible is to provision for embedded flicker mitigation. Reactive power based mitigation can be one method that may be provisioned in order to minimize the likelihood of a potential flicker problem as discussed in chapters 4 and 5. Moreover, the use of energy storage, capable of removing power fluctuations in the band of 0.1 to 1Hz, commonly used in power smoothing applications, such as in ref [66],[67], can also be a viable technique, although this has not been deeply discussed in this dissertation. On another note, eqn. (2.14) detailed the maximum flicker allowance which could be attributed to the wind farm, while maintaining EMC of the power system. Thus, if a global network flicker analysis is conducted in the pre-connection study and little or no flicker emitting industrial loads are

present in the distribution network, the utility may also choose to allocate a larger part of the flicker emission allowance to the wind farm, such that the project can be accepted. As specified in chapter 2, the French grid code allows for a similar measure, allowing a maximum $P_{st} = 0.44$ for large distribution-connected wind project.

In the third and final case, whereby a detailed flicker study is required, the wind installation does not pass the screening test and should not be installed, without a detailed flicker study, even if flicker mitigation techniques are provisioned for. The detailed flicker pre-connection study to be conducted will involve detailed knowledge of all industrial flicker emitting loads present, feeder and wind farm components, in order to determine if flicker will indeed be a problem. The utility also has two other trivial solutions possible; 1) reduce the level of wind penetration and 2) connect the wind farm at a stiffer point in the network, typically located at a shorter distance from the substation.

6.2 Summary

In this dissertation, a general methodology to quantify and assess flicker emissions from distribution-connected wind energy has been detailed. This included a review of the main applicable IEC EMC standards dealing with the measurement and assessment of flicker produced from wind energy, notably IEC 641000-4-15, IEC 61400-21 and IEC 61000-4-7. Flicker oriented modeling was discussed based on factors which influence flicker. This involved an understanding of which components in the equivalent wind speed model, turbine model and network model influenced flicker emissions. Based on the flicker oriented modeling, the behavior and degree in which key parameters affect flicker were reviewed and quantified. Using Opal-RT®'s real time simulator and associated software tools, a real distribution network was decoupled to permit computational speed-ups via parallel computing and a flicker study was conducted. This included a more comprehensive representation of the wind farm using time shifted wind speeds and the distribution network. The interaction between the wind farm and flicker producing industrial loads, represented by high powered, frequently starting induction motors was studied. Furthermore, a reactive power based, flicker mitigation technique, which dispatches reactive power to handle power fluctuations in the flicker

frequency range was tested and proven to be potentially be a viable solution. Lastly a rule of thumb to be used as a flicker screening technique, during a pre-connection study was formulated.

6.3 Conclusion

Large, distribution-connected wind farms may result in a voltage flicker problem and thus, limit the greatest level of wind penetration possible. Flicker emissions from a modern day Type 3 or Type 4 WTG are mainly influenced by turbulent and gusty winds and network characteristics. In situations where the severity of flicker emissions is anticipated to exceed the allocated emission limits, the provisioning of flicker mitigation techniques and emission coordination become essential. Thus, pre-connection studies are required to determine if flicker amongst other issues will be a limiting technical factor hindering the implementation of a wind project. The rule of thumb developed for flicker assessment is one tool utilities can now use to analyze large distribution-connected wind projects.

6.4 Recommendations for further work

Despite the research effort conducted in quantifying and assessing flicker emissions from distribution-connected wind farms, more work is required to keep up with future revisions of the IEC Flickermeter instrument, that may eventually consider modern lighting, revised flicker emission limits provided by emerging grid codes and economically viable flicker mitigation techniques. This section enumerates some ideas for extending the scope of the work.

6.4.1 Adaptable reactive power based flicker mitigation technique

There is no need for a flicker mitigation technique to operate and dispatch reactive power continuously. Flicker emissions from a distribution-connected wind farm will only exceed emission limits during certain time periods categorized by highly turbulent and gusty winds. Hence, there are significant opportunities in operating flicker mitigation scheme in an “only when needed” basis, (i.e. when emission limits allocated to the fluctuation installation are surpassed). This type of strategy would lead a more efficient use of reactive power. Figure 6-3

present a modification to the controller presented in section 4.5.3. Essentially, Q_{Pst} is set to $Q_{Pst} = 0$ when flicker emissions are not deemed a problem and set to $Q_{Pst} = -K\frac{R_L}{X_L}P_{fluctuations}$ when flicker emissions are deemed a problem.

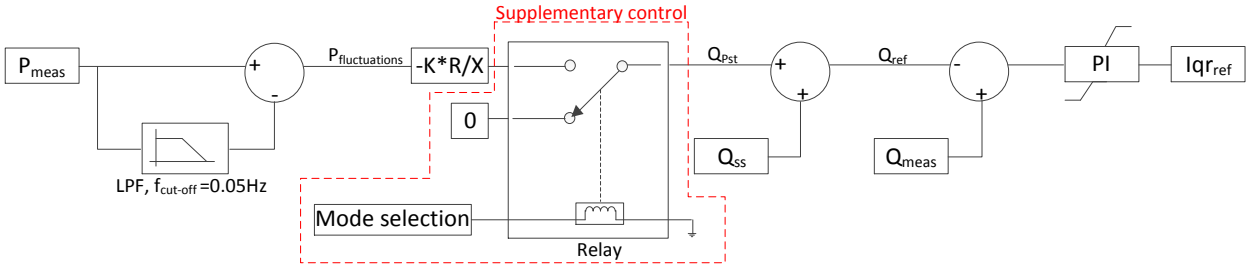

Figure 6-3 Controller diagram

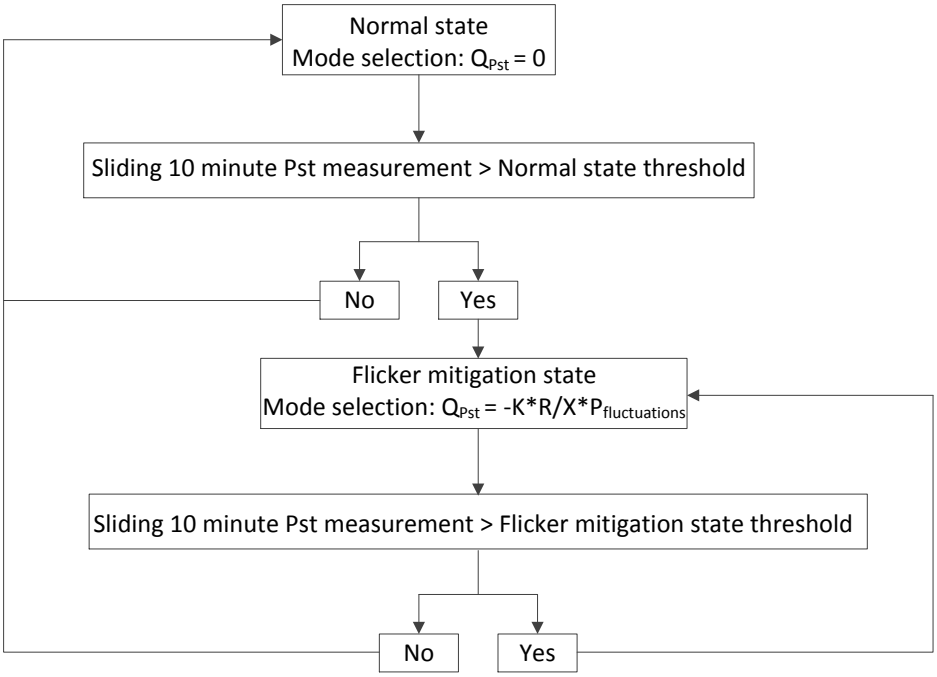

Figure 6-4 Supplementary control algorithm

Figure 6-4 describes the algorithm which will select which mode the turbine will operate in. The first mode, called the "Normal state" does not involve any flicker mitigation. The second mode, called "Flicker mitigation state" activates the flicker mitigation scheme. The trigger, which would determine the WTGs operating mode would be a 10 minute sliding flicker measurement taken at the PCC compared to a flicker emission threshold. There would also be one threshold associated with each state. Thus, in the normal state with no flicker mitigation,

flicker would need to be above a certain emission threshold to activate the flicker mitigation scheme and once the flicker mitigation scheme was activated, emissions would need to be below a second smaller emission threshold for the turbine to return to its normal state. These emission thresholds would need to be tuned on a case by case basis in accordance to the distribution feeder under study and emission limits granted. The implementation and benefits of the adaptable mitigation scheme would need to be tested for a much longer time frame, over a range of grid and wind conditions.

6.4.2 Flicker mitigation via energy storage

Recommendations for further work can also be with flicker mitigation techniques involving the use of ESSs. Currently, energy storage has been mostly used for power smoothing applications as in [66]-[69]. It would be interesting to investigate the level in which energy storage can attenuate flicker emissions and if it can be optimally sized to be practically viable. Hence, this research would involve the design of an embedded ESS, of optimal size to reduce WTG flicker emissions.

Appendix

Appendix A

Parameter	Value
Rated power	2 MW
Rated frequency	60 Hz
Rated voltage	0.575 kV
Rated speed	16.7 r/min
Stator resistance	0.023 pu
Stator reactance	0.18 pu
Rotor resistance	0.016 pu
Rotor reactance	0.016 pu
Pole pairs	3
Generator inertia (H_G)	0.8 s
Turbine inertia (H_T)	4.2 s
Shaft stiffness (K_{shaft})	1.52 pu
Shaft mutual damping (D_m)	3.4 pu
Rotor radius (R)	35 m
Hub height (H)	80 m
Tower radius (a)	2 m
Distance from blade origin to tower midline (x)	3 m
Empirical wind shear exponent (α)	0.3
Lambda opt (λ^*)	9.9495
Power coefficient ($C_{P,max}$)	0.5
Coefficients ($c_1 - c_8$)	
c_1	0.6450
c_2	116
c_3	0.4
c_4	5
c_5	21
c_6	0.00912
c_7	0.08
c_8	0.035
Air density (ρ)	1.29 Kg/m^3

Parameters of the DFIG WTG

Appendix B

Transformer	Rated Power	X/R ratio	Primary/Secondary Voltages
Substation transformer	15 MVA	25	114.3 kV/24.94 kV
DG transformer	17 MVA	10	0.575 kV/24.94 kV

Distribution feeder transformer parameters

Line	From	To	R_1 (Ω)	R_0 (Ω)	L_1 (mH)	L_0 (mH)
Z_{grid}	HV Substation	HV/MV Transformer	6.4438	0.1	5.13	0.3

Distribution feeder grid impedance parameters

Line	From	To	L (km)	R_1 (Ω/km)	R_0 (Ω/km)	L_1 (mH/km)	L_0 (mH/km)	C_1 (nF/km)	C_0 (nF/km)
TL-1	B-1	B-2	4.167	0.1140	0.3774	1.030	3.449	1.011	0.544
TL-2	B-2	B-3	2.291	0.116	0.384	1.0478	3.509	11.504	4.812
TL-3	B-3	B-4	2.04	0.1159	0.3838	1.047	3.5077	0.918	0.484
TL-4	B-4	B-5	6.517	0.1155	0.3824	1.043	3.4948	0.975	0.497
TL-5	B-6	B-7	0.97	1.469	1.469	3.649	3.647	1.213	0.603
TL-6	B-7	B-8	8.527	0.1134	0.3753	1.024	3.430	0.897	0.411
TL-7	B-8	B-9	10.67	0.116	0.384	1.0478	3.509	11.504	4.812
TL-8	B-8	B-10	1.59	0.1134	0.3753	1.024	3.430	0.969	0.534
TL-9	B-10	B-11	0.452	0.116	0.384	1.0478	3.509	10.434	4.121
TL-10	B-11	B-13	1.05	0.1157	0.3829	1.0448	3.5	0.983	0.531
TL-11	B-13	B-14	1.21	0.2860	0.5289	1.050	3.2819	0.997	0.476
TL-12	B-14	B-15	0.3	0.851	1.211	1.342	4.154	9.316	4.403
TL-13	B-13	B-16	0.423	0.2437	0.4971	1.065	3.393	0.989	0.513
TL-14	B-16	B-17	2.91	0.2648	0.4822	0.9464	2.943	1.133	0.579
TL-15	B-17	B-18	5.45	0.4238	0.6701	0.9330	2.969	1.138	0.583

Distribution feeder overhead line parameters

References

[1] Global Wind Energy Council (2012, February). Global Wind Statistics 2011. [Online]. Available:http://www.gwec.net/fileadmin/images/News/Press/GWEC_-Global_Wind_Statistics_2011.pdf

[2] Global Wind Energy Council (2012, March). Global Wind Report. [Online]. Available:http://www.gwec.net/fileadmin/documents/NewsDocuments/Annual_report_2011_lowres.pdf

[3] Hydro Québec (2009, August). Strategic Plan 2009-2013. [Online].Available: http://www.hydroquebec.com/publications/en/strategic_plan/pdf/plan-strategique-2009-2013.pdf

[4] T. Ackerman, G. Anderson, and L. Soder, "Distributed generation: a definition," Electric Power System Research, vol. 57, pp. 195–204, 2001.

[5] Quebec Government Department of Natural Resources and Wildlife (2005, June). Hydro-Québec Integrated Network Integration Capability with Respect to the Addition of Wind Energy Generation. [Online]. Available: http://www.mrnf.gouv.qc.ca/english/publications/energy/capacite-integration-version-anglaise-RSW.pdf

[6] Li, H.; Chen, Z.; , "Overview of different wind generator systems and their comparisons," *Renewable Power Generation, IET* , vol.2, no.2, pp.123-138, June 2008

[7] Polinder, H.; , "Overview of and trends in wind turbine generator systems," *Power and Energy Society General Meeting, 2011 IEEE* , vol., no., pp.1-8, 24-29 July 2011

[8] A. D. Hansen, F. Iov, F. Blaabjerg, and L. H. Hansen, "Review of contemporary wind turbine concepts and their market penetration," Wind Engineering, vol. 28, no. 3, pp. 247-263, 2004.

[9] T. Xu and P. Taylor, "Voltage control techniques for electrical distribution networks including distributed generation," presented at the Proc. 17th World Congress The International Federation of Automatic Control,Seoul, 2008.

[10] Stavros A. Papathanassiou, A technical evaluation framework for the connection of DG to the distribution network, Electric Power Systems Research, Volume 77, Issue 1, Pages 24-34, January 2007.

[11] Deutsches Windenergie-Institut GmbH in Germany; Tech-wise A/S in Denmark and DM Energy in United Kingdom: "Wind Turbine Grid Connection and Interaction", 2001.

[12] BC Hydro, "Power Quality: A guide to voltage fluctuation and light flicker," March 2005 [Online]. Available: http://www.bchydro.com/etc/medialib/internet/documents/psbusiness/pdf/power_quality_a_guide_to_voltage_fluctuation_and_light_fl.Par.0001.File.power_quality_a_guide_to_voltage_fluctuation_and_light_fl.pdf

[13] Owen, E.L.; , "Power disturbance and quality: light flicker voltage requirements ," *Industry Applications Magazine, IEEE* , vol.2, no.1, pp.20-27, Jan/Feb 1996

[14] Bayo, A. H. (2008) Voltage Fluctuations and Flicker, in Handbook of Power Quality (ed A. Baggini), John Wiley & Sons, Ltd, Chichester, UK.

[15] IEC 61000-4-15:2003, Electromagnetic Compatibility (EMC)—Part 4: Testing and measurement techniques—Section 15: Flickermeter—Functional and design specifications.

[16] Halpin, S.M.; Bergeron, R.; Blooming, T.M.; Burch, R.F.; Conrad, L.E.; Key, T.S.; , "Voltage and lamp flicker issues: should the IEEE adopt the IEC approach?," *Power Delivery, IEEE Transactions on* , vol.18, no.3, pp. 1088- 1097, July 2003

[17] Cooper Development Association (2005, October). Voltage Disturbances: Flicker Measurement. [Online]. Available: http://www.copperinfo.co.uk/power-quality/downloads/pqug/523-flicker-measurement.pdf

[18] De Lange H., “Eye’s response at flicker fusion to square-wave modulation of a test field surrounded by a large steady field of equal mean luminance,” Journal of the Optical Society of America, vol. 51, pp. 415–421, 1961

[19] Rashbass C., “The visibility of transient changes of luminance,” Journal of Physiology, vol. 210, pp. 165–186, 1970

[20] "IEEE Application Guide for IEEE Std 1547, IEEE Standard for Interconnecting Distributed Resources with Electric Power Systems," *IEEE Std 1547.2-2008* , vol., no., pp.1-207, April 15 2009.

[21] Larsson, A.; , "Flicker Emission of Wind Turbines during Continuous Operation," Power Engineering Review, IEEE , vol.22, no.2, pp.59, Feb. 2002

[22] Tao Sun; Zhe Chen; Blaabjerg, F.; , "Flicker study on variable speed wind turbines with doubly fed induction generators," *Energy Conversion, IEEE Transactions on* , vol.20, no.4, pp. 896- 905, Dec. 2005

[23] Weihao Hu; Zhe Chen; Yue Wang; Zhaoan Wang; , "Flicker study on variable speed wind turbines with permanent magnet synchronous generator," *Power Electronics and Motion Control Conference, 2008. EPE-PEMC 2008. 13th* , vol., no., pp.2325-2330, 1-3 Sept. 2008

[24] Papadopoulos, M.P.; Papathanassiou, S.A.; Tentzerakis, S.T.; Boulaxis, N.G.; , "Investigation of the flicker emission by grid connected wind turbines," *Harmonics and Quality of Power Proceedings, 1998. Proceedings. 8th International Conference On* , vol.2, no., pp.1152-1157 vol.2, 14-18 Oct 1998

[25] Chun Wei; Minxiao Han; Wenli Yan; , "Voltage fluctuation and flicker assessment of a weak system integrated wind farm," *Power and Energy Society General Meeting, 2011 IEEE* , vol., no., pp.1-5, 24-29 July 2011

[26] Thiringer, T.; Petru, T.; Lundberg, S.; , "Flicker contribution from wind turbine installations," *Energy Conversion, IEEE Transactions on* , vol.19, no.1, pp. 157- 163, March 2004

[27] Thiringer, T.; Petru, T.; Liljegren, C.; , "Power quality impact of a sea located hybrid wind park," Energy Conversion, IEEE Transactions on , vol.16, no.2, pp.123-127, Jun 2001

[28] Fadaeinedjad, R.; Moschopoulos, G.; Moallem, M.; , "The Impact of Tower Shadow, Yaw Error, and Wind Shears on Power Quality in a Wind–Diesel System," *Energy Conversion, IEEE Transactions on* , vol.24, no.1, pp.102-111, March 2009

[29] Dolan, D.S.L.; Lehn, P.W.; , "Simulation model of wind turbine 3p torque oscillations due to wind shear and tower shadow," *Energy Conversion, IEEE Transactions on* , vol.21, no.3, pp.717-724, Sept. 2006

[30] Swagata Das, Neeraj Karnik, and Surya Santoso, "Time-Domain Modeling of Tower Shadow and Wind Shear in Wind Turbines," ISRN Renewable Energy, vol. 2011, Article ID 890582, 11 pages, 2011.

[31] Schoene, J.; McDermott, T.E.; Smith, C.; Zavadil, R.; Lamoree, J.; , "Flicker from distributed wind generation," *Power and Energy Society General Meeting, 2011 IEEE* , vol., no., pp.1-9, 24-29 July 2011

[32] Scott, N.C.; Atkinson, D.J.; Morrell, J.E.; , "Use of load control to regulate voltage on distribution networks with embedded generation," *Power Systems, IEEE Transactions on* , vol.17, no.2, pp.510-515, May 2002

[33] Montanari, G.C.; Loggini, M.; Cavallini, A.; Pitti, L.; Zaninelli, D.; , "Arc-furnace model for the study of flicker compensation in electrical networks," Power Delivery, IEEE Transactions on , vol.9, no.4, pp.2026-2036, Oct 1994

[34] Ruiz, J.; Gutierrez, J.J.; Lazkano, A.; Ruiz de Gauna, S.; , "A Review of Flicker Severity Assessment by the IEC Flickermeter," *Instrumentation and Measurement, IEEE Transactions on* , vol.59, no.8, pp.2037-2047, Aug. 2010

[35] Bhattacharyya, S., Cobben, S., Myrzik, J. and Kling, W. (2010), Flicker propagation and emission coordination study in a simulated low voltage network. Euro. Trans. Electr. Power, 20: 52–67.

[36] Deokar, S.A.; Waghmare, L.M.; Jadhav, G.N.; , "Voltage flicker assessment of induction motors used in the integrated water pumping station," *Power Electronics, Drives and Energy Systems (PEDES) & 2010 Power India, 2010 Joint International Conference on* , vol., no., pp.1-7, 20-23 Dec. 2010

[37] Weihao Hu; Zhe Chen; Yue Wang; Zhaoan Wang; , "Flicker Mitigation by Active Power Control of Variable-Speed Wind Turbines With Full-Scale Back-to-Back Power Converters," *Energy Conversion, IEEE Transactions on* , vol.24, no.3, pp.640-649, Sept. 2009

[38] Tan Luong Van; Thanh Hai Nguyen; Dong-Choon Lee; , "Flicker mitigation in DFIG wind turbine systems," *Power Electronics and Applications (EPE 2011), Proceedings of the 2011-14th European Conference on* , vol., no., pp.1-10, Aug. 30 2011-Sept. 1 2011

[39] Sun, T.; Chen, Z.; Blaabjerg, F.; , "Flicker mitigation of grid connected wind turbines using STATCOM," *Power Electronics, Machines and Drives, 2004. (PEMD 2004). Second International Conference on (Conf. Publ. No. 498)* , vol.1, no., pp. 175- 180 Vol.1, 31 March-2 April 2004

[40] Moataz Ammar, "Flicker emission of distributed wind power: a review of impacts, modeling, grid codes and mitigation techniques", IEEE PES General Meeting 22 Jul - 27 Jul 2012, San Diego, USA.

[41] Liu, M.B.; Canizares, C.A.; Huang, W.; , "Reactive Power and Voltage Control in Distribution Systems With Limited Switching Operations," Power Systems, IEEE Transactions on , vol.24, no.2, pp.889-899, May 2009

[42] Mohamed Machmoum, Ahmad Hatoum, Toufik Bouaouiche, Flicker mitigation in a doubly fed induction generator wind turbine system, Mathematics and Computers in Simulation, Volume 81, Issue 2, October 2010, Pages 433-445

[43] Yun-Seong Kim; Dong-Jun Won; , "Mitigation of the Flicker Level of a DFIG Using Power Factor Angle Control," *Power Delivery, IEEE Transactions on* , vol.24, no.4, pp.2457-2458, Oct. 2009

[44] Meegahapola, L.; Fox, B.; Flynn, D.; , "Flicker mitigation strategy for DFIGs during variable wind conditions," *Power and Energy Society General Meeting, 2010 IEEE* , vol., no., pp.1-8, 25-29 July 2010

[45] M. Tsili and S. Papathanassiou, "A review of grid code technical requirements for wind farms," IET Renewable Power Generation, vol. 3, no. 3, pp. 308–332, 2009.

[46] Xiao Hui; Liu Yong; Liu Huijing; , "Comparison of Two Calculation Methods of Flicker Caused by Wind Power," *Power and Energy Engineering Conference (APPEEC), 2011 Asia-Pacific* , vol., no., pp.1-4, 25-28 March 2011

[47] IEC 61400-21:2008, Wind turbines—Part 21: Measurement of assessment of power quality characteristics of grid connected wind turbines.

[48] IEC/TR 61000-3-7:2008, Electromagnetic Compatibility (EMC)—Part 3-7: Limits—Assessment of emission limits for the connection of fluctuating installations to MV, HV and EHV power systems.

[49] European Commission, "Commission Regulation (EC) No 244/2009 of 18 March 2009 implementing Directive 2005/32/EC of the European Parliament and of the Council with regard to ecodesign requirements for non-directional household lamps", Official Journal of the European Union, n.76, March, 24th, 2009, pp. 3-16.

[50] Keppler, T.; Watson, N.R.; Arrillaga, J.; Shiun Chen; , "Theoretical assessment of light flicker caused by sub- and interharmonic frequencies," *Power Delivery, IEEE Transactions on* , vol.18, no.1, pp. 329- 333, Jan 2003

[51] Xu, W.; , "Deficiency of the IEC flicker meter for measuring interharmonic-caused voltage flickers," Power Engineering Society General Meeting, 2005. IEEE , vol., no., pp. 2326-2329 Vol. 3, 12-16 June 2005

[52] Drapela, J.; Toman, P.; , "Interharmonic - Flicker Curves of Lamps and Compatibility Lever for Interharmonic Voltages," *Power Tech, 2007 IEEE Lausanne* , vol., no., pp.1552-1557, 1-5 July 2007

[53] Chen, S.; Lo, C.M.; Foo, M.K.; How, K.T.; , "Testing of fluorescent lamps for its flickering susceptibility towards interharmonic voltages," *Power Engineering Conference, 2007. IPEC 2007. International* , vol., no., pp.326-331, 3-6 Dec. 2007

[54] Emanuel, A.E.; Peretto, L.; , "The response of fluorescent lamp with magnetic ballast to voltage distortion," *Power Delivery, IEEE Transactions on* , vol.12, no.1, pp.289-295, Jan 1997

[55] De Jaeger, Emmanuel; , "Disturbance emission level assessment techniques (CIGRE-CIRED joint working group C4.109)," *Electricity Distribution - Part 2, 2009. CIRED 2009. The 20th International Conference and Exhibition on* , vol., no., pp.1-2, 8-11 June 2009

[56] Yang, X.; Gauthier, J.; , "How can flicker level be determined before a customer is connected to the electric grid," *Power & Energy Society General Meeting, 2009. PES '09. IEEE* , vol., no., pp.1-6, 26-30 July 2009

[57] E. Welfonder, R. Neifer, M. Spanner, Development and experimental identification of dynamic models for wind turbines, Control Engineering Practice, Volume 5, Issue 1, Pages 63-73, January 1997

[58] Liu Yanjie; Wang Jun; , "A large time scale wind velocity simulation method," *Computer Design and Applications (ICCDA), 2010 International Conference on* , vol.4, no., pp.V4-282-V4-286, 25-27 June 2010

[59] Poul Sørensen, Anca D. Hansen, Pedro André Carvalho Rosas, Wind models for simulation of power fluctuations from wind farms, Journal of Wind Engineering and Industrial Aerodynamics, Volume 90, Issues 12–15, Pages 1381-1402, December 2002

[60] Amadou D. Diop, Emil Ceanga, Jean-Louis Rétiveau, Jean-François Méthot, Adrian Ilinca, Real-time three-dimensional wind simulation for windmill rig tests, Renewable Energy, Volume 32, Issue 13, Pages 2268-2290, October 2007

[61] Nichita, C.; Luca, D.; Dakyo, B.; Ceanga, E.; , "Large band simulation of the wind speed for real time windturbine simulators," *Energy Conversion, IEEE Transactions on* , vol.17, no.4, pp. 523- 529, Dec 2002

[62] Petru, T.; Thiringer, T.; , "Modeling of wind turbines for power system studies," *Power Systems, IEEE Transactions on* , vol.17, no.4, pp. 1132- 1139, Nov 2002

[63] Ming Yin; Gengyin Li; Ming Zhou; Guoping Liu; Chengyong Zhao; , "Study on the control of DFIG and its responses to grid disturbances," *Power Engineering Society General Meeting, 2006. IEEE* , vol., no., pp.6 pp.,

[64] Moataz Ammar, Geza Joos, "Combined active/reactive power control for flicker mitigation in distributed wind power", 2012 IEEE Energy Conversion Congress and Exposition (ECCE), Raleigh, North Carolina.

[65] Moataz Ammar, Philippe Venne, Chad Abbey, Geza Joos, A methodology for assessing the impact of distributed wind power on voltage flicker", Cigre International Symposium on the Electric Power System of the Future, 13-15 September 2011, Bologna, Italy.

[66] Wei Li; Joos, G.; Abbey, C.; , "Attenuation of Wind Power Fluctuations in Wind Turbine Generators using a DC Bus Capacitor Based Filtering Control Scheme," *Industry Applications Conference, 2006. 41st IAS Annual Meeting. Conference Record of the 2006 IEEE* , vol.1, no., pp.216-221, 8-12 Oct. 2006

[67] Wei Li; Joos, G.; Abbey, C.; , "Wind Power Impact on System Frequency Deviation and an ESS based Power Filtering Algorithm Solution," *Power Systems Conference and Exposition, 2006. PSCE '06. 2006 IEEE PES* , vol., no., pp.2077-2084, Oct. 29 2006-Nov. 1 2006

[68] Shajari, S.; Key Pour, R.; , "Reduction of battery size and charge-discharge for active power smoothing of DFIG," *Environment and Electrical Engineering (EEEIC), 2012 11th International Conference on* , vol., no., pp.112-114, 18-25 May 2012

[69] Aghatehrani, R.; Kavasseri, R.; Thapa, R.C.; , "Power smoothing of the DFIG wind turbine using a small energy storage device," *Power and Energy Society General Meeting, 2010 IEEE* , vol., no., pp.1-6, 25-29 July 2010

[70] White, L.W.; Bhattacharya, S.; , "A Discrete Matlab–Simulink Flickermeter Model for Power Quality Studies," Instrumentation and Measurement, IEEE Transactions on , vol.59, no.3, pp.527-533, March 2010

[71] Soo-Hwan Cho, Jae-Ahn Jung, Gilsoo Jan, Sae-Hyuk Kwon and Moon-Ho Kang;, "Development of Matlab/Simulink Module for Voltage Flicker Simulationin Distribution Power Systems," Journal of Electrical Engineering & Technology, Vol. 3, No. 3, pp. 314-319, 2008

[72] Bertola, A.; Lazaroiu, G.C.; Roscia, M.; Zaninelli, D.; , "A Matlab-Simulink flickermeter model for power quality studies," Harmonics and Quality of Power, 2004. 11th International Conference on , vol., no., pp. 734- 738, 12-15 Sept. 2004

[73] Mombauer, W.; , "Flicker-simulation and minimization," Electricity Distribution, 1989. CIRED 1989. 10th International Conference on, vol., no., pp.102-106 vol.2, 8-12 May 1989

[74] Drapela, J., Slezingr, J. A Light-flickermeter – Part I: Design.Proceedings of the 11th Conference Electric Power Engineering 2010.Brno University of Technology, 2010, pp.453-458

[75] Miller, N.W.; Sanchez-Gasca, J.J.; Price, W.W.; Delmerico, R.W.; , "Dynamic modeling of GE 1.5 and 3.6 MW wind turbine-generators for stability simulations," *Power Engineering Society General Meeting, 2003, IEEE* , vol.3, no., pp. 1977- 1983 Vol. 3, 13-17 July 2003

[76] P. C. Krause, O.Wasynczuk, and S. D. Sudhoff, *Analysis of Electric Machinery*, IEEE Press, 1995.

[77] Emanuel, H.; Schellschmidt, M.; Wachtel, S.; Adloff, S.; , "Power quality measurements of wind energy converters with full-scale converter according to IEC 61400-21," *Electrical Power Quality and Utilisation, 2009. EPQU 2009. 10th International Conference on* , vol., no., pp.1-7, 15-17 Sept. 2009

[78] Stavros A. Papathanassiou, Spyros J. Kiartzis, Michael P.Papadopoulos, Antonios G. Kladas, "Wind Turbine Flicker Calculation using Neural Networks," Wind Engineering, vol. 24, no. 5, pp. 317-335, 2000.

[79] Gagnon, R.; Fecteau, M.; Prud'Homme, P.; Lemieux, E.; Turmel, G.; Pare, D.; Duong, F.; , "Hydro-Québec Strategy to Evaluate Electrical Transients Following Wind Power Plant Integration in the Gaspésie Transmission System," *Sustainable Energy, IEEE Transactions on* , vol.3, no.4, pp.880-889, Oct. 2012

[80] C. Larose, R. Gagnon, G. Turmel, P. Giroux, J. Brochu, D. McNabb, and D. Lefebvre, "Large wind power plant modeling techniques for power system simulation studies," in *Proc. 8th Int. Workshop Large-Scale Integration of Wind Power Into Power Systems*, Bremen, Germany, Oct. 2009, pp. 472–478.